ANALYSIS AND DESIGN OF ARRAY ANTENNA RADIATION PATTERNS USING ANALYTIC SIGNAL THEORY

By

CHING-SONG CHUANG

A DISSERTATION PRESENTED TO THE GRADUATE SCHOOL
OF THE UNIVERSITY OF FLORIDA IN PARTIAL FULFILLMENT
OF THE REQUIREMENTS FOR THE DEGREE OF
DOCTOR OF PHILOSOPHY

UNIVERSITY OF FLORIDA

1989

The author proudly dedicates this dissertation to his family.

ACKNOWLEDGEMENTS

The author wishes to express his sincere thanks to the chairman of his advisory committee, Dr. L. W. Couch, for suggesting this project, and for his patient advice, guidance and infinite encouragement throughout the course of this research. The author also appreciates the help of the other members of his supervisory committee, Drs. P. Z. Peebles, J. T. Tou, J. C. Principe, and James Keesling, for the time they spent reviewing his research program frequently and enthusiastically. Their comments and suggestions have been invaluable.

In addition, the author would like to thank Drs. D. G. Chang and S. M. Juang, who are working in the antenna area in CSIST, Taiwan, for their interest and helpful discussion relating to this research project, and Mr. S. F. Law for his help in editing of this manuscript.

Special thanks are given to his family for their moral support and encouragement.

The author is indebted to the people and the government in Taiwan, Republic of China, for their providing the scholarship for his graduate research in the United States.

TABLE OF CONTENTS

page

ACKNOWLEDGEMENTS iii

LIST OF TABLES vii

LIST OF FIGURES viii

ABSTRACT xi

CHAPTERS

I INTRODUCTION 1

1.1 Motivation and Objectives of the Research 1
1.2 Areas of Research 2
1.3 Organization of the Dissertation 6

II THE DISCRETE-TIME ANALYTIC SIGNAL AND HILBERT TRANSFORNATION 8

2.1 Introduction 8
2.2 Review of the One-Dimensional Analytic Signal Theory and Hilbert Transform 9
2.3 The 2-D Discrete-Time Analytic Signal and 2-D Discrete-Time Hilbert Transform 19
  2.3.1 The definition of 2-D discrete-time ãnalytic signals 21
  2.3.2 The definition of 2-D discrete-time Hilbert transforms 22
  2.3.3 The properties of the general expression of 2-D discrete-time Hilbert transform 24
    2.3.3.1 The impulse response of the general expression of 2-D discrete-time Hilbert transform 25
    2.3.3.2 The properties of the transformation using impulse response $h_g(m,n)$ 29
  2.3.4 The generation of a 2-D ãnalytic signal--Type I using two stages of transfromations (Case Ia) 31
    2.3.4.1 The 2-D discrete-time Hilbert transform (Type I) 31
    2.3.4.2 The generation of a 2-D ãnalytic signal--Type I 36

2.3.5 The generation of a 2-D ãnalytic signal--Type I using two 1-D ãnalytic signals (Case Ib) 38
2.3.6 The generation of a 2-D ãnalytic signal--Type II using 2-D discrete-time Hilbert transform(Type II) (Case II) 39
2.4 Summary 43

III ANALYSIS OF BROADSIDE NARROW BEAMWIDTH ARRAY RADIATION PATTERNS USING ANALYTIC EXCITATIONS 45

3.1 Introduction 45
3.2 Fundamentals of an Array Antenna Theory 46
3.2.1 The generalized structure of an array antenna system 46
3.2.2 The linear array antenna system 51
3.2.3 The planar rectangular grid array antenna system 54
3.3 Analysis of Broadside Narrow Beamwidth Array Radiation Patterns using Analytic Excitations 58
3.3.1 The potential advantages of broadside narrow beamwidth array radiation patterns using ãnalytic excitations 61
3.3.1.1 The generation of a half-sided narrow beamwidth radiation pattern using an ãnalytic excitation 62
3.3.1.2 The symmetry property of an ãnalytic excitation 65
3.3.1.3 The improvement of Radiation efficiency (η) of a tapered excitation using an ãnalytic excitation 67
3.3.2 The analysis of broadside narrow beamwidth array radiation patterns using realizable ãnalytic excitations 69
3.3.3 Analysis examples 77
3.4 Discussion and Summary 90

IV THE BROADSIDE NARROW BEAMWIDTH ASYMMETRIC SIDELOBE ARRAY RADIATION PATTERN DESIGN USING ANALYTIC EXCITATION 92

4.1 Introduction 92
4.2 The Fundamental Theories for Designing a Broadside Narrow Beamwidth Asymmetric Sidelobe Array Radiation Pattern 93
4.3 System Design Constraint 96
4.4 System Analysis and Performance Evaluation 97
4.5 System Design Procedure 102
4.6 Design Examples 107

4.7 The Generation of Narrow Beamwidth Asymmetric Sidelobe Planar Array Radiation Pattern 120
  4.7.1 The generation of the half-plane asymmetric sidelobe radiation pattern using Type II ãnalytic excitation 121
  4.7.2 The generation of the quadrant-plane asymmetric sidelobe radiation pattern using Type I ãnalytic excitation 124
4.8 Discussion and Summary 125

V THE SHAPED BEAM ARRAY ANTENNA RADIATION PATTERN DESIGN USING ANALYTIC EXCITATION 131

5.1 Introduction 131
5.2 The Basic Concepts for Shaped Beam Radiation Pattern Design using Analytic Excitation 132
5.3 System Design Constraint 137
5.4 System Design Example using Windowing Method .. 139
5.5 Discussion and Summary 150

VI ANALYSIS AND DESIGN OF RADIATION PATTERNS FOR A MONOPULSE ARRAY ANTENNA SYSTEM USING ANALYTIC SIGNAL THEORY 152

6.1 Introduction 152
6.2 The Generations of Radiation Patterns for a Monopulse Array Antenna Radar System using Analytic Signal Concept 154
6.3 Analysis of Radiation Patterns of a Monopulse Array Antenna Radar System using Realizable Hilbert Transformer 159
6.4 System Analysis and Design Example 162
6.5 Discussion and Summary 170

VII CONCLUSION 172

APPENDIX THE DOLPH-CHEBYSHEV LINEAR ARRAY SYSTEM 177

REFERENCES 182

BIOGRAPHICAL SKETCH 188

LIST OF TABLES

Table

3.1 The characteristics of the broadside narrow beamwidth radiation patterns excited by Hamming and the two corresponding ãnalytic excitations .. 82

3.2 The normalized Hamming and the corresponding ãnalytic excitations 84

3.3 The characteristics of the broadside narrow beamwidth radiation patterns excited by the Dolph-Chebyshev and the two corresponding ãnalytic excitations 87

4.1 The characteristics of the radiation patterns excited by Hamming and the corresponding modulated ãnalytic excitations 108

4.2 The ãnalytic excitation for (35/23) asymmetric sidelobe radiation pattern 118

4.3 The characteristics of the shifted (35/23) asymmetric sidelobe and (35/35) Taylor symmetric sidelobe radiation patterns 118

5.1 The excitations of the realized cosecant-squared power patterns 149

5.2 The characteristics of the realized cosecant-squared power patterns 149

6.1 The characteristics of the difference pattern as functions of the number of array elements 163

6.2 The characteristics of the difference pattern as functions of truncation windows 166

6.3 The excitations for the realized sum and difference patterns of a monopulse array antenna radar system 170

LIST OF FIGURES

Figure

2.1 The spectrum transformation between the analog and discrete-time analytic signals 13

2.2 The impulse response of one-dimensional discrete-time Hilbert transform 18

2.3 The 2-D quadrant-plane and half-plane spectra ... 22

2.4 The impulse response and spectrum of $h_g(m,n)$ .. 28

2.5 The 2-D discrete-time Hilbert transform (Type I) 35

2.6 A general 2-D ãnalytic signal--TYpe I generator 36

2.7 The 2-D discrete-time Hilbert transform (Type II) 42

3.1 The generalized geometrical structure of an array antenna system 47

3.2 The linear array antenna system 51

3.3 The rectangular grid planar array antenna system 54

3.4 The broadside narrow beamwidth radiation patterns excited by a uniform excitation and the corresponding ideal ãnalytic excitation 65

3.5 The pictorial illustration of the complemental property of the real and the imaginary parts of a typical ãnalytic excitation 68

3.6 The illustration of periodic convolution 73

3.7 The generations of the realizable ãnalytic excitation and the corresponding asymmetric radiation pattern 76

3.8 The Hamming and the corresponding realized asymmetric radiation patterns 80

3.9 The Chebyshev (R=30dB) and the corresponding realized asymmetric radiation patterns 86

3.10 The peak sidelobe ratios of the asymmetric radiation patterns as function of the number of array elements 89

4.1 The decomposed mainbeam and sidelobe patterns of a real modulated excitation 98

4.2 The parameters used to define the SSG_{peak} and SRPR 102

4.3 The Hamming $F_{ham}(u)$ and the corresponding realized asymmetric sidelobe $F_{ma}(u+u_c)$ radiation patterns 108

4.4 The 25dB Taylor pattern and mainbeam widths 114

4.5 The relations of the asymmetric sidelobes SLL_{peak} and SLR_{peak} and the Taylor patterns with various peak sidelobes 116

4.6 The realized shifted (35/23) asymmetric sidelobe and the Taylor symmetric sidelobe (35dB) radiation patterns 117

4.7 The nonseparable Kaiser circular and the corresponding half-plane asymmetric sidelobe planar array patterns 127

4.8 The 11x11 separable Taylor and the corresponding half-plane asymmetric sidelobe planar array patterns 129

5.1 Sketches of the desired shaped beam pattern, the symmetricalized shaped beam pattern and the realized shaped beam pattern 134

5.2 The definitions of the roll-off regions of the realized symmetricalized shaped beam pattern and the spectrum of the realizable Hilbert transformer 138

5.3 The desired cosecant-squared shaped beam power pattern 141

5.4 The desired and realized cosecant-squared shaped power patterns 146

5.5 The realized cosecant-squared shaped power pattern with increasing number of array elements 148

6.1 Sketches of the typical radiation patterns of an amplitude monopulse array antenna radar system .. 153

6.2 The desirable radiation patterns of an amplitude monopulse array antenna radar system 159

6.3 The directivity and difference slope of a difference pattern as functions of the number of array elements 164

6.4 The difference slopes and the peak sidelobes of a difference pattern as functions of the truncation windows 167

6.5 The realized sum and difference patterns using the Hilbert transfrom method 169

Abstract of Dissertation Presented to the Graduate School
of the University of Florida in Partial Fulfillment of the
Requirements for the Degree of Doctor of Philosophy

ANALYSIS AND DESIGN OF ARRAY ANTENNA RADIATION PATTERNS USING ANALYTIC SIGNAL THEORY

By

CHING-SONG CHUANG

August, 1989

Chairman: Dr. Leon W. Couch
Major Department: Electrical Engineering

A new concept and design methods for the radiation patterns of an array antenna system are introduced and developed. It is well known that the analysis and design problems of the array antenna system are analogous to those of a discrete-time signal and system. Through the analogy, the utilization of the analytic signal concept for the design of an array antenna system is fully exploited and investigated.

First, the equivalent one-dimensional and two-dimensional discrete-time analytic signals and the associated Hilbert transforms are defined and derived. There are two types of two-dimensional discrete-time analytic signals that are found to be useful for the planar array antenna system.

Using the spectrum property as well as the spectrum relations between the real part and the imaginary part of an analytic signal, these design concepts, are theoretically discussed and physically evaluated in order to improve the beamwidth resolution of a conventional broadside symmetric radiation pattern and to implement the sum and difference patterns for a monopulse array antenna radar system. The achievements depend on and are determined by the realizable Hilbert transformer.

This analytic signal concept, along with the modulation theory, is then used to design various desirable asymmetric sidelobe radiation patterns which include linear and planar broadside narrow beamwidth patterns and shaped beam patterns. By comparing the characteristics of the asymmetric sidelobe patterns to the conventional symmetric patterns, we found that the asymmetric patterns have a large advantage. The features of those design methods compared to the others are conceptual simplicity, computational effectiveness and use of analytic design procedures.

In summary, the analytic signal theory provides a new concept and methods for designing various desirable radiation patterns of an array antenna system.

CHAPTER I

INTRODUCTION

1.1 Motivation and Objectives of the Research

The fundamental theory and principles of an array antenna system are so widely known that they can be found everywhere in textbooks and published literature [1-11]. Since the far field radiation pattern and current excitation of an array antenna system can be formed as Fourier transform relations (discrete-time), it has long been recognized that there are analogies in the design problems between the array antenna system and the discrete-time signal and system. Various useful analysis and design concepts and theories have been exploited and beneficially shared on both areas [5,7,12-13].

The analytic signal, first introduced by Gabor in 1946, has been playing an important role in signal processing and communication systems. Specifically speaking, wherever the Fourier transform is applicable, the analytic signal concept always provides both theoretical interest and practical useful results. Surprisingly, no attention has been paid to the use of the analytic signal concept in the design of the radiation patterns of an array antenna system. Such a design idea to the author's knowledge is still ignored by the experts in the antenna area and thus not found in the published literature. However, there are several properties of an analytic signal which are well suited for the design of the radiation patterns of an antenna system. It is the purpose of this dissertation to exploit and exhibit the advantages of the design of the radiation patterns of an array antenna system using analytic signal theory.

1.2 Areas of Research

Basically, there are two main trends in designing the radiation patterns of an array antenna system: either to maximize some pattern characteristics [14-18] or to approximate a prescribed pattern shape [19-21]. This dissertation concentrates on the study of the latter trend by applying the analytic signal concept. The function of the radiation pattern of an antenna system can be alternatively interpreted as a spatial filter. Consequently, the required shapes of the radiation patterns may very much depend on the applications. Detection and discrimination of spatial targets may require a narrow beamwidth radiation pattern, and tracking a moving target may require an even symmetric and an odd symmetric narrow beamwidth radiation pattern. Some special-purpose applications may require particular, shaped beam patterns, such as the cosecant-squared shaped power pattern for an air surveillance or ground mapping radar system.

The analytic signal can be formed by a Hilbert transform pair [22], and there are several interesting properties related to the analytic signal which are well understood [23-26]:

1. The spectrum of the analytic signal vanishes for negative frequency while its dual (its complex conjugate) vanishes for positive frequency.
2. The real and imaginary parts of the analytic signal have an identical power spectrum.
3. If the real part of the analytic signal is even symmetric, then its imaginary part is odd symmetric.
4. The analytic signal is completely described by its real or imaginary part.

By carefully associating the required shapes of the radiation patterns of an antenna system with the spectral properties of an analytic signal, we find that Property 1 indicates the beamwidth resolution can doubly be increased, and one of the sidelobes will be eliminated compared to a typical broadside symmetric antenna radiation pattern. Properties 2,3,4 provide a new idea for designing the radiation patterns of a monopulse radar system using the excitations corresponding to the real and the imaginary parts of the analytic signal. Those design concepts will be fully exploited and analyzed in this dissertation.

The design of a broadside narrowest beamwidth radiation pattern with a specified symmetric sidelobe level for an equal interelement distance linear array antenna system has been proposed by Dolph [19] and extended to continuous sources by Taylor [20]. Lopez [27] and Elliott [28] have pointed out that the symmetric sidelobes of an antenna radiation pattern are neither a requirement, nor even desirable, because most operation environments have a situation where the effects of the interferences (either intentional or unintentional clutters) are unevenly distributed in the space. For instance, a ground base radar system is desirable to have a lower sidelobe below the horizon than above the horizon so as to minimize the effect of the ground clutter. Thus, by using an asymmetric sidelobe radiation pattern, there would be advantages in a narrowing of the beamwidth and an increase in gain relative to the symmetric case with both sides of sidelobes having the same sidelobe level as that below the horizon of the asymmetric radiation pattern. However, the design of an asymmetric sidelobe radiation pattern is not as straightforward as symmetric one. In [28-29], Elliott was able to generate an asymmetric sidelobe aperture radiation pattern by independently specifying peak sidelobes on both sides of the Taylor aperture pattern. However, his is a special design case. Then, he has published several papers [30-34] related to the asymmetric sidelobe narrow beamwidth and shaped beam radiation patterns by adjusting the nulls of the radiation pattern using the numerical iterative method. However, skill and luck are often required in the numerical manipulations.

In this dissertation, using the analytic signal concept, we introduce a generalized theory to design the desirable asymmetric sidelobe array radiation patterns. The meaning of generalization is that this design method can be equally applied to a broadside narrow beamwidth radiation pattern and a shaped beam pattern. It will be shown that this design methodology appears to have several advantages compared to others. It is conceptually simple and straightforward. It is computationally inexpensive. It provides, for the first time, a design method, related to an asymmetric radiation pattern, which is supported by a generalized theory, implying that this design method can be analytically carried out.

One of the most widely used antenna radiation patterns is the shaped beam pattern. Various techniques have been suggested for synthesis of the shaped beam pattern [13,21,35-42]. However, the equiripple (minmax) design criterion (Dolph-Chebyshev synthesis) has never been applied to the synthesis of an asymmetric shaped beam pattern, because of the complex polynomial representation of such a pattern. In this research, by applying the analytic signal concept, we will show the feasibility of applying the equiripple design criterion to the design of asymmetric shaped beam patterns, although the realized asymmetric shaped beam patterns may not have the equiripple result because of the operation of the Hilbert transformation.

Various practical examples are chosen and simulated to demonstrate the applications and to show the feasibility of the proposed design methodology. It will be shown that the contributions of the analytic signal concept to the design of array radiation patterns are practical and valuable.

1.3 Organization of the Dissertation

In order to equally apply the analytic signal concept to the design of the linear and planar array antenna systems, Chapter II is devoted to defining the equivalent one-dimensional and two-dimensional discrete-time analytic signals by way of sampling theory and variable transformation, and to deriving the associated required mathematical tool--two-dimensional discrete-time Hilbert transforms. In Chapter III, the broadside narrow beamwidth array radiation patterns using the excitations corresponding to both theoretical and realizable analytic signals are derived and quantitatively analyzed. Several properties of the broadside narrow beamwidth radiation patterns using the analytic signal concept are discussed. In Chapter IV, the general theory and procedures for designing a broadside narrow beamwidth asymmetric sidelobe radiation patterns of an array antenna system using the analytic signal concept are derived. Examples are given to demonstrate the introduced design method and to compare the performance between the asymmetric sidelobe radiation pattern and the typical broadside symmetric radiation pattern. Chapter V extends the design concepts and modifies the design procedures presented in Chapter IV to design an asymmetric shaped beam pattern. In Chapter VI, the association of the generation of radiation patterns for a monopulse array antenna radar system with the analytic signal concept is addressed. Then, performance is analyzed and design procedure is formalized for the generation of the radiation patterns of a monopulse array antenna radar system using the analytic signal concept. Finally, conclusions are presented in Chapter VII.

CHAPTER II

THE DISCRETE-TIME ANALYTIC SIGNAL AND HILBERT TRANSFORMATION

2.1 Introduction

The fundamental properties and applications of the analog analytic signal and Hilbert transform are well developed [22-26,43-54]. The comparable one-dimensional discrete-time analytic signal and the associated Hilbert transform can be found in [55-57]. In order to apply the analytic signal concept to the planar array antenna system, the purposes of this chapter are to deduce the two-dimensional (hereafter written as 2-D) discrete-time analytic signals and to derive the associated Hilbert transforms. First, the discrete-time analytic signals will be defined for both 1-D and 2-D cases. Then, it will be shown that there are two types of 2-D discrete-time analytic signals and Hilbert transforms which provide both theoretical interest and practical usefulness, and thus will be applied in later chapters.

From the application point of view, the spectrum property of the discrete-time analytic signal, which is directly related to the radiation pattern of an array antenna system, is emphasized. There is no intention to exhaustively discuss all possible properties of such analytic signals.

2.2 Review of the One-Dimensional Analytic Signal Theory and Hilbert Transform

An analytic function[1] is defined as a function where all derivatives exist and are continuous over a region. Furthermore, a complex function $f(x+jy)=u(x,y)+jv(x,y)$ is analytic in a complex region R, if the partial derivatives of its real part $u(x,y)$ and imaginary part $v(x,y)$ are continuous over the region R and satisfy the following Cauchy-Riemann conditions [58-59]

$$\frac{\partial u}{\partial x} = \frac{\partial v}{\partial y} \qquad \text{and} \qquad \frac{\partial u}{\partial y} = - \frac{\partial v}{\partial x} \tag{2.1}$$

For a real continuous signal $z_r(t)$, an analog analytic signal $z(t)$ can be formed by [22]

$$z(t) = z_r(t) + jz_i(t) \tag{2.2}$$

where $z_i(t)$ is the analog Hilbert tranform of $z_r(t)$ and the Hilbert transform is given by

$$\begin{aligned} z_i(t) &= \hat{z}_r(t) = z_r(t) * h(t) = z_r(t) * \frac{1}{\pi t} \\ &= \frac{1}{\pi} \, p \int_c \frac{r(\xi)}{(t-\xi)} \, d\xi \end{aligned} \tag{2.3}$$

where

---

[1] Later in Definition 2.1 the term ãnalytic function (note tilde used) will be defined. The ãnalytic function is not analytic since its derivatives do not exist and, consequently, it does not satisfy the Cauchy-Riemann conditions given by (2.1).

$\hat{z}(\cdot)$ represents the Hilbert transform of $z(\cdot)$.

$*$ indicates the convolution operation.

$h(t)=(1/\pi t)$ is the impulse response of an analog Hilbert transform.

$P\int_C \langle\cdot\rangle$ denotes the Cauchy principal value.

From Equation (2.3), the Hilbert transform of a continuous signal can be obtained from the residue values evaluated on the real axis, provided that the signal is analytic (derivatives exist) over upper half complex plane. The spectrum $H(\omega)$, the Fourier transform of $h(t)$, is

$$H(\omega) = \int_{-\infty}^{\infty} h(t)e^{-j\omega t}\,dt = -j\mathrm{sgn}(\omega) \tag{2.4}$$

where

$$\mathrm{sgn}(\omega) = \begin{cases} 1 & \omega > 0. \\ -1 & \omega < 0. \end{cases} \tag{2.5}$$

It is well known that the analytic signal $z(t)$ has positive-sided spectrum (i.e. $Z(\omega)=0$ for $\omega<0$). A dual analytic signal which is formed as $z_d(t)=z_r(t)-jz_i(t)$ has negative-sided spectrum (i.e. $Z(\omega)=0$ for $\omega>0$).

In the discrete-time signals domain, the analyticity concept defined in the continuous signals will be meaningless, since the discrete-time signals are mathematically represented as sequences of numbers, and their spectra are inherently periodic. However, in order to equally share the analytic terminology in the complex discrete-time signal, we can first generate a complex discrete-time signal by sampling an analog analytic signal, then from the property of the spectrum of such a complex sampled analytic signal, a general discrete-time analytic signal and the concept of a periodic half-sided spectrum could be appropriately defined.

Let's assume a bandlimited analog analytic signal $z(t)=z_r(t)+jz_i(t)$, which has a maximum spectrum content ω_m, is sampled with an impulse (impulse sampling [60]); the sampling rate is $\omega_s=(2\pi/\Delta_t)$ and $\omega_s \geq 2\omega_m$. Δ_t is the sampling interval. The sampled analog analytic signal, denoted as $z_s(t)$, is [60]

$$z_s(t) = \sum_{k=-\infty}^{\infty} [z_r(k\Delta_t)+jz_i(k\Delta_t)]\delta(t-k\Delta_t) \tag{2.6}$$

Using the sampling theory, the spectrum $Z_s(\omega)$ of the sampled $z(t)$ is

$$Z_s(\omega) = (\omega_s/2\pi) \sum_{k=-\infty}^{\infty} Z(\omega-k\omega_s) \tag{2.7}$$

where

$$Z(\omega) = \int_{-\infty}^{\infty} z(t)e^{-j\omega t}\,dt$$

Next, by taking the Fourier transformation on both sides of Equation (2.6), an alternative spectrum representation for $z_s(t)$ is

$$Z_s(\omega) = \int_{-\infty}^{\infty} [\sum_{k=-\infty}^{\infty} \{[z_r(k\Delta_t)+jz_i(k\Delta_t)]\delta(t-k\Delta_t)\}]e^{-j\omega t}\, dt$$

$$= \sum_{k=-\infty}^{\infty} \{[z_r(k\Delta_t)+jz_i(k\Delta_t)][\int_{-\infty}^{\infty} \delta(t-k\Delta_t)e^{-j\omega t}dt]\}$$

$$= \sum_{k=-\infty}^{\infty} [z_r(k\Delta_t)+jz_i(k\Delta_t)]e^{-j\omega k\Delta_t} \tag{2.8}$$

That is, both Equation (2.7) and Equation (2.8) should represent the same spectrum of the sampled z(t), which is periodic with periodicity ω_s. Let's take a linear transformation of the variables from ω to u with $u=\omega\Delta_t$; that is, we map the spectrum from $-(\omega_s/2)$ to $(\omega_s/2)$ in ω into $-\pi$ to π in u, and the mapping procedure is periodic with ω_s in ω and 2π in u. After changing the variable, Equation (2.8) becomes

$$Z_s(u)= \sum_{k=-\infty}^{\infty} [z_r(k\Delta_t)+jz_i(k\Delta_t)]e^{-juk} \tag{2.9}$$

Now, the spectrum in Equation (2.9) is a periodic funtion of u with periodicity 2π. If the spectrum $Z(\omega)$ of the original analog analytic signal is as depicted in Figure 2.1(a), the spectrum $Z_s(\omega)$ of the sampled analog analytic signal in either

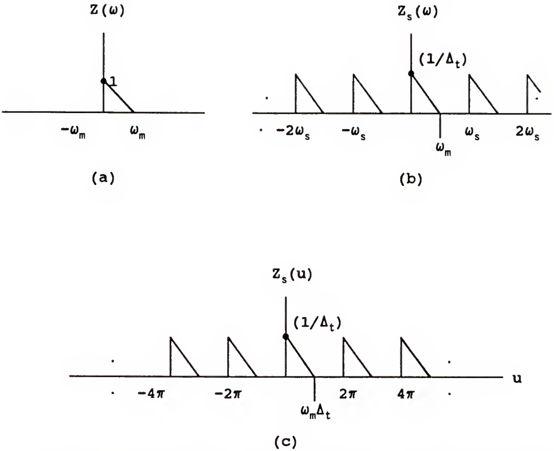

Figure 2.1 The spectrum transformation between the analog and discrete-time analytic signals.
(a) The spectrum of an analog analytic signal.
(b) The spectrum of the sampled analytic signal of (a).
(c) The spectrum of a discrete-time analytic signal transformed from (b).

Equation (2.7) or Equation (2.8) (because both of them represent the same spectrum) and the variable transformed spectrum in Equation (2.9) will be shown as in Figure 2.1(b) and Figure 2.1(c) respectively. As seen from Figure 2.1, the original single-sided bandlimited spectrum $Z(\omega)$ of an analog analytic signal is mapped into a periodic half-sided spectrum $Z_s(u)$, by ways of sampling and variable transformation. That is, the single-sided spectrum $Z(\omega)=0$ for $\omega<0$ is mapped into the periodic half-sided spectrum $Z_s(u)=0$ for $-\pi \le u<0$ of each period, provided that $\omega_s \ge 2\omega_m$.

In essence, the sampled signal $[z_r(k\Delta_t)+jz_i(k\Delta_t)]$ in Equation (2.9) will be defined as a discrete-time analytic signal. Consequently, the transformation format in Equation (2.9) can be regarded as the Fourier transform for a discrete-time signal, which is formally stated as follows.

The Fourier transformation of an absolutely summable discrete-time signal x(n) is defined as [56,p.45]

$$X(u) = \sum_{n=-\infty}^{\infty} x(n) e^{-jun} \tag{2.10}$$

Hereafter, X(u) is called the spectrum of the discrete-time signal x(n). Note that, in Equation (2.10), the function variable n is an integer and the spectrum variable u is continuous. The spectrum X(u) of a general discrete-time signal is inherently periodic with periodicity 2π. For a finite length discrete-time signal x(n) with length N, the spectrum calculated using the discrete Fourier transform (DFT) [60], where the resultant spectrum is both discrete and periodic, is the sampled version of the spectrum in Equation (2.10) with sampling period $(2\pi/N)$.

Since the spectrum is a periodic function of u, Equation (2.10) can be viewed as a Fourier series representation of X(u). According to the theory of the Fourier series, the discrete-time signal x(n) can be derived from x(u) as

$$x(n) = \frac{1}{2\pi} \int_{-\pi}^{\pi} X(u)\, e^{jun}\, du \tag{2.11}$$

Equations (2.10) and (2.11) thus form a transform pair which is commonly defined as the discrete-time Fourier transform pair, and denoted as $x(n) \leftrightarrow X(u)$. Since we are dealing with a discrete system--array antenna system, hereafter, any statement of relations between the spectrum and the discrete-time signal will be directly related to the Fourier transform pair of Equations (2.10) and (2.11).

From the illustrated periodic half-sided spectrum of the sampled analog analytic signal in Figure 2.1(c), we then could define an equivalent discrete-time analytic signal by the notion that a complex discrete-time signal which has the periodic half-sided spectrum is the discrete-time analytic signal, and neglect the analyticity requirement in the continuous case. Thus, let's formally define the periodic half-sided spectrum (due to the periodic property, we only need to explicitly define the $-\pi$ to π interval) and a discrete-time analytic signal as follows.

Definition 2.1 A spectrum X(u) of a discrete-time signal is said to be periodic half-sided, if $X(u)=0$ for $-\pi \le u < 0$, with period of 2π (refer to Figure 2.1(c)). A complex discrete-time signal $z(n)$ is defined as an ãnalytic signal, if its spectrum $Z(u)$ is periodic half-sided.[2]

After establishing the meaning of the discrete-time ãnalytic signal, the impulse response $h(n)$ of the discrete-time Hilbert transform can be derived from the spectrum property of the ãnalytic signal [56]. Let's denote the defined half-sided periodic spectrum as $Z(u)$, and its corresponding ãnalytic signal as $z(n)$. Based on the property of the discrete-time Fourier transform, $z(n)$ should be complex and can be alternatively expressed as

$$z(n) = z_r(n) + jz_i(n) \tag{2.12}$$

where both $z_r(n)$ and $z_i(n)$ are real and represent the real and imaginary part of $z(n)$, respectively. It is easily shown that $z_r(n)=[(1/2)(z(n)+z^*(n))]$ and $z_i(n)=[(-j/2)(z(n)-z^*(n))]$, where $z^*(\cdot)$ represents the complex conjugate of $z(\cdot)$. With $Z_r(u)$ and $Z_i(u)$ denoting the spectra of $z_r(n)$ and $z_i(n)$, it is straightforward to show that

$$\begin{aligned} Z_r(u) &= (1/2)[Z(u) + Z^*(-u)] \\ Z_i(u) &= (-j/2)[Z(u) - Z^*(-u)] \end{aligned} \tag{2.13}$$

---

[2] Henceforth we will use the "ãnalytic signal" (with a tilde on the first letter of the word "analytic") to denote the discrete-time analytic signal whenever it is necessary to clearly distinguish it from "analytic signal" which is used in the continuous case. Furthermore, there are two kinds of ãnalytic signals related to the positive ($X(u)=0$ for $-\pi \le u<0$) and negative (where $X(u)=0$ for $0<u<\pi$) periodic half-sided spectra.

Applying the half-sided spectrum property of Z(u), the relations among Z(u), $Z_r(u)$, $Z_i(u)$ are

$$\begin{aligned} Z(u) &= 2Z_r(u) = 2jZ_i(u) && \text{for } 0 < u < \pi \\ Z^*(-u) &= 2Z_r(u) = -2jZ_i(u) && \text{for } -\pi \le u < 0 \end{aligned} \tag{2.14}$$

Thus, from Equation (2.14), $Z_r(u)$ and $Z_i(u)$ are related as follows

$$\begin{aligned} Z_i(u) &= H(u)Z_r(u) \\ Z_r(u) &= -H(u)Z_i(u) \end{aligned} \tag{2.15}$$

where H(u) is called the discrete-time Hilbert transformer and defined as

$$H(u) = -j\,\mathrm{sgn}(u) \tag{2.16}$$

and

$$\mathrm{sgn}(u) = \begin{cases} -1 & -\pi \le u < 0. \\ 1 & 0 < u < \pi \end{cases} \tag{2.17}$$

Then, the impulse response h(n) of the discrete-time Hilbert transform is the Inverse Fourier transform of H(u) in Equation (2.16), that is

$$h(n) = \frac{1}{2\pi} \int_{-\pi}^{\pi} H(u) e^{jun}\, du$$

After a straightforward integration, h(n) becomes

$$h(n) = \begin{cases} \dfrac{1}{n\pi}(1-\cos n\pi), & \text{if } n \neq 0 \\ 0, & \text{if } n = 0 \end{cases} \tag{2.18}$$

which is odd symmetric sequence about the origin and depicted in Figure 2.2.

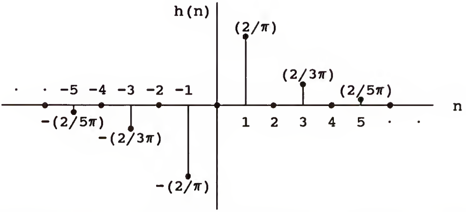

Figure 2.2 The impulse response of one-dimensional discrete-time Hilbert transform.

Using Equation (2.15), the relationship between the real and the imaginary parts of an ãnalytic signal z(n) in Equation (2.12) can be represented by the following discrete-time convolution pair,

$$z_i(n) = \sum_{k=-\infty}^{\infty} z_r(k)h(n-k) \tag{2.19}$$

$$z_r(n) = -\sum_{k=-\infty}^{\infty} z_i(k)h(n-k) \tag{2.20}$$

Equations (2.19) and (2.20) form the desired one-dimensional discrete-time Hilbert transform relations between the real and the imaginary parts of an ãnalytic signal. It should be noted that, for any real discrete-time signal, whether finite length or not, the corresponding ãnalytic signal is unrealizable since it always has an infinite sequence. This is due to the fact that the impulse response of the discrete-time Hilbert transform in Equation (2.18) is an infinite sequence. Some of the properties related to the discrete-time Hilbert transform can be found in [56], and those related to the design of the radiation pattern of an array antenna will be stated and proved later whenever it becomes necessary and appropriate.

2.3 The 2-D Discrete-Time Analytic Signal and 2-D Discrete-Time Hilbert Transform

In the 2-D signal theory, there appears to be no defined analog analytic signal, and so we could not obtain the meanning of a 2-D discrete-time ãnalytic signal from a comparable 2-D continuous analytic signal. We will, nevertheless, propose a definition, by maintaining the physical meaning and the terminologies used in the 1-D case and meeting the application requirement of finding a 2-D complex discrete-time signal whose spectrum is periodic quadrant-plane or periodic half-plane[3] as will be defined later. Consequently, we will define a 2-D complex discrete-time signal, which possesses the spectrum property, as an ãnalytic signal and derive the associated Hilbert transform which will generate the desired 2-D ãnalytic signal.

---

[3] Both quadrant-plane spectrum and half-plane spectrum are useful concepts and properties for the design of the radiation pattern of a planar array antenna system.

First, the Fourier transform of an absolutely summable 2-D discrete-time signal x(m,n) is defined as [61,p.32]

$$X(u,v)=\sum_{m=-\infty}^{\infty}\sum_{n=-\infty}^{\infty} x(m,n)\,e^{-j(um+vn)} \tag{2.21}$$

X(u,v) is called the spectrum of the 2-D discrete-time signal x(m,n). Note that the spectrum of a 2-D discrete signal is generally continuous and periodic in both spectrum variables u and v with period of 2π.

Since Equation (2.21) is similar to the Fourier series representation for X(u,v), the 2-D discrete-time signal x(m,n) can be derived from X(u,v) by using the orthogonal property of the transformation kernel (over 2π period) in Equation (2.21); that is,

$$x(m,n)=\frac{1}{4\pi^2}\int_{-\pi}^{\pi}\int_{-\pi}^{\pi} X(u,v)\,e^{j(um+vn)}\,dudv \tag{2.22}$$

Thus, Equations (2.21) and (2.22) form a transformation pair which is defined as the 2-D discrete-time Fourier transform pair, and denoted as $x(m,n) \leftrightarrow X(u,v)$.

2.3.1 The definition of 2-D discrete-time ãnalytic signals

As mentioned earlier, by maintaining the concepts used in a 1-D case and meeting the application requirement, a 2-D discrete-time ãnalytic signal can be defined. However, one generalization is formulated by requiring that the spectrum be zero over some specific region within each period of the 2-D spectrum, rather than half-side interval within each period of the spectrum in the 1-D discrete-time case. Thus, there are two 2-D discrete-time ãnalytic signals. Both of them and their associated spectra are defined as follows.

Definition 2.2 A spectrum $X(u,v)$ of a 2-D discrete-time signal is said to be periodic quadrant-plane, if $X(u,v)$ is

$$X(u,v) = 0 \qquad \text{for } (-\pi \le u < 0 \text{ or } -\pi \le v < 0)$$

with period of 2π in both u and v. A typical rectangular periodic quadrant-plane spectrum is depicted in Figure 2.3(a). Consequently, a 2-D complex discrete-time signal $z(m,n)$ is defined as a 2-D ãnalytic signal--Type I, if its spectrum $Z(u,v)$ is periodic quadrant-plane.[4]

Definition 2.3 A spectrum $X(u,v)$ of a 2-D discrete-time signal is said to be periodic half-plane, if $X(u,v)$ is

$$X(u,v) = 0 \qquad \text{for } (-\pi \le u < 0)$$

with period of 2π in both u and v. A typical rectangular periodic half-plane spectrum is depicted in Figure 2.3(b). Consequently, a complex 2-D discrete-time signal $z(m,n)$ is defined as a 2-D ãnalytic signal--Type II, if its spectrum Z(u,v) is periodic half-plane.[5]

---

[4] There are four possible 2-D Type I ãnalytic signals corresponding to the four periodic quadrant-plane spectra.

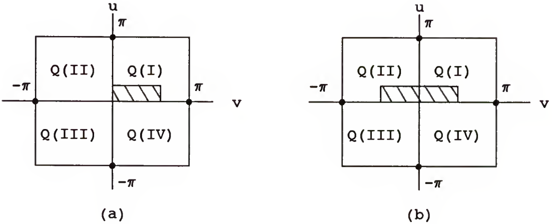

Figure 2.3 The 2-D quadrant-plane and half-plane spectra.
(a)The 2-D quadrant-plane spectrum (Type I).
(b)The 2-D half-plane spectrum (Type II).

2.3.2 The definition of 2-D discrete-time Hilbert transforms

A generalized one-dimensional discrete-time Hilbert transform which is capable of generating an ãnalytic signal with half-sided spectrum is indicated in Equation (2.19). Using the same token, a generalized 2-D discrete-time Hilbert transform of a real discrete-time signal $z_r(m,n)$ can be expressed as the following 2-D discrete-time convolution,

$$z_i(m,n) = z_r(m,n)**h(m,n)$$

$$= \sum_{\ell=-\infty}^{\infty} \sum_{k=-\infty}^{\infty} z_r(\ell,k)h(m-\ell,n-k), \text{ for } -\infty < m,n < \infty \tag{2.23}$$

---

[5] There are four possible 2-D Type II ãnalytic signals corresponding to the four periodic half-plane spectra.

where $z_i(m,n)$ denotes the 2-D discrete-time Hilbert transform of $z_r(m,n)$, $**$ represents the 2-D discrete-time convolution, and $h(m,n)$ is the impulse response of the 2-D discrete-time Hilbert transform.

Applying the 2-D discrete-time convolution theorem to Equation (2.23), the generalized spectrum relation of the Hilbert transformation is

$$Z_i(u,v) = H(u,v)Z_r(u,v) \tag{2.24}$$

where $Z_i(u,v)$, $Z_r(u,v)$ and $H(u,v)$ are the spectrums of the 2-D discrete-time signal $z_i(m,n)$, $z_r(m,n)$ and the impulse response $h(m,n)$, respectively.

However, in order to be consistent with the physical meaning of a Hilbert transformer, the 2-D discrete-time Hilbert transforms should be further restrictedly defined as follows: the 2-D discrete-time convolution in Equation (2.23) can be defined as the 2-D discrete-time Hilbert transform of the real signal $z_r(m,n)$, if the spectrum, $H(u,v)$, of the impulse response $h(m,n)$ in Equation (2.23) has the format as $H(u,v)=-j\mathrm{sgn}(u,v)$, where $\mathrm{sgn}(u,v)$ represents the 2-D version of sgn function, that is, depending on u and v, its value is always either 1 or 0 in the 2-D plane (reference to Equation (2.40)). Consequently, $z_r(m,n)$ and $z_i(m,n)$ in Equation (2.23) are said to be a 2-D discrete-time Hilbert transform pair. Based on the definition, it will be shown that there are two types of 2-D discrete-time Hilbert transforms related to the defined Type I and Type II ãnalytic signals in the 2-D case.

Having defined the 2-D ãnalytic signals and the format of 2-D discrete-time Hilbert transform, we first show that no 2-D Type I ãnalytic signal (i.e. the periodic quadrant-plane spectrum) can be derived in general using $H(u,v)=-j\mathrm{sgn}(u,v)$. However, after a complete consideration and exploration, there are three methods that can be used to generate the 2-D ãnalytic signals (either Type I or Type II) which have these desired quadrant-plane and half-plane spectra. These three methods are stated in the following cases, and their associated discrete-time Hilbert transforms will be discussed and derived in Section 2.3.4 through Section 2.3.6.

Case Ia. It is possible to obtain a 2-D Type I ãnalytic signal using two stages of transformations.

Case Ib. It is possible to obtain a 2-D Type I ãnalytic signal using two 1-D ãnalytic signals.

Case II. It is possible to obtain a 2-D Type II ãnalytic signal using a 2-D discrete-time Hilbert transform.

2.3.3 The Properties of the general expression of 2-D discrete-time Hilbert transform

Formally, we can directly derive the 2-D impulse response $h(m,n)$ from the general expression of the 2-D discrete-time Hilbert transform in Equation (2.23), and explore the general properties of the 2-D discrete-time Hilbert transform.

2.3.3.1 The impulse response of the general expression of 2-D discrete-time Hilbert transform

Let's first try to derive a generalized 2-D Hilbert transform, $h_g(m,n)$, and then examine its spectral properties where $H_g(u,v)$ is the 2-D Fourier transform of $h_g(m,n)$. The derivation of $H_g(u,v)$ can be carried out as follows: let the kernel of the 2-D discrete-time Hilbert transform in Equation (2.23) be separable (just like the separability of the kernel of the 2-D Fourier transformation); that is,

$$h_g(m-\ell,n-k)=h(m-\ell)h(n-k).$$

where h(n) is defined in Equation (2.18). Thus, the discrete convolution in Equation (2.23) becomes

$$z_i(m,n)=\sum_{\ell}\sum_{k} z_r(\ell,k)h(m-\ell)h(n-k), \quad -\infty < m,n,\ell,k < \infty \tag{2.25}$$

By taking the 2-D discrete-time Fourier transformation on both sides of Equation (2.25), the spectrum of $z_i(m,n)$, denoted as $Z_i(u,v)$, is

$$\begin{aligned} Z_i(u,v) &= \sum_{m}\sum_{n}\Big[\sum_{\ell}\sum_{k} z_r(\ell,k)h(m-\ell)h(n-k)\Big]e^{-j(um+vn)} \\ &= \sum_{\ell}\sum_{k}\Big[\sum_{m}\sum_{n} z_r(\ell,k)h(m-\ell)h(n-k)\Big]e^{-j(um+vn)} \\ &= \sum_{\ell}\sum_{k} z_r(\ell,k)\Big\{\Big[\sum_{m} h(m-\ell)e^{-jum}\Big]\Big[\sum_{n} h(n-k)e^{-jvn}\Big]\Big\} \end{aligned} \tag{2.26}$$

From Equation (2.18), the impulse response h(n) is an odd symmetric function; that is,

$$h(n-k) = h[-(k-n)] = -h(k-n)$$

Then, one of the discrete convolutions of the complex exponential e^{-jum} in Equation (2.26) becomes

$$\sum_{m} h(m-\ell)e^{-jum} = -[\sum_{m} h(\ell-m)e^{-jum}] = -[h(\ell)*e^{-ju\ell}]$$
$$= -[\sum_{m} h(m)e^{-ju(\ell-m)}] = -e^{-ju\ell}[\sum_{m} h(m)e^{jum}]$$
$$= -e^{-ju\ell}[-j\mathrm{sgn}(-u)] = -j\mathrm{sgn}(u)e^{-ju\ell} \quad (2.27)$$

where sgn(u) is defined in Equation (2.17). Using the result of Equation (2.27), the spectrum $Z_i(u,v)$ in Equation (2.26) becomes

$$Z_i(u,v)= \sum_{\ell}\sum_{k} z_r(\ell,k)[j\mathrm{sgn}(u)e^{-ju\ell}][j\mathrm{sgn}(v)e^{-jvk}]$$
$$= [-\mathrm{sgn}(u)\mathrm{sgn}(v)] \sum_{\ell}\sum_{k} z_r(\ell,k)e^{-j(u\ell+vk)}$$
$$= [-\mathrm{sgn}(u)\mathrm{sgn}(v)]Z_r(u,v) \quad (2.28)$$

where $Z_r(u,v)$ is the spectrum of $z_r(m,n)$. Comparing Equations (2.24) and (2.28), the spectrum of the generalized 2-D discrete-time impulse response, denoted as $H_g(u,v)$, is

$$H_g(u,v) = [-\mathrm{sgn}(u)\mathrm{sgn}(v)] \quad (2.29)$$

Then, by taking the 2-D discrete-time inverse Fourier transform of $H_g(u,v)$ in Equation (2.29), the 2-D discrete-time impulse response, denoted as $h_g(m,n)$, is

$$h_g(m,n) = \frac{1}{4\pi^2}\int_{-\pi}^{\pi}\int_{-\pi}^{\pi}[-\mathrm{sgn}(u)\,\mathrm{sgn}(v)]\,e^{j(um+vn)}\,du\,dv$$

After some mathematical manipulation, $h_g(m,n)$ becomes

$$h_g(m,n) = \begin{cases} 0, & \text{for } m=n=0 \text{ or } m=o \text{ or } n=0. \\ \dfrac{1}{(mn)\pi^2}\,[\cos(m\pi)\cos(n\pi)-\cos(m\pi)-\cos(n\pi)+1], & \text{elsewhere.} \end{cases} \qquad (2.30)$$

Examining the values of $h_g(m,n)$ for all possible combinations of m and n in Equation (2.30), $h_g(m,n)$ becomes

$$h_g(m,n) = \begin{cases} \dfrac{4}{(mn)\pi^2}, & \text{both m and n are odd} \\ 0, & \text{elsewhere} \end{cases} \qquad (2.31)$$

From Equation (2.31), the 2-D impulse response derived from the general expression of 2-D discrete-time Hilbert transform has cross-quadrant even symmetry and adjacent-quadrant odd symmetry. The impulse response $h_g(m,n)$ and the spectrum of a uniformly truncated version of $h_g(m,n)$ (where the lengths of both m and n are 11) are plotted in Figure 2.4(a) and (b).

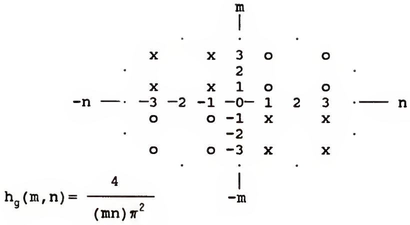

$$h_g(m,n) = \frac{4}{(mn)\pi^2}$$

o:positive value, x:negative value, otherwise, zero value.

(a)

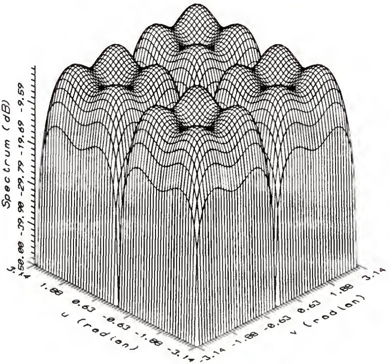

(b)

Figure 2.4 The impulse response and spectrum of $h_g(m,n)$.
(a)The impulse response $h_g(m,n)$.
(b)The spectrum of uniformly truncated version of (a). (M=N=11)

2.3.3.2 The properties of the transformation using impulse response $h_g(m,n)$

Using the impulse response $h_g(m,n)$ in Equation (2.31), a 2-D complex discrete-time signal $z(m,n)$ can be formed as

$$z(m,n) = z_r(m,n) + jz_i(m,n) \tag{2.32}$$

where $z_r(m,n)$ is a real 2-D discrete-time signal and $z_i(m,n)=[z_r(m,n)**h_g(m,n)]$. From Equation (2.28), the spectrum of $z_i(m,n)$, denoted as $Z_i(u,v)$, is

$$Z_i(u,v) = (-1)\mathrm{sgn}(u)\mathrm{sgn}(v)Z_r(u,v)$$

Thus, the spectrum of the $z(m,n)$ in Equation (2.32), denoted as $Z(u,v)$, becomes

$$\begin{aligned} Z(u,v) &= Z_r(u,v) - j[\mathrm{sgn}(u)\mathrm{sgn}(v)Z_r(u,v)] \\ &= Z_r(u,v)[1 - j\mathrm{sgn}(u)\mathrm{sgn}(v)] \end{aligned} \tag{2.33}$$

The result shown in Equation (2.33) indicates that the spectrum of the 2-D complex discrete-time signal in Equation (2.32), which is formed by using the impulse response $h_g(m,n)$, does not possess the previously defined quadrant-plane or half-plane spectrum, and consequently, the complex signal $z(m,n)$ in Equation (2.32) is not a 2-D ãnalytic signal.

Again, using $z_r(m,n)$ and $z_i(m,n)$ in Equation (2.32), let's form another 2-D discrete-time signal as

$$\begin{aligned} z(m,n) &= z_r(m,n) + (j)^2z_i(m,n) \\ &= z_r(m,n) - z_i(m,n) \end{aligned} \tag{2.34}$$

Note that z(m,n) becomes a real 2-D discrete-time signal, and consequently, is not an ãnalytic signal. However, it is easy to show that the spectrum of z(m,n) in Equation (2.34), denoted as Z(u,v), is

$$\begin{aligned} Z(u,v) &= Z_r(u,v) + \mathrm{sgn}(u)\mathrm{sgn}(v)Z_r(u,v) \\ &= Z_r(u,v)[1+\mathrm{sgn}(u)\mathrm{sgn}(v)] \end{aligned}$$

that is,

$$Z(u,v) = \begin{cases} 2Z_r(u,v), & \text{for } (-\pi \le u < 0 \text{ and } -\pi \le v < 0) \text{ or } \\ & \quad (0 < u < \pi \text{ and } 0 < v < \pi) \\ Z_r(u,v), & \text{for } (u=v=0 \text{ or } u=0 \text{ or } v=0) \\ 0, & \text{otherwise} \end{cases} \qquad (2.35)$$

which is a cross-quadrant spectrum (spectrum vanishes in both Quadrant II and IV). We will define this cross-quadrant spectrum as a Type III spectrum.

It needs to be pointed out that the 2-D signal pair $z_r(m,n)$ and $z_i(m,n)$ in either Equation (2.32) or Equation (2.34) never forms a 2-D discrete-time Hilbert transform pair. This is because the spectrum, $H_g(u,v)$, of the 2-D impulse response $h_g(m,n)$ in Equation (2.31) is not consistent with the format of H(u,v)=-jsgn(u,v) for the 2-D discrete-time Hilbert transform which was defined in Section 2.3.2. Thus, based on the separable assumption, derivation and discussion above, we can establish a conclusion in Lemma 2.1

Lemma 2.1 In the 2-D signal domain, there is no generalized 2-D discrete-time Hilbert transform which can produce a 2-D ãnalytic signal, whose spectrum is quadrant-plane. However, the 2-D impulse response which is derived from the general expression of the 2-D discrete-time Hilbert transform is capable of generating a 2-D real discrete-time signal, whose spectrum is cross-quadrant (i.e. Type III).

2.3.4 The generation of a 2-D ãnalytic signal--Type I using two stages of transformations (Case Ia)

According to Lemma 2.1, given a general real 2-D discrete-time signal, the 2-D impulse response in Equation (2.31) is capable of generating another real 2-D discrete-time signal whose spectrum is cross-quadrant (Type III). The purposes of this section are to derive a 2-D discrete-time Hilbert transform (Type I), so that a 2-D ãnalytic signal with quadrant-plane spectrum--Type I can be obtained from a special real 2-D discrete-time signal whose spectrum is cross-quadrant (Type III), and to devise a two-stage transformation, so that a 2-D ãnalytic signal with quadrant-plane spectrum--Type I can be obtained from a general real 2-D discrete-time signal.

2.3.4.1 The 2-D discrete-time Hilbert transform (Type I)

Consider a special case where a 2-D real discrete-time signal $z_{rr}(m,n)$ has a cross-quadrant spectrum (Type III) which is denoted as $Z_{rr}(u,v)$; that is,

$$Z_{rr}(u,v)=\sum_{m}\sum_{n} z_{rr}(m,n)\,e^{-j(um+vn)} = 0,$$

$$\text{for } (0 < u < \pi \text{ and } -\pi \le v < 0)$$
$$\text{or } (-\pi \le u < 0 \text{ and } 0 < v < \pi$$

Then, let's form a complex signal $z(m,n)$ whose real part is $z_{rr}(m,n)$; that is, $z(m,n)= z_{rr}(m,n)+j\ z_{ii}(m,n)$. Now, we want to deduce a 2-D discrete-time Hilbert transform (Type I) which is capable of generating $z_{ii}(m,n)$ from $z_{rr}(m,n)$, such that the spectrum of the complex signal $z(m,n)$, denoted as $Z(u,v)$, is a quadrant-plane; that is,

$$Z(u,v) = 0, \quad \text{for } (-\pi \le u < 0 \ \text{ or } \ -\pi \le v < 0) \qquad (2.36)$$

Since $z(m,n)=z_{rr}(m,n)+jz_{ii}(m,n)$, it is true that

$$z_{rr}(m,n) = (1/2)[z(m,n)+z^*(m,n)]$$
$$jz_{ii}(m,n) = (1/2)[z(m,n)-z^*(m,n)]$$

where $z^*(\cdot,\cdot)$ is the complex conjugate of $z(\cdot,\cdot)$. With $Z_{rr}(u,v)$ and $Z_{ii}(u,v)$ denoting the spectra of $z_{rr}(m,n)$ and $z_{ii}(m,n)$, it can be shown that

$$Z_{rr}(u,v) = (1/2)[Z(u,v) + Z^*(-u,-v)]$$
$$jZ_{ii}(u,v) = (1/2)[Z(u,v) - Z^*(-u,-v)]$$

Let's presume that the cross-quadrant spectrum property of $Z(u,v)$ in Equation (2.36) is valid. Then the relations among $Z(u,v)$, $Z_{rr}(u,v)$ and $Z_{ii}(u,v)$ are

$$Z(u,v)= 2Z_{rr}(u,v)= 2jZ_{ii}(u,v), \quad (0 \le u < \pi \text{ and } 0 < v < \pi) \ (\text{except } u=v=0)$$

$$Z^*(-u,-v)=2Z_{rr}(u,v)=-2jZ_{ii}(u,v), (-\pi \le u \le 0 \text{ and } -\pi\le v\le 0) \ (\text{except } u=v=0) \qquad (2.37)$$

Thus, from Equation (2.37), the $Z_{rr}(u,v)$ and $Z_{ii}(u,v)$ should be related as follows

$$Z_{ii}(u,v) = H_I(u,v)Z_{rr}(u,v)$$
$$Z_{rr}(u,v) = -H_I(u,v)Z_{ii}(u,v) \qquad (2.38)$$

where

$$H_I(u,v) = -j\mathrm{sgn}_I(u,v) \qquad (2.39)$$

and

$$\mathrm{sgn}_I(u,v) = \left[\begin{array}{ll} 1 & 0 \le u < \pi \text{ and } 0 \le v < \pi \\ -1 & -\pi \le u \le 0 \text{ and } -\pi \le v \le 0 \\ 0 & u=v=0 \text{ and elsewhere} \end{array}\right. \qquad (2.40)$$

Then the impulse response of the 2-D discrete-time Hilbert transform (Type I), denoted as $h_I(m,n)$, can be obtained by taking the 2-D discrete-time inverse Fourier transform of $H_I(u,v)$ in Equation (2.39),

$$h_I(m,n) = \frac{1}{4\pi^2}\left\{\int_{-\pi}^{0}\int_{-\pi}^{0} je^{j(um+vn)}\,dudv - \int_{0}^{\pi}\int_{0}^{\pi} je^{j(um+vn)}\,dudv\right\}$$

After taking the integration with all possible combinations of m and n, the impulse response $h_I(m,n)$ is

$$h_I(m,n) = \begin{cases} \dfrac{1-\cos(n\pi)}{2n\pi}, & m = 0 \text{ and } n \neq 0 \\ \dfrac{1-\cos(m\pi)}{2m\pi}, & n = 0 \text{ and } m \neq 0 \\ 0, & \text{otherwise} \end{cases} \tag{2.41}$$

The impulse response $h_I(m,n)$ in Equation (2.41) and the spectrum $H_I(u,v)$ of a uniformly truncated version (the lengths of both m and n are 11) of $h_I(m,n)$ are plotted in Figure 2.5(a) and (b).

From Equation (2.38), the relations between $z_{rr}(m,n)$ and $z_{ii}(m,n)$ are

$$\begin{aligned} z_{ii}(m,n) &= z_{rr}(m,n)**h_I(m,n) \\ z_{rr}(m,n) &= -z_{ii}(m,n)**h_I(m,n) \end{aligned} \tag{2.42}$$

It is straightforward to prove that if the real signal $z_{rr}(m,n)$ has cross-quadrant spectrum (Type III), then the 2-D complex signal $z(m,n)=z_{rr}(m,n)+jz_{ii}(m,n)$ has quadrant-plane spectrum (Type I). Thus, $h_I(m,n)$ in Equation (2.41) is the desired impulse response for the 2-D discrete-time Hilbert transform (Type I). Furthermore, by definition, the 2-D discrete-time convolution in Equation (2.42) forms the desired 2-D discrete-time Hilbert transform relations (Type I) between the signal pair $z_{rr}(m,n)$ and $z_{ii}(m,n)$.

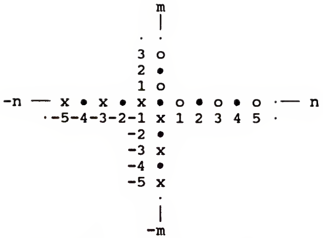

$$h_I(m) = \frac{1}{m\pi}, \quad h_I(n) = \frac{1}{n\pi}$$

o:positive value, x:negative value, otherwise, zero value.

(a)

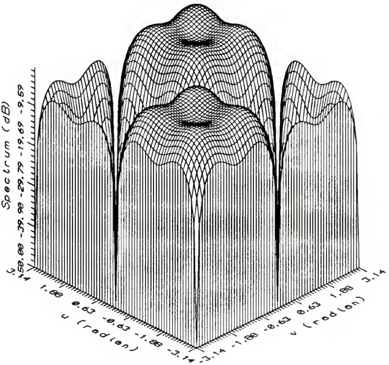

(b)

Figure 2.5 The 2-D discrete-time Hilbert transform (Type I).
(a)The impulse response $h_I(m,n)$.
(b)The spectrum of uniformly truncated version of (a). (M=N=11)

2.3.4.2 The generation of a 2-D ãnalytic signal--Type I

After deriving the two required 2-D transformations in Section 2.3.3 and Section 2.3.4.1, the two-stage transformation and the procedures used to produce a 2-D ãnalytic signal with quadrant-plane spectrum (Type I) from a real 2-D signal $z_r(m,n)$ can be depicted in Figure 2.6.

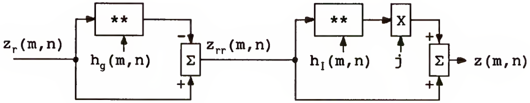

Σ:Summation
X:Multiplication
**:2-D discrete-time convolution

Figure 2.6 A general 2-D ãnalytic signal--Type I generator.

In Figure 2.6, $h_g(m,n)$ and $h_I(m,n)$ denote the 2-D impulse responses in Equation (2.31) and Equation (2.41). $z_r(m,n)$ is a real 2-D discrete-time signal, and the 2-D signal $z_{rr}(m,n)$ is formed as

$$z_{rr}(m,n) = z_r(m,n) - [z_r(m,n)**h_g(m,n)] \qquad (2.43)$$

According to Equation (2.34) and (2.35), the spectrum of $z_{rr}(m,n)$, denoted as $Z_{rr}(u,v)$, is cross-quadrant; that is,

$$Z_{rr}(u,v) = \begin{cases} 2Z_r(u,v), & \text{for } (-\pi \le u < 0 \text{ and } -\pi \le v < 0) \text{ or} \\ & \quad (0 < u < \pi \text{ and } 0 < v < \pi) \\ Z_r(u,v), & \text{for } (u=v=0 \text{ or } u=0 \text{ or } v=0) \\ 0, & \text{otherwise} \end{cases} \qquad (2.44)$$

where $Z_r(u,v)$ is the spectrum of $z_r(m,n)$. Note that $z_{rr}(m,n)$ is a real 2-D signal and has cross-quadrant spectrum $Z_{rr}(u,v)$. Finally, $z(m,n)$, the output at the second stage, can be expressed as

$$z(m,n) = z_{rr}(m,n) + j[z_{rr}(m,n)**h_I(m,n)] \tag{2.45}$$

The spectrum of $z(m,n)$, denoted as $Z(u,v)$, is

$$Z(u,v) = Z_{rr}(u,v) + j[Z_{rr}(u,v)H_I(u,v)] \tag{2.46}$$

where $H_I(u,v)$ is the spectrum of the impulse response $h_I(m,n)$ in Equation (2.41). After applying the spectrum property of $H_I(u,v)$ in Equation (2.39), the spectrum $Z(u,v)$ in Equation (2.46) becomes

$$Z(u,v) = \begin{cases} 4Z_r(u,v), & (0 < u < \pi \text{ and } 0 < v < \pi) \\ 2Z_r(u,v), & (u=v=0) \text{ or } (u=0 \text{ and } 0 < v < \pi) \\ & \text{or } (v=0 \text{ and } 0 < u < \pi) \\ 0\ , & \text{otherwise} \end{cases} \tag{2.47}$$

Because $z_r(m,n)$ is assumed to be real, $z_{rr}(m,n)$ is also real, and consequently $z(m,n)$ in Equation (2.45) is complex. Since $z(m,n)$ is complex and has the quadrant-plane spectrum (Type I), by definition, it is a 2-D ãnalytic signal--Type I corresponding to a general real signal $z_r(m,n)$. Thus, we have Lemma 2.2 which is stated as follows.

Lemma 2.2 In a 2-D signal domain, a 2-D ãnalytic signal, whose spectrum is the quadrant-plane (Type I) of a 2-D real discrete-time signal, can be generated by using two stages of transformations. (Refer to Figure 2.6)

2.3.5 The generation of a 2-D ãnalytic signal--Type I using two 1-D ãnalytic signals (Case Ib)

It is also possible to obtain the desired 2-D ãnalytic signal--Type I using two one dimensional ãnalytic signals. Let's assume a 2-D complex discrete-time signal z(m,n) is separable, that is z(m,n)=z(m)z(n), where z(m) and z(n) are two 1-D complex signals. We want to show that if both z(m) and z(n) are ãnalytic, then z(m,n) is also a 2-D ãnalytic signal with the defined quadrant-plane spectrum (Type I). The 2-D complex signal z(m,n) can be alternatively expressed as

$$\begin{aligned} z(m,n) &= z(m)\ z(n) \\ &= [z_r(m) + jz_i(m)][z_r(n) + jz_i(n)] \\ &= [z_r(m)z_r(n) - z_i(m)z_i(n)] \\ &\quad +j[z_r(m)z_i(n) + z_r(n)z_i(m)] \end{aligned} \tag{2.48}$$

where $z_r(\cdot)$ and $z_i(\cdot)$ represent the real and imaginary parts of $z(\cdot)$, both of them are real and $z_i(\cdot)$ is the discrete-time Hilbert transform of $z_r(\cdot)$. Since both $z_r(\cdot)$ and $z_i(\cdot)$ are real, the 2-D signal z(m,n) in Equation (2.48) is complex. Furthermore, by using the spectrum relations between the real and imaginary part of a 1-D ãnalytic signal in Equation (2.15), it is straightforward to show that the spectrum of z(m,n) in Equation (2.48), denoted as Z(u,v), is

$$\begin{aligned} Z(u,v) &= Z_r(u)Z_r(v) - [-j\mathrm{sgn}(u)Z_r(u)][-j\mathrm{sgn}(v)Z_r(v)] \\ &\quad +j[-j\mathrm{sgn}(v)Z_r(v)Z_r(u)] + j[-j\mathrm{sgn}(u)Z_r(u)Z_r(v)] \\ &= Z_r(u)Z_r(v)[1 + \mathrm{sgn}(u)\mathrm{sgn}(v) + \mathrm{sgn}(u) + \mathrm{sgn}(v)] \end{aligned}$$

that is,

$$Z(u,v) = \begin{cases} 4Z_r(u)Z_r(v), & \text{for } (0 < u < \pi \text{ and } 0 < v < \pi) \\ 2Z_r(u)Z_r(v), & \text{for } (u=0 \text{ and } 0 < v < \pi) \text{ or} \\ & \quad (v=0 \text{ and } 0 < u < \pi) \\ Z_r(u)Z_r(v), & \text{for } u=v=0 \\ 0, & \text{otherwise} \end{cases} \tag{2.49}$$

which is quadrant-plane spectrum. Since the 2-D discrete-time signal z(m,n) in Equation (2.48) is complex and has quadrant-plane spectrum (Type I), by definition, it is a 2-D ãnalytic signal--Type I.

The above derivation also shows that a 2-D separable ãnalytic signal--Type I can be generated by using 1-D discrete-time Hilbert transform, and thus leads to Lemma 2.3, the main result in this section.

Lemma 2.3 A complex 2-D discrete-time signal formed by the product of two 1-D ãnalytic signals is also ãnalytic, and consequently has a periodic quadrant-plane spectrum (Type I).

2.3.6 The generation of a 2-D ãnalytic signal--Type II using 2-D discrete-time Hilbert transform (Type II) (Case II)

Theoretically, the concept and procedures of deducing the 2-D discrete-time Hilbert transform (Type II) used to generate the desired ãnalytic signal with a half-plane spectrum (Type II) are similar to those used to deduce the discrete-time Hilbert tansform (Type I) in Section 2.3.4.1. Thus referring to Figure 2.3(b), by definition the spectrum of the 2-D ãnalytic signal--Type II, denoted as Z(u,v), is

$$Z(u,v) = 0, \qquad \text{for } (-\pi \le u < 0) \qquad (2.50)$$

Let's denote the 2-D discrete-time signal corresponding to $Z(u,v)$ as $z(m,n)$ which must be complex, due to the asymmetric property of $Z(u,v)$. Thus, $z(m,n)$ can be represented by its real and imaginary parts, that is, $z(m,n)= z_r(m,n)+jz_i(m,n)$, where both $z_r(m,n)$ and $z_i(m,n)$ are real. It can be shown that

$$z_r(m,n) = (1/2)[z(m,n)+z^*(m,n)]$$
$$jz_i(m,n) = (1/2)[z(m,n)-z^*(m,n)]$$

where $z^*(\cdot,\cdot)$ is the complex conjugate of $z(\cdot,\cdot)$. With $Z_r(u,v)$ and $Z_i(u,v)$ denoting the spectra of $z_r(m,n)$ and $z_i(m,n)$, it is easy to show that

$$Z_r(u,v) = (1/2)[Z(u,v) + Z^*(-u,-v)]$$
$$jZ_i(u,v) = (1/2)[Z(u,v) - Z^*(-u,-v)]$$

Using the periodic half-plane spectrum property of $Z(u,v)$, the relations among $Z(u,v)$, $Z_r(u,v)$ and $Z_i(u,v)$ are

$$Z(u,v) = 2Z_r(u,v) = 2jZ_i(u,v), \quad \text{for } (0 < u < \pi)$$
$$Z^*(-u,-v)=2Z_r(u,v)=-2jZ_i(u,v), \quad \text{for } (-\pi \le u < 0) \qquad (2.51)$$

Thus, from Equation (2.51), $Z_r(u,v)$ and $Z_i(u,v)$ are related as follows

$$Z_i(u,v) = H_{II}(u,v)Z_r(u,v)$$
$$Z_r(u,v) = -H_{II}(u,v)Z_i(u,v) \qquad (2.52)$$

where

$$H_{II}(u,v) = -j\,\mathrm{sgn}_{II}(u,v) \tag{2.53}$$

and

$$\mathrm{sgn}_{II}(u,v) = \left[\begin{array}{ll} 1 & (0 < u < \pi) \text{ and } (-\pi \le v < \pi) \\ -1 & (-\pi \le u < 0) \text{ and } (-\pi \le v < \pi) \end{array}\right. \tag{2.54}$$

The impulse response $h_{II}(m,n)$ corresponding to $H_{II}(u,v)$ can be obtained by carrying out the 2-D discrete-time inverse Fourier transformation of $H_{II}(u,v)$ in Equation (2.53); that is,

$$h_{II}(m,n) = \frac{1}{4\pi^2}\left\{\int_{-\pi}^{0}\int_{-\pi}^{\pi} j\, e^{j(um+vn)}\,dudv - \int_{0}^{\pi}\int_{-\pi}^{\pi} j\, e^{j(um+vn)}\,dudv\right\}$$

After taking the integration with all possible combinations of m and n, $h_{II}(m,n)$ is found to be

$$h_{II}(m,n) = \left[\begin{array}{ll} \dfrac{1-\cos(m\pi)}{m\pi}, & n = 0 \text{ and } m \neq 0 \\ 0, & \text{otherwise} \end{array}\right. \tag{2.55}$$

Again, the 2-D impulse response $h_{II}(m,n)$ in Equation (2.55) and the spectrum of a uniformly truncated version of $h_{II}(m,n)$ (the lengths of both m and n are 11) are shown in Figure 2.7(a) and (b).

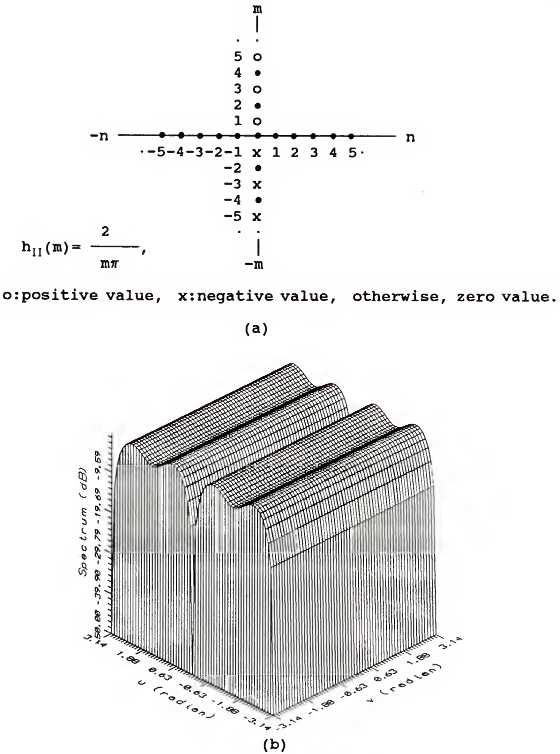

Figure 2.7 The 2-D discrete-time Hilbert transform (Type II).
(a) The impulse response $h_{II}(m,n)$.
(b) The spectrum of uniformly truncated version of (a). (M=N=11)

After deriving the 2-D impulse response $h_{II}(m,n)$ of the 2-D discrete-time Hilbert transform (Type II), it is easy to show that, for an arbitrary real 2-D discrete-time signal $z_r(m,n)$, the 2-D complex signal $z(m,n)=z_r(m,n)+jz_i(m,n)$ has a half-plane spectrum. Thus, by definition, $z(m,n)$ is a 2-D ãnalytic signal--Type II which can be generated by using the 2-D discrete-time Hilbert transform (Type II).

Furthermore, according to Equation (2.52), the desired discrete-time Hilbert transform relations (Type II) between the real and imaginary part of a Type II ãnalytic signal can be expressed as

$$\begin{aligned} z_i(m,n) &= z_r(m,n)**h_{II}(m,n) \\ z_r(m,n) &= -z_i(m,n)**h_{II}(m,n) \end{aligned} \qquad (2.56)$$

It should be noted that based on the property of the 2-D impulse response $h_{II}(m,n)$ in Equation (2.55), the discrete-time Hilbert transform relations (Type II) in Equation (2.56) can be simplified as a 1-D discrete-time convolution, that is

$$\begin{aligned} z_i(m,n) &= \sum_k z_r(k,n)h_{II}(m-k) \\ z_r(m,n) &= -\sum_k z_i(k,n)h_{II}(m-k) \end{aligned} \qquad (2.57)$$

2.4 Summary

From the application point of view, the 2-D discrete-time ãnalytic signals and their associated discrete-time Hilbert transforms have been discussed and derived in this chapter.

The derivation procedures can be extended to continuous as well as multi-dimensioned signals. However, in order to compatible with the planar array antenna system, only the 2-D case is emphasized. It was found that it is possible to obtain the quadrant-plane spectrum (Type I) of a real 2-D discrete-time signal by using two stages of transformations. If the original 2-D signal is separable, it was found that the 2-D ãnalytic signal--Type I can be obtained from the product of the associated 1-D ãnalytic signal. Furthermore, a technique was developed to obtain 2-D ãnalytic signal with half-plane spectrum (Type II). As far as application is concerned, these concepts of the ãnalytic signals and the associated half-sided, quadrant-plane and half-plane spectra will provide an important contribution to the area in the design of the radiation patterns of an array antenna system.

CHAPTER III

ANALYSIS OF BROADSIDE NARROW BEAMWIDTH ARRAY RADIATION PATTERNS USING ANALYTIC EXCITATIONS

3.1 Introduction

Having defined the discrete-time analytic signals and derived the required mathematical tool - discrete-time Hilbert transforms, we will fully analyze the utilization of the ãnalytic excitation[1] for an array antenna system. To do so, we first show the discrete-time Fourier transform relations between the radiation pattern and its element's excitation of an array antenna system. It is this relationship that shows why the concept of the ãnalytic signal theory is applicable to the design of the array antenna radiation pattern. Then, the performance of a narrow beamwidth radiation pattern using an ãnalytic excitation which is directly corresponding to an even symmetric broadside array excitation is analyzed. The analysis procedures will be divided into two steps. In the first step, the attractive properties of the array antenna radiation pattern using an ãnalytic excitation are illustrated. These attractive properties stimulate the idea using the ãnalytic excitation in the design of the array antenna radiation patterns. In the second step, the performance of radiation patterns using a realizable ãnalytic excitation is quantitatively analyzed. From there, several properties related to this new realization technique are extracted. The properties are useful and essential for designing several array antenna radiation patterns that will be developed in the next chapters.

---

[1] The "ãnalytic signal" mentioned in Chapter II will be replaced by "ãnalytic excitation" whenever the signal is the excitation of an array antenna system.

3.2 Fundamentals of an Array Antenna Theory

This section begins with a description of a generalized far field radiation pattern of an Array Antenna System. Two basic but important array structures, linear and rectangular grid planar array antennas, will be studied in this dissertation. Consequently, the discrete-time Fourier transform relations between the far field radiation pattern and its element's excitation will be shown.

3.2.1 The generalized structure of an array antenna system

Generally, the phasor for a spherical wave that propagates along a radially outward direction can be expressed as [3]

$$E(r,\theta,\phi) = [A(\theta,\phi)/r]e^{-jkr} \qquad (3.1)$$

Where $A(\theta,\phi)$ is the complex amplitude of the propagated wave, $k=(2\pi/\lambda)$ is the wave number, λ is the wavelength of the propagated wave, r is the distance between the radiation source and the observation point in the space, and (1/r) is the expression for the law of energy conservation. The actual waveform is $e(t)=Re\ [E(r,\theta,\phi)e^{j(\omega_c t)}]$, this representation assumes that the propagated waveform is a temporal narrow band signal, and to shorten the notation the temporal variation is omitted in the wave function of Equation (3.1). Two propagated waves with same temporal frequency may be summed so that they combine or interfere with each other, and it is this principle that forms the array antenna radiation pattern.

An antenna array is a collection of a specific spatial distribution of several identical and similarly oriented radiation elements, and can be considered as the sampled version of an aperture antenna. An array antenna with N arbitrary elements is described in Figure 3.1, where one of the elements, the n^{th} element, is explicitly shown.

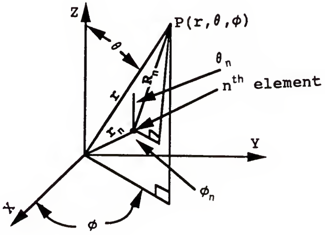

Figure 3.1 A generalized geometrical structure of an array antenna system.

In Figure 3.1, a phase reference is assumed to be the coordinate origin. The position vector of the nth array element with respective to the phase origin is $\mathbf{r}_n$

$$\mathbf{r}_n = x_n\mathbf{x}_o + y_n\mathbf{y}_o + z_n\mathbf{z}_o$$

where the boldface letter represents a vector,[2] $\mathbf{x}_o$, $\mathbf{y}_o$ and $\mathbf{z}_o$ are unit vectors in the x, y, and z direction respectively. The far electromagnetic field that launched from this nth element, according to Equation (3.1), is proportional to [3]

$$E_n = \{[J(n)\ f_n(\theta_n,\phi_n)]/R_n\}e^{-jkR_n} \tag{3.2}$$

where $J(n)$ and $f_n(\theta_n,\phi_n)$ are the complex current excitation and the far field pattern of the nth array element respectively, and R_n is the distance between the nth array element and the observation point P. Let's assume that all individual elements have the same radiation pattern, denoted as $f(\theta,\phi)$, and they are distributed within a volume with radius a, which is much smaller than the distance, r, from the phase reference to the observation point ($a \ll r$). This assumption,[3] by using the Taylor series expansion, assures a good approximation [3], $(1/R_n) \approx (1/r)$, $\theta_n \approx \theta$, $\phi_n \approx \phi$, and

---

[2] Hereafter, the boldface denotes a vector. Thus, $\mathbf{r}_n$ is a vector, and r_n is a scalar quantity.

[3] For the far field radiation pattern, this assumption is always valid. Generally, the distance, r, shall be equal to or greater than $(2d^2/\lambda)$ to be considered as the far field region, where d is the size of measurement device in the far field observation point. In the far field region, a spherical wave can be locally represented as a plane wave, and thus simplify many propagated wave analysis problems.

$$\begin{aligned} e^{-jkR_n} &\approx e^{-jkr}\, e^{jk(x_n\sin\theta\cos\phi\, +\, y_n\sin\theta\sin\phi\, +\, z_n\cos\theta)} \\ &\approx e^{-jkr}\, e^{jk(\mathbf{r}_u\cdot\mathbf{r}_n)} \end{aligned}$$

where $\mathbf{r}_u$ is the normalized unit vector along the r direction, which is defined as

$$\mathbf{r}_u = \left[\frac{\mathbf{r}}{|\mathbf{r}|}\right] = \sin\theta\cos\phi\mathbf{x}_o + \sin\theta\sin\phi\mathbf{y}_o + \cos\theta\mathbf{z}_o$$

$(\mathbf{r}_u\cdot\mathbf{r}_n)$ represents the inner product of $\mathbf{r}_u$ and $\mathbf{r}_n$, and $k(\mathbf{r}_u\cdot\mathbf{r}_n)$ is the measurement of the phase difference between the phase reference and the n^{th} element as measured along the $\mathbf{r}_u$ direction. Then, by virtue of the superposition principle, the total far field strength of an array antenna, denoted as $E_s(r,\theta,\phi)$, is proportional to [3]

$$E_s(r,\theta,\phi) = (e^{-jkr}/r)f(\theta,\phi)\left[\sum_{n=1}^{N} J(n)e^{jk(\mathbf{r}_u\cdot\mathbf{r}_n)}\right] \tag{3.3}$$

where $J(n)$ is the normalized complex excitation of n^{th} array element, and the component in the bracket of the right-hand side, denoted as $A(\theta,\phi)$,

$$A(\theta,\phi) = \left[\sum_{n} J(n)e^{jk(\mathbf{r}_n\cdot\mathbf{r}_n)}\right] \tag{3.4}$$

is usually called the array factor or space factor, because it depends on the geometrical structure in the array system, for given a specified set of excitation $\{J(n)\}$ and the number of array elements N.

As mentioned earlier, the factor (e^{-jkr}/r) in Equation (3.3) is the expression for the law of energy conservation and the phase reference and is not a function of direction. In antenna theory, the far field radiation pattern $F(\theta,\phi)$ of an array antenna system, which is defined as the function of direction only, is identified with the multiplicative of the element factor $f(\theta,\phi)$ and the array factor $A(\theta,\phi)$ in Equation (3.4);[4] that is,

$$F(\theta,\phi) = f(\theta,\phi)\left[\sum_{n=1}^{N} J(n)e^{jk(\mathbf{r}_u \cdot \mathbf{r}_n)}\right] \qquad (3.5)$$

The objective of this research is to apply a complex excitation so that the far field radiation patterns are obtained. We shall not deal with the problems related to designing the element factor, $f(\theta,\phi)$, for the individual radiation elements. Hence, without loss of any generality, an isotropical element factor is assumed and consequently, the array factor $A(\theta,\phi)$ and the array radiation pattern $F(\theta,\phi)$ are assumed to be interchangable throughout this dissertation.

In general, a linear phase gradient is fed along with the individual array element, such that the mainbeam of the narrow beamwidth radiation pattern can be steered at a specific direction (θ_o,ϕ_o). Mathematically, the normalized steering vector in the (θ_o,ϕ_o) direction, denoted as $\mathbf{r}_s$, can be expressed as

---

[4] This is the well-known principle of the pattern multiplication of an array antenna system.

$$\mathbf{r}_s = \sin\theta_0\cos\phi_0\mathbf{x}_0 + \sin\theta_0\sin\phi_0\mathbf{y}_0 + \cos\theta_0\mathbf{z}_0 \qquad (3.6)$$

Then, the required phase gradient on each array element can be obtained by k times the inner product of $\mathbf{r}_s$ and $\mathbf{r}_n$, and the generalized far field radiation pattern (strictly speaking, the array factor) of an N elements array antenna becomes

$$F(\theta,\phi) = \sum_{n=1}^{N} J(n)\, e^{jk[(\mathbf{r}_u\cdot\mathbf{r}_n)-(\mathbf{r}_s\cdot\mathbf{r}_n)]} \qquad (3.7)$$

Two specific array antenna structures, the linear and the planar rectangular grid array systems are used to illustrate the principle of the general array antenna theory. For some other structures, the reader can refer to [3].

3.2.2 The linear array antenna system

A typical linear array antenna which consists of N linearly oriented array elements along z axis is depicted in Figure 3.2.

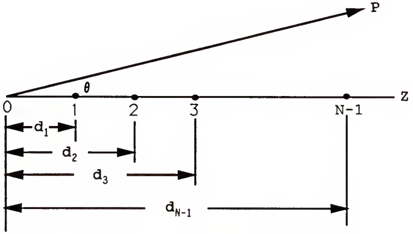

Figure 3.2 The linear array antenna system.

In Figure 3.2, the phase reference of the array system is assumed to be at the origin of the coordinates. d_n is the distance between the n^{th} element and the coordinate origin. Let's assume that the interelement distance is constant (assume d). Then, the location of the n^{th} element with respect to the coordinate origin can be expressed as

$$\mathbf{r}_n = nd\mathbf{z}_o$$

and the phase difference between the n^{th} array element and the phase origin is

$$k(\mathbf{r}_u \cdot \mathbf{r}_n) = knd\cos\theta$$

Further assume that a constant linear phase gradient

$$k(\mathbf{r}_s \cdot \mathbf{r}_n) = knd\cos\theta_o$$

is applied along with the array elements, such that the mainbeam maximum of the radiation pattern is oriented at the angular direction θ_o. Then, based on Equation (3.7), the far field radiation pattern of the linear array antenna system is

$$F(\theta) = \sum_{n=0}^{N-1} J(n) e^{jn(kd\cos\theta - kd\cos\theta_o)} \tag{3.8}$$

It is normally more convenient to represent the linear array radiation pattern given in Equation (3.8) as function of u, where

$$u(\theta) = kd(\cos\theta - \cos\theta_o)$$

Then, the linear array far field radiation pattern is alternatively expressed as

$$F(u) = \sum_{n=0}^{N-1} J(n) e^{jun} \tag{3.9}$$

which shows the linear array far field radiation pattern and its element's current excitation forming a Fourier transform relationship (with reversed sign in u).[5] Refering to Figure 3.2, for $\theta_0=(\pi/2)$, the linear array is called broadside array, and for $\theta_0=0$, is called the endfire array. For a broadside array system, the angle (θ) of the radiation pattern from 0 to π corresponding to the range of u from +kd to -kd, is called the visible range. The far field radiation pattern of a linear array system is inherently a periodic function of u with periodicity 2π. However, it is different from the

---

[5] It is without loss of generality that the index n of the summation in Equation (3.9) can be extended from $-\infty$ to $+\infty$ so as to meet the format of the Fourier transform in Equation (2.10), although the number of array elements is finite.

It is also possible to transform an N elements linear array system into a (N-1)-order polynomial function of z, by letting $z = e^{-ju}$, and the array function in Equation (3.9) becomes

$$F(z) = \sum_{n} J(n)\ z^{-n}$$

Since u is always real, the magnitude of z is always equal to unity, and the array pattern thus is evaluated along with a Schelkunoff unit circle in the complex plane. For an N elements array system, there are (N-1) roots in polynomial F(z), and the locations of these roots determine the shape of the array radiation pattern. For the analysis of the array radiation pattern using z transform, the reader can refer to [5-7].

spectrum of a discrete-time signal in that only the pattern corresponding to the visible range need to be noteworthy. It is easy to show that if the interelement distance d is larger than $(\lambda/2)$, then the visible range will be greater than 2π. Thus, for a steering angle of $\theta_0=0$ (on the endfire direction), a second radiation peak (called grating lobe) will appear within the visible range of the radiation pattern. Commonly, the interelement distance d of a linear array system is assumed to be smaller than $(\lambda/2)$, so as to eliminate grating lobe within the visible range.[6]

3.2.3 The planar rectangular grid array antenna system

A planar rectangular grid array antenna system, whose elements are distributed in x-y plane with constant interelement distances d_x and d_y is depicted in Figure 3.3.

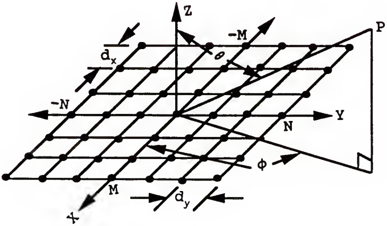

Figure 3.3 The rectangular grid planar array antenna system.

---

[6] The interelement distance will be assumed to be half of the wavelength $(d=\lambda/2)$ throughout this dissertation.

In Figure 3.3, it is assumed that there are 2M+1 and 2N+1 elements in each column (x axis) and row (y axis). The reference element is exactly positioned at the coordinate origin, the interelement distances in x and y axes are constant and denoted as d_x and d_y respectively. Thus, the location of m^{th} element in x axis is $x_m=md_x$, and the n^{th} element in y axis is $y_n=nd_y$, in which $-M \le m \le M$, $-N \le n \le N$. Again, both d_x and d_y are smaller or equal to $(\lambda/2)$, such that the effect of grating lobe is eliminated. Then, the location of the mn^{th} element of the rectangular grid planar array system can be expressed as

$$\mathbf{r}(\mathbf{m},\mathbf{n}) = md_x\mathbf{x}_o + nd_y\mathbf{y}_o$$

and the phase difference between the mn^{th} element and the phase origin is

$$k[\mathbf{r}_u\cdot\mathbf{r}(\mathbf{m},\mathbf{n})] = k[md_x\sin\theta\cos\phi + nd_y\sin\theta\sin\phi]$$

Again, a constant phase gradient is required to apply to each planar array element, such that the radiation pattern maximum can be steered to a specific direction (θ_o,ϕ_o), and the phase gradiant, according to Equation (3.6), should be

$$k[\mathbf{r}_s\cdot\mathbf{r}(\mathbf{m},\mathbf{n})] = k[md_x\sin\theta_o\cos\phi_o + nd_y\sin\theta_o\sin\phi_o]$$

Then, based on Equation (3.7), the far field radiation pattern of the rectangular grid planar array antenna system is proportional to

$$F(\theta,\phi)=\sum_m\sum_n J(m,n)\exp\{j[kmd_x(\sin\theta\cos\phi-\sin\theta_0\cos\phi_0)] +j[knd_y(\sin\theta\sin\phi-\sin\theta_0\sin\phi_0)]\} \quad (3.10)$$

where J(m,n) is the complex excitation of the mn^{th} array element. From analysis point of view, once an excitation function is given, the characteristics of the field pattern can be evaluated by using Equation (3.10). However, from the design point of view, it is more convenient to have the following variable transformations. Let's assume

$$u(\theta,\phi) = kd_x(\sin\theta\cos\phi - \sin\theta_0\cos\phi_0)$$
$$v(\theta,\phi) = kd_y(\sin\theta\sin\phi - \sin\theta_0\sin\phi_0) \quad (3.11)$$

Then, the planar far field radiation pattern in Equation (3.10) becomes

$$F(u,v) = \sum_m\sum_n J(m,n)e^{j(um+vn)} \quad (3.12)$$

which again exactly shows the 2-D discrete-time Fourier transform relations (with reversed sign in both u and v) between the far field radiation pattern of the rectangular grid planar array system and its element's current excitation. Due to the periodic property of an exponential function, the planar far field radiation pattern in Equation (3.12) is a periodic function on both u and v with the period of 2π. Once a desired field pattern $F(\theta,\phi)$ is specified, it can be mapped into F(u,v) via Equation (3.11). Thus, any available techniques of 2-D waveform design can be applied to the design of the radiation pattern of this planar array system.

It is always true that the array excitation J(m,n) is controllable, such that the following separable condition is realized [8]

$$J(m,n) = J(m,o)J(o,n) \tag{3.13}$$

Thus, the radiation pattern of the planar array antenna as given by Equation (3.12) can be mathematically expressed as the product of two linear array radiation patterns; that is,

$$\begin{aligned} F(u,v) &= \Big[\sum_{m} J(m,o)e^{jum}\Big]\Big[\sum_{n} J(o,n)e^{jvn}\Big] \\ &= F(u)F(v) \end{aligned} \tag{3.14}$$

The separable consequence shown in Equation (3.14) provides a useful idea in designing the radiation pattern of a planar array antenna by applying the well-developed design technique in the linear array system. This is the reason why most efforts in dealing with the radiation pattern of an array antenna have been concentrated on the linear array system.

Having shown the Fourier transform relations of the far field radiation pattern and its element's current excitation of an array antenna system, we can now apply any concepts in the traditional waveform problem to the design of radiation pattern for an array antenna system. Since several properties of an ãnalytic signal are so attractive, the potential advantages of using such an ãnalytic excitation for an array antenna will be formally exploited and analyzed in the following sections. It is noted that, in order to be compatible with a traditional signal analysis representation, hereafter, it is desirable to change the variables u, v to -u, -v in Equation (3.9) and (3.12), which reverse the radiation pattern. However it does not change the shape and characteristics of the radiation pattern. First, we discuss and analyze the application of the ãnalytic excitation for designing narrow beamwidth radiation patterns. The procedures will be extended to designing patterns for monopulse tracking radar systems which is the subject of Chapter VI. Due to the similarity of the error analysis between the linear and the planar array systems, the derivation and analysis will be emphasized on the linear array antenna system.

3.3 Analysis of Broadside Narrow Beamwidth Array Radiation Patterns using Analytic Excitations

The frequent need to both detect the long range radar targets and discriminate among closedly-spaced radar targets has led to the high beamwidth resolution, and high antenna directivity radiation pattern design. Both requirements are describable in terms of the shape of the radiation pattern. A high beamwidth resolution pattern implies the pattern has a narrow mainlobe beamwidth and low sidelobe, while a high antenna directivity implies a large amount of energy radiated toward the designated direction relative to the total energy radiated. It has been recognized that a uniformly excited array antenna system which has half wavelength interelement distance provides the maximum directivity and the radiation efficiency. However, the high sidelobe ratio of the uniform array antenna is unacceptable in most of the radar applications. The optimal linear in-phase excited array antenna system in trade-off between the mainbeam width and the sidelobe ratio has been highlighted by the work of Dolph [19]. Since it will be extensively applied throughout this dissertation, the procedures to derive the Dolph-Chebyshev array system [19] is attached in Appendix.

In the following sections, we present and analyze a new concept to improve the characteristics of a typical symmetric broadside narrow beamwidth radiation pattern of an array antenna system, such as directivity, the radiation efficiency and the beamwidth resolutions. For the sake of convenience, these characteristic indices of a narrow beamwidth radiation pattern to be studied are collectively defined as follows.

a. The directivity of an array antenna is a dimensionless quantity and defined as the ratio of the power radiated in the direction of mainbeam maximum (θ_0,ϕ_0) to the average power density from the antenna. It is mathematically expressed as

$$D = \frac{|F(\theta_0,\phi_0)|^2}{\frac{1}{4\pi}\int_0^{2\pi}\int_0^{\pi}|F(\theta,\phi)|^2 \sin\theta d\theta d\phi} \qquad (3.15)$$

b. The main-beam radiation efficiency (η) of an N elements array antenna is a dimensionless quantity and defined as the normalized ratio of the power radiated in the direction of mainbeam maximum (θ_o,ϕ_o) to the total power of the current excitation of the individual array element. It is mathematically expressed as [16][7]

$$\eta = \frac{|F(\theta_o,\phi_o)|^2}{N[\sum_n (J(n)^2]} \tag{3.16}$$

c. Half power (or 3dB power) beam-width (HPBW) of a narrow beamwidth radiation pattern of a linear array system is defined as the angular width of the mainbeam between the angular points half power (3dB) lower than the mainbeam maximum in the direction (θ_o); that is,

$$\text{HPBW} = \theta_2 - \theta_1 \tag{3.17}$$

where $F(\theta_2)=F(\theta_1)=0.707F(\theta_o)$

d. First null beam-width (BW_{null}) of a narrow beamwidth

---

[7] It has been shown [16] that $\eta=1$ which is the possible maximum value of η for uniform cophasal excitation. Furthermore, for an N elements broadside linear array antenna system ($\theta_o=\pi/2$ or u=0), based on Equation (3.9), the numerator in Equation (3.16) is proportional to the algebraic sum of all the current excitation, thus the radiation efficiency (η) in Equation (3.16) can be simplified as:

$$\eta = \frac{[\sum_n J(n)]^2}{N[\sum_n J(n)^2]}$$

radiation pattern of a linear array system is defined as the angular width between the first zero crossing on either side of the mainbeam maximum, which is used to measure the mainbeam width of the pattern; that is,

$$BW_{null} = \hat{\theta}_2 - \hat{\theta}_1 \tag{3.18}$$

where $F(\hat{\theta}_2)=F(\hat{\theta}_1)=0$.

e. The peak sidelobe (SL_{peak}) is the ratio of the maximum strength of the radiation pattern outside the mainbeam to the strength of the mainbeam maximum.

The directivity (D) is used to measure the transmitting power gain of the radiation pattern of an antenna system. The main beam radiation efficiency (η) is used to measure the radiation intensity in the main beam direction and the excitation efficiency of the current excitation of an array antenna system. The half-power beamwidth (HPBW), first-null beamwidth (BW_{null}) and the peak sidelobe ratio (SL_{peak}) are the pattern characteristics which are associated with the capability of detection and tracking in the radar application.

3.3.1 The potential advantages of broadside narrow beamwidth array radiation patterns using ãnalytic excitations

The potential advantages of the broadside narrow beamwidth array radiation pattern using ãnalytic excitation are first illustrated in this section. The performance of the broadside narrow beamwidth array radiation pattern excited by a realizable ãnalytic excitation will be analyzed in the following Section 3.3.2.

3.3.1.1 The generation of a half-sided narrow beamwidth radiation pattern using an ãnalytic excitation

Consider we are given a conventional real excitation $J_r(n)$ which produces a symmetric broadside narrow beamwidth radiation pattern denoted as $F_r(u)$. A desired ãnalytic excitation $J_d(n)$ can be generated from $J_r(n)$ by applying the discrete-time Hilbert transform in Equation (2.19); that is,

$$J_d(n) = J_r(n) + jJ_i(n) \tag{3.19}$$

where $J_i(n)$ is the discrete-time Hilbert transform of $J_r(n)$. After using the spectrum relations of the real and imaginary part of an ãnalytic signal in Equation (2.15), the radiation pattern, denoted as $F_h(u)$, corresponding to the ãnalytic excitation in Equation (3.19) is

$$\begin{aligned} F_h(u) &= F_r(u) + j[-j\,\mathrm{sgn}(u)F_r(u)] \\ &= F_r(u)\ [1 + \mathrm{sgn}(u)] \end{aligned}$$

That is,

$$F_h(u) = \begin{cases} 2F_r(u), & 0 < u < \pi \\ F_r(u), & u=0 \\ 0\quad, & -\pi \le u < 0 \end{cases} \tag{3.20}$$

Equation (3.20) shows that the radiation pattern excited by an ãnalytic excitation is half-sided. As a result, both the

HPBW and the BW_{null} beamwidths of $F_h(u)$ are exactly half of those in $F_r(u)$.

Using the same procedures for given a typical 2-D real symmetric excitation $J_r(m,n)$ which produces a narrow beamwidth planar radiation pattern, denoted as $F_r(u,v)$, with mainbeam maximum at u=v=0, a half-plane radiation pattern of a planar array system, denoted as $F_h(u,v)$ (assumed in u plane), can be produced by using a 2-D ãnalytic excitation--Type II which is denoted as $J_d(m,n)$ and is formed as

$$J_d(m,n) = J_r(m,n) + jJ_i(m,n) \tag{3.21}$$

where $J_i(m,n)$ is the Hilbert transform of $J_r(m,n)$ using the 2-D discrete-time Hilbert transform (Type II). It is easy to show that the half-plane pattern $F_h(u,v)$ is

$$F_h(u,v) = \left[\begin{array}{ll} 2F_r(u,v), & \text{for } (0 < u < 0) \text{ and } (-\pi \le v < \pi) \\ F_r(u,v), & \text{for } (u=0) \text{ and } (-\pi \le v < \pi) \\ 0, & \text{for } (-\pi \le u < 0) \text{ and } (-\pi \le v < \pi) \end{array}\right. \tag{3.22}$$

It is obvious that both HPBW and BW_{null} beamwidths of the half-plane radiation pattern $F_h(u,v)$ as given by Equation (3.22) are half of those in $F_r(u,v)$ in u plane. Furthermore, a desired quadrant-plane radiation pattern can be produced from the real excitation $J_r(m,n)$ by using the procedures as given in Section 2.3.3.2. (the procedures will not be repeated here). Thus, according to Equation (2.47), the quadrant-plane radiation pattern $F_q(u,v)$ is expressed as

$$F_q(u,v) = \begin{cases} 4F_r(u,v), & \text{for } (0 < u < \pi \text{ and } 0 < v < \pi) \\ 2F_r(u,v), & \text{for } (u=v=0) \text{ or } (u=0 \text{ and } 0 \le v < 0) \\ & \quad \text{or } (v=0 \text{ and } 0 \le u < 0) \\ 0, & \text{otherwise} \end{cases} \tag{3.23}$$

As a result, both HPBW and BW_{null} of $F_q(u,v)$ in Equation (3.23) are half of those in $F_r(u,v)$ in both u and v planes.

The common features of these asymmetric radiation patterns as given by Equation (3.20), (3.22) and (3.23) are that the beamwidths (both HPBW and BW_{null}) are reduced by one half, and the radiation strengths over the radiation region are two times uniformly increased in the half-sided pattern $F_h(u)$ and the half-plane pattern $F_h(u,v)$, and four times uniformly increased in the quadrant-plane pattern $F_q(u,v)$. Therefore, the beamwidth resolutions are doubly increased, and the directivity and the peak sidelobe remain the same compared to the conventional broadside narrow beamwidth symmetric radiation patterns. Furthermore, the undesired sidelobes in either half-side, half-plane or three of four quadrants of $F_h(u)$, $F_h(u,v)$ and $F_q(u,v)$ respectively are totally eliminated. Thus, we have the following first assertion related to the utilization of an ãnalytic excitation for an array system.

Assertion 3.1 An ãnalytic excitation can theoretically produce a desired asymmetric radiation pattern whose beamwidth resolutions are doubly increased and half of the sidelobe region is totally eliminated, without sacrificing the directivity and peak sidelobe compared to a conventional symmetric broadside radiation pattern of an array antenna system.

Two linear broadside array radiation patterns excited by a uniform excitation and the corresponding theoretical ideal ãnalytic excitation are plotted in Figure 3.4(a) and (b).

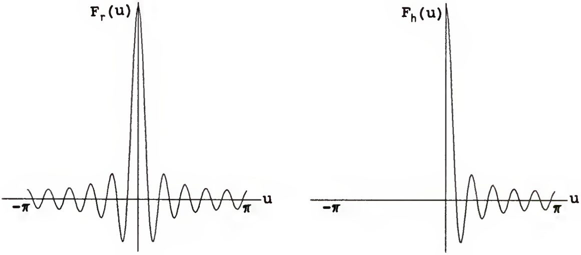

(a) (b)

Figure 3.4 The broadside narrow beamwidth radiation patterns excited by a uniform excitation and the corresponding ideal ãnalytic excitation.
(a)The uniform excitation.
(b)The corresponding ãnalytic excitation.

3.3.1.2 The symmetry property of an ãnalytic excitation

One of the desirable excitation characteristics for a large array antenna system is the symmetric property of the magnitude of the excitation. This is because the symmetric property reduces the required categories of power divider by one half in the physical realization of the beamforming network. Therefore, most of the excitations related to a large array antenna system have the symmetric property.

Assume that $J_r(n)$ is a typical real even symmetric excitation (i.e. $J_r(-n)=J_r(n)$), for an array antenna system.

Then based on the properties of discrete-time Fourier transform, the corresponding radiation pattern, denoted as $F_r(u)$, should be real and even symmetry. That is, $F_r(-u)=F_r(u)$. The radiation pattern $F_i(u)$ generated by the Hilbert transform of $F_r(u)$, that is $F_i(u)=[-j\text{sgn}(u)F_r(u)]$, should be pure imaginary and odd symmetry. Thus, the excitation $J_i(n)$ corresponding to $F_i(u)$ should be real and odd symmetry. The above deductions show the fact that the Hilbert transform of a real even symmetric excitation is always a real odd symmetric excitation. Thus, if an ãnalytic excitation $J(n)$ is formed as

$$\begin{aligned} J(n) &= J_r(n) + j\, J_i(n) \\ &= a(n)\ \tan^{-1}\left(\frac{J_i(n)}{J_r(n)} \right) \end{aligned} \tag{3.24}$$

where $a(n)=[J_r^2(n)+J_i^2(n)]^{1/2}$ is the magnitude and $\tan^{-1}(\cdot)$ is the phase of $J(n)$, respectively. Then, based on the even and odd symmetric property of $J_r(n)$ and $J_i(n)$, it is easy to show that $J(-n)$ is complex conjugate of $J(n)$. Due to the complex conjugate symmetric property, the desirable even symmetric property in the magnitude of the excitation is maintained in the ãnalytic excitation. Thus, the symmetric property of an ãnalytic excitation is stated as follows:

Assertion 3.2 The analytic excitation generated from a real even symmetric excitation has the property of complex conjugate symmetry, that is, its magnitude is even symmetry while its phase is odd.

3.3.1.3 The improvement of radiation efficiency (η) of a tapered excitation using an ãnalytic excitation

The radiation efficiency (η) plays an important role in the radiation pattern design of an antenna system. This is because the transmitting efficiency of an array antenna system is related to this parameter. It will be shown that an ãnalytic excitation which is generated by a real tapered excitation always has better radiation efficiency than the original real tapered excitation, especially compared to a heavily tapered real excitation.

Assume that an ãnalytic excitation $J(n)$ is generated from a real excitation $J_r(n)$; that is,

$$J(n) = J_r(n) + jJ_i(n) \tag{3.25}$$

where $J_i(n)$ is the discrete-time Hilbert transform of $J_r(n)$. As deduced in the preceeding section, $J_i(n)$ should be an odd symmetric excitation. Now, let's examine what will later be defined as the complemental property of the real and imaginary parts of an ãnalytic excitation by using a pictorial illustration. If a given (N=9) conventional normalized array excitation $J_r(n)$ is as depicted in Figure 3.5(a), then, based on the operation process of the discrete-time convolution and the sequence of the impulse response of the discrete-time Hilbert transform $h(n)$ in Equation (2.18), it is not hard to show that $J_i(n)$ will be as in Figure 3.5(b).

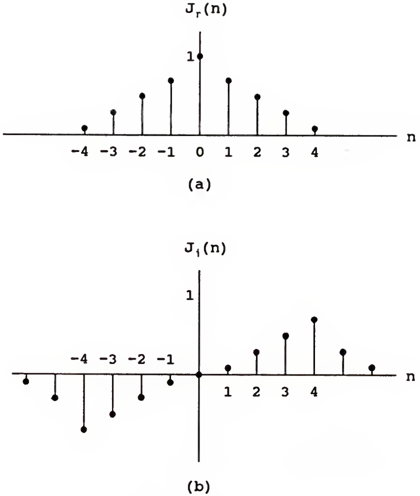

Figure 3.5 The pictorial illustration of the complemental property of the real and the imaginary parts of a typical ãnalytic excitation. (a)$J_r(n)$. (b)$J_i(n)$.

The meaning of the pictorial results shown in Figure 3.5 can be stated as follows: whenever $J_r(n)$ approaches maximum value, $J_i(n)$ always approaches a zero value, and at the two tapered terminals of $J_r(n)$, $J_i(n)$ normally becomes dilated. This is the complemental property between the real and imaginary parts of an analytic excitation. An extremely evident example of the complemental property of an ãnalytic excitation is the sinusoidal excitation, that is, an ãnalytic excitation is formed as a sum of a sine and cosine excitation, that is, J(n)=cos(n)+jsin(n) (it is well known that the cos(n) and sin(n) form a Hilbert transform pair), and it is easy to show that the magnitude of J(n) is always unity for all the array elements. Furthermore, the following inequality holds

$$|J(n)| = |J_r(n) + j\ J_i(n)| \geq |J_r(n)| \tag{3.26}$$

The complemental property of the real and imaginary parts of an ãnalytic excitation illustrated in Figure 3.5 and the inequality equation of (3.26) assure the improvement of tapering condition as well as radiation efficiency (η) of the ãnalytic excitation over the real symmetric excitation (will be seen from computer simulations later). Therefore, the assertion 3.3, the result of this section, can be stated as follows:

Assertion 3.3 Due to the complemental property of the real and the imaginary parts, an ãnalytic excitation always provides higher radiation efficiency than a tapered real excitation for an array antenna system.

3.3.2 The analysis of broadside narrow beamwidth array radiation patterns using realizable ãnalytic excitations

In the previous Section 3.3.1, we have illustrated the outstanding and special characteristics of the broadside narrow beamwidth array radiation pattern using a theoretical ãnalytic excitation. However, such a theoretical ãnalytic excitation is unrealizable, because it can be achieved only with an infinite number of array elements. A physically realizable array antenna system consists of a finite number of array elements. Thus, the realization of an ãnalytic excitation in the array antenna system becomes an approximation problem.

Consider an $N=2M+1$ elements linear broadside array antenna system, where M is an integer, and a typical conventional real excitation $J_r(n)$, where $-M \le n \le M$. Accordingly, the desired ãnalytic excitation $J_d(n)$ can be generated by

$$J_d(n) = J_r(n) + j[J_r(n)*h(n)] \tag{3.27}$$

where * denotes the discrete-time convolution, and h(n) is the impulse response of 1-D discrete-time Hilbert transform defined in Equation (2.18). Then, the desired half-sided radiation pattern $F_d(u)$ corresponding to $J_d(n)$ is

$$\begin{aligned} F_d(u) &= F_r(u) + j\{F_r(u)[-j\mathrm{sgn}(u)]\} \\ &= F_r(u) + [F_r(u)\mathrm{sgn}(u)] \end{aligned} \tag{3.28}$$

where $F_r(u)$ is the radiation pattern corresponding to $J_r(n)$. It is obvious that the analysis of the half-sided radiation pattern $F_d(u)$ using a realizable ãnalytic excitation is equivalent to the analysis of the approximation to the ideal transformed pattern $[-jF_r(u)\mathrm{sgn}(u)]$. Based on the property of the discrete-time Hilbert transformation, the excitation of $[J_r(n)*h(n)]$ corresponding to the pattern of $[-jF_r(u)\mathrm{sgn}(u)]$ is an infinite sequence, due to the infinite length of h(n).

For a finite elements array antenna system, the most straightforward approach to obtain a realizable ãnalytic excitation is to truncate the infinite sequence of $[J_r(n)*h(n)]$ into a length of N with some suitable window function;[8] that is, the truncated analytic excitation $J_t(n)$ can be represented as

$$J_t(n) = J_r(n) + j[J_r(n)*h(n)]w(n) \qquad (3.29)$$

where w(n) represents a typical N points truncation window,

$$w(n) = 0 \qquad M < |n|$$

By applying the window theorem [17,pp.59], the realizable radiation pattern $F_t(u)$ corresponding to $J_t(n)$ in Equation (3.29), becomes

$$\begin{aligned} F_t(u) &= F_r(u) + j\{F_r(u)[-j\mathrm{sgn}(u)]\}*W(u) \\ &= F_r(u) + [F_r(u)\mathrm{sgn}(u)]*W(u) \qquad (3.30) \end{aligned}$$

where W(u) is the spectrum of the selected window function w(n), and $\{[F_r(u)\mathrm{sgn}(u)]*W(u)\}$ represents the periodic convolution of the ideal transformed pattern $[F_r(u)\mathrm{sgn}(u)]$ and the spectrum, W(u), of the window function. With $F_i(u)$ denoting the resulting spectrum after periodic convolution, the periodic convolution is defined as [56]

---

[8] In this dissertation, our principal interest is to convey a new concept to the design of the radiation pattern of an array antenna system, and the window method will be adopted in the analysis and design of the radiation pattern using ãnalytic excitation.

$$F_i(u) = \frac{1}{2\pi} \int_{-\pi}^{\pi} [F_r(\xi)\,\mathrm{sgn}(\xi)]W(u-\xi)\, d\xi \qquad (3.31)$$

Actually, the realization of the ideal pattern $[F_r(u)\mathrm{sgn}(u)]$ which has discontinuity in the u=0 direction by using windowing method is similar to the realization of an ideal finite impulse response (FIR) discrete filter by using windowing method [56-57], a subject which has received a great deal of study, and a particular set of tapering windows which moderated the Gibbs phenomenon [56] at the discontinuity has been found [12]. Thus, it is well known that due to the effects of the window function, the realized pattern $F_i(u)$ in Equation (3.31) becomes a smeared version of $[F_r(u)\mathrm{sgn}(u)]$. Using a typical even symmetric pattern $F_r(u)$ and a typical spectrum W(u) of a window function, the periodic convolution in Equation (3.30) is illustrated in Figure 3.6. Figure 3.6(a) is the typical symmetric broadside radiation pattern $F_r(u)$, Figure 3.6(b) shows the convolution process at u=0, and the pattern in Figure 3.6(c) represents the relizable transformed pattern $F_i(u)$ which is the smeared version of the desired pattern $[F_r(u)\mathrm{sgn}(u)]$. As seen from Figure 3.6, the most familiar effects of the window method are that the discontinuity of the pattern $[F_r(u)\mathrm{sgn}(u)]$ at u=0 becomes a roll-off region, and the pattern of $[F_r(u)(\mathrm{sgn}\ u)]$ is also leaked by the spectrum, W(u), of the window function for all range of u. However, a quantitative estimation of the width

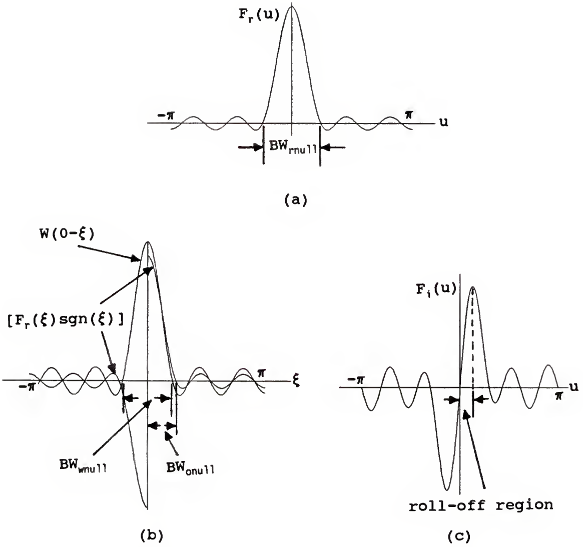

Figure 3.6 The illustration of periodic convolution.
(a)The symmetric broadside pattern $F_r(u)$.
(b)The convolution process at u=0.
(c)The realized transformed pattern $F_i(u)$.

of the roll-off region and the extent of the leakage effect of the windowing method is unobtainable. This is because not only they depend on both the overall shapes of the original symmetric pattern $F_r(u)$ and the spectrum $W(u)$ of the truncation window, but also the symmetric pattern $F_r(u)$ and the spectrum W(u) always have approximately the same mainbeam width and mainlobe width under this realization situation. Nevertheless, it will be shown by computer simulations that the performance of the realized asymmetric radiation pattern using a realizable ãnalytic excitation is found to be proportional to the parameter Main-Lobe Width Ratio (MLWR), which is defined as

$$\text{MLWR} = \frac{BW_{wnull}}{BW_{inull}} = \frac{2BW_{wnull}}{BW_{rnull}} \tag{3.32}$$

where BW_{wnull} and BW_{rnull} are the mainlobe width of the spectrum W(u) of the window function and the mainbeam width of the original even symmetric pattern $F_r(u)$ respectively, and BW_{inull} is the half-side mainbeam width of the pattern $[F_r(u)\text{sgn}(u)]$ which is half of BW_{rnull}. For the definitions of BW_{wnull}, BW_{rnull} and BW_{inull}, please refer to Figure 3.6.

It is clear that the performance of the realizable asymmetric radiation pattern $F_t(u)$ in Equation (3.30) is determined by the extent of the pattern $F_i(u)$ approximation to the ideal pattern $[F_r(u)\text{sgn}(u)]$. As far as the distortion which results from the truncation window is concerned, it should be equivalent to the extent of the distortion of the ideal pattern $[F_r(u)\text{sgn}(u)]$ around the u=0 results from a realizable Hilbert transformer that is also assumed to be implemented by the windowing method. Consequently, the selection of the truncation window becomes the narrower the mainlobe width the better. That is, the spectrum of the window function should possess the narrowest mainlobe width under a specified sidelobe ratio, or vice versa. It is well known that the optimal window function which possesses the required properties is the Dolph-Chebyshev window [12]. Actually, the Dolph-Chebyshev window is exactly the same as the Dolph-Chebyshev linear array system where the interelement distance is set to half of the wavelength.[9] For the derivation of the optimal Dolph-Chebyshev window, refer to Appendix. The property of the Dolph-Chebyshev window function is that whenever the sidelobe ratio R is specified, the mainlobe width is automatically minimized.

After acquiring the optimal truncation window, the performance of an array antenna radiation pattern using realizable ãnalytic excitation can be thoroughly analyzed. However, a generalized error analysis is unobtainable. By using computer simulation, two specific linear array antenna systems are used to demonstrate the achievements of this new realization technique. The procedures used to analyze and to simulate the realizable ãnalytic excitation and its corresponding asymmetric radiation pattern are described in Figure 3.7.

---

[9] Refer to Equation (3.9), when $d=(\lambda/2)$, the visible range of the linear array system is from $-\pi$ to π (total 2π range), which is exactly the same as the periodicity of the spectrum of the discrete-time signal. Thus the Dolph-Chebyshev linear array radiation pattern is equivalent to the spectrum of a discrete-time window function which is optimal in the narrowest mainlobe width.

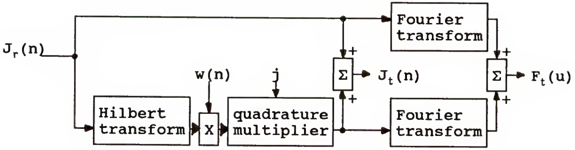

X:multiplication.
Σ:summation.

Figure 3.7 The generations of the realizable ãnalytic excitation and the corresponding asymmetric radiation pattern.

From Figure 3.7, once a real excitation $J_r(n)$ is specified, the imaginary part of a realizable ãnalytic excitation can be obtained from $J_r(n)$ by carrying out the discrete-time Hilbert transform, and multiplying it with a selected truncation window w(n). The analytic excitation $J_t(n)$ is then the quadrature summation of the real excitation $J_r(n)$ and the truncated version of Hilbert transform of $J_r(n)$. Accordingly, the corresponding asymmetric array radiation pattern $F_t(u)$ is the Fourier transform of the finite length ãnalytic excitation $J_t(n)$. In doing the computer simulation, there are two steps that need to be emphasized. The first one is that based on the discrete-time convolution operation, the length of the impulse response h(n) of the discrete-time Hilbert transfrom which is required to compute the N points imaginary part of an ãnalytic excitation is reduced to the points from -(N-1) to (N-1), for total (2N-1) points. The second one is that the Romberg integration [62-63], which applies the Richardson extrapolation process to improve the accuracy of the trapezoidal integration rule, is used to compute the average radiation power in the denominator of Equation (3.15) that is required to evaluate the antenna directivity given a particular set of excitation.

3.3.3 Analysis examples

Example 1 In this first analysis example, we use the heavily tapered Hamming function as an original real even symmetric excitation to generate the desired ãnalytic excitation. Then, the performance of the radiation patterns excited by the Hamming and the corresponding realizable ãnalytic excitations are analyzed and compared.

The Hamming excitation of an N (N=2M+1, M is an integer) elements array system can be expressed as [12]

$$J_h(n) = \begin{cases} 0.54 + 0.46\cos(\frac{2n\pi}{N-1}), & -M \le n \le M, \\ 0, & \text{otherwise} \end{cases} \qquad (3.33)$$

and its radiation pattern, denoted as $F_{ham}(u)$, is

$$F_{ham}(u) = 0.54\left(\frac{\sin[(\frac{N}{2})u]}{\sin(\frac{u}{2})}\right) + 0.23\left(\frac{\sin[(\frac{N}{2})(u-(\frac{2\pi}{(N-1)})]}{\sin[(\frac{1}{2})(u-(\frac{2\pi}{(N-1)})]}\right)$$

$$+0.23\left(\frac{\sin[(\frac{N}{2})(u+(\frac{2\pi}{(N-1)})]}{\sin[(\frac{1}{2})(u+(\frac{2\pi}{(N-1)})]}\right) \qquad (3.34)$$

Equation (3.34) shows that the pattern excited by the Hamming function is the summation of three weighted and shifted [sin(Nx)/sin(x)] waveforms that effectively eliminate the peak sidelobe of the [sin(Nx)/sin(x)] waveform, thus its normalized peak sidelobe can be as low as -41 dB. However, the mainbeam width (BW_{null}) is wider than that of uniformly excited array system (about $10\pi/N$) [12]. Due to being heavily tapered, the radiation efficiency of the Hamming excitation is poor. The truncated (or realizable) ãnalytic excitation related to the Hamming excitation can be obtained by implementing the transformation and truncation processes in Figure 3.6. Thus, the truncated ãnalytic excitation, denoted as $J_{th}(n)$ and the corresponding asymmetric radiation pattern, denoted as $F_{th}(u)$, are expressed as

$$J_{th}(n) = J_h(n) + j[J_h(n)*h(n)]w(n)$$

$$F_{th}(u) = F_{ham}(u) + [F_{ham}(u)\,\mathrm{sgn}(u)]*W(u) \qquad (3.35)$$

where W(u) is the spectrum of the Dolph-Chebyshev truncation window mentioned earlier. The various radiation patterns used to analyze and to compare the performance of the Hamming excitation and the corresponding realizable ãnalytic excitation are plotted in Figure 3.8(a) through Figure 3.8(d), where the number of array elements is assumed to be 21 (N=21). Figure 3.8(a) overlaps the even symmetric radiation pattern $F_{ham}(u)$ excited by the Hamming excitation and the transformed pattern $\{[F_{ham}(u)(\mathrm{sgn}\ u)]*W(u)\}$ corresponding to the excitation $\{[J_h(n)*h(n)]w(n)\}$, where the truncation window is the Dolph-Chebyshev window with sidelobe ratio R=30dB. The Hamming pattern $F_{ham}(u)$ and the realized asymmetric radiation pattern, let it be denoted as $F_{th}(u)$ R=30, corresponding to the summation of the two patterns in Figure 3.8(a) are plotted together in Figure 3.8(b). Both Figure 3.8(c) and Figure 3.8(d) have the same interpretations as Figure 3.8(a) and Figure 3.8(b) respectively. However, the truncation window is the Dolph-Chebyshev window with sidelobe ratio R=20dB, thus, let the realized asymmetric pattern in Figure 3.8(d) be denoted as $F_{th}(u)$ R=20. Let's first examine the shapes of the realized asymmetric radiation pattern $F_{th}(u)$ R=30 in Figure 3.8(b). The most noticeable phenomenon is a high peak sidelobe that appears within the sidelobe region of $u < 0$. The cause of this high peak sidelobe can be examined from Figure 3.8(a), which shows the peak sidelobe is the result of the mis-match of the mainbeams between the Hamming symmetric pattern and its Hilbert transformed pattern. It is the consequence of the periodic convolution between the idealized Hilbert transformed pattern and the spectrum of the truncation window, that induces the mainbeam mis-match phenomenon. Next, by examining the realized asymmetric pattern $F_{th}(u)$ R=20 in Figure 3.8(d), we find that the mainbeam mis-match phenomenon is moderated. This is because the Dolph-Chebyshev truncation window used to realize the asymmetric pattern $F_{th}(u)$ R=20 has a higher

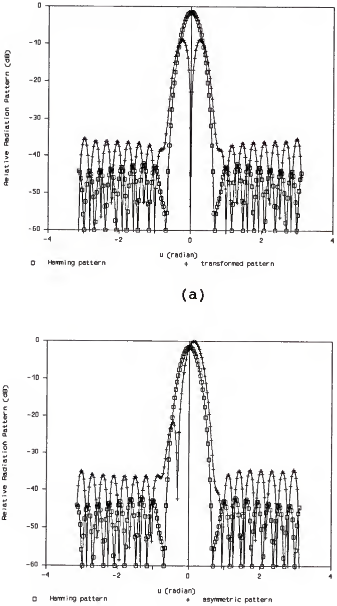

(a)

(b)

Figure 3.8 The Hamming and the corresponding realized asymmetric patterns.

(a) The Hamming and its Hilbert transformed patterns. (w(n)=Dolph-Chebyshev with R=30 dB)

(b) The Hamming and the realized asymmetric pattern $F_{th}(u)$ R=30, corresponding to (a).

(c) The Hamming and its Hilbert transformed patterns. (w(n)=Dolph-Chebyshev with R=20 dB)

(d) The Hamming and the realized asymmetric pattern $F_{th}(u)$ R=20, corresponding to (c).

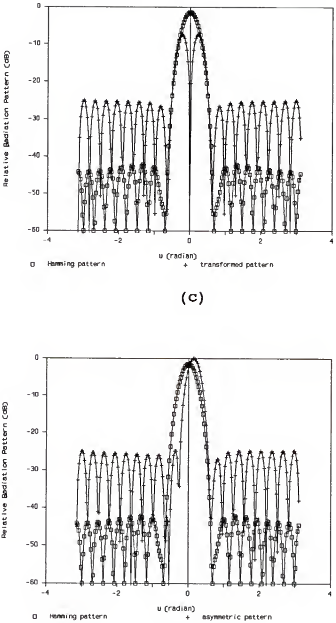

(c)

(d)

Figure 3.8 --- continued

sidelobe ratio and consequently narrower mainlobe width compared to that of the window used to generate the pattern $F_{th}(u)$ R=30. This is an increase in the parameter the Main-Lobe Width Ratio, (MLWR). The improvement of the mainbeam mis-match phenomenon can be seen from Figure 3.8(c). As a result, the peak sidelobe produced by the mainbeam mis-match is dwindled in the asymmetric pattern $F_{th}(u)$ R=20 of Figure 3.8(d). However, theaccomplishment of the dwindled peak sidelobe is achieved by sacrificing the overall peak sidelobe of the realized asymmetric pattern. The quantitative characteristics of the patterns of $F_{ham}(u)$, $F_{th}(u)$ R=30 and $F_{th}(u)$ R=20 are listed in Table 3.1. In the characteristic of peak sidelobe, the overall peak sidelobe scenario SL_{peak} is further decomposed into left SLL_{peak} and right SLR_{peak} sidelobe regions with respect to the mainbeam of the asymmetric pattern, in order to clearly describe the inherent property of the asymmetric radiation pattern.

Table 3.1 The characteristics of the broadside narrow beamwidth radiation patterns excited by Hamming and the two corresponding analytic excitations.

type of pattern	HPBW (Rad)	BW_{null} (Rad)	MLWR (None)	η (None)	D (None)	SLL_{peak} (dB)	SLR_{peak} (dB)
$F_{ham}(u)$	.401	1.359	-	.709	14.885	-40.64	-40.64
$F_{th}(u)$ R=30	.361	1.268	1.55	.789	16.575	-21.64	-34.63
$F_{th}(u)$ R=20	.322	.907	2.01	.877	18.419	-24.85	-24.79

By comparing the quantitative analysis results of these three radiation patterns tabulated in Table 3.1, we find that the patterns excited by the analytic excitations have the advantages stated in Section 3.3.1, that is, they have higher beamwidth resolutions in both HPBW and BW_{null}, and have higher antenna directivity and radiation efficiency. However, the higher peak sidelobes that appear in the realized asymmetric patterns, especially the undesired peak sidelobe produced by the convolution process, has greatly demolished these advantages gained from the ãnalytic excitation. By examining the tabulated characterictics of the two realized asymmetric radiation patterns $F_{th}(u)$ R=30 and $F_{th}(u)$ R=20, we find that the shapes of both realized asymmetric radiation patterns are, as expected, very much determined by the spectrum characteristics of the Dolph-Chebyshev truncation window. The sidelobes of both realized asymmetric radiation patterns are leaked by the sidelobe of the truncation window which is normally higher than that of the original symmetric pattern. It also indicates that the higher the Main-Lobe Width Ratio (MLWR), the more advantages obtained from the ãnalytic excitation, which include the HPBW, BW_{null}, directivity (D), radiation efficiency (η), and the lower peak sidelobe which is produced by the periodic convolution process. However, those advantages are limited by the required sidelobe ratio of the realized asymmetric radiation pattern.

The excitations for the symmetric radiation patterns $F_{ham}(u)$ and $F_{th}(u)$ R=20 are listed in Table 3.2, where only half of the element's excitations are tabulated, and the another half of the element's excitations are just the complex conjugate of the tabulated results, that is, $J(-n)=J^*(n)$. Comparing the two excitation sets listed in Table 3.2 show that the heavily tapered amplitudes of the original Hamming excitation are greatly improved in the corresponding ãnalytic excitation, which is another important advantage of the ãnalytic excitation.

Table 3.2 The normalized Hamming and the corresponding ãnalytic excitations.
($N=21$, $J(-n)=J^*(n)$)

n	J(n)		
	$F_{ham}(u)$	$F_{th}(u)$ R=20	
	(amplitude)	(amplitude)	(phase)
10	.080	.504	80.87
9	.103	.254	66.17
8	.168	.361	62.26
7	.270	.480	55.84
6	.398	.614	49.64
5	.540	.737	42.85
4	.682	.842	35.90
3	.810	.918	28.02
2	.912	.967	19.43
1	.978	.992	9.94
0	1.000	1.000	0.00

Example 2 The purpose of this example is to analyze the performance of a Dolph-Chebyshev excited linear array system and its corresponding ãnalytic excitations (instead of Hamming excitation as used in Example 1), so that a deeper insight into the pattern characteristics of an ãnalytic excitation can be obtained.

The radiation pattern of an N elements Dolph-Chebyshev linear array system can be expressed as (refer to Appendix)

$$F_c(u) = T_{N-1}(x_0\cos(u/2)) \qquad (3.36)$$

where $T_{N-1}(x)$ is the $(N-1)^{th}$ Chebyshev polynomial, x_0 is chosen such that $T_{N-1}(x_0)=R$, and R is the required peak sidelobe ratio. Let's assume that the sidelobe ratio R=30dB Dolph-Chebyshev array system is the original real excitation, and the two truncation windows used to realize the ãnalytic excitations are Dolph-Chebyshev windows with R=25 dB and R=18dB. The number of array elements is the same as that in Example 1 (N=21). The symmetric radiation pattern $F_c(u)$ of a Dolph-Chebyshev array system and the corresponding two realized asymmetric radiation patterns, denoted as $F_{tc}(u)$ R=25 and $F_{tc}(u)$ R=18, are plotted together in Figure 3.9(a) and Figure 3.9(b) respectively, and their quantitative pattern characteristics are listed in the first three rows of Table 3.3, where they are indicated as $F_c(u)\{30\}$, $F_{tc}(u)$ R=25 and $F_{tc}(u)$ R=18. By examining and comparing the shapes of the radiation patterns in Figure 3.9, and the quantitative characteristics of these radiation patterns in Table 3.3, we can conclude that the analysis results related to the pattern characteristics of an ãnalytic excitation are very much similar to those of Example 1. That is, the advantages gained from the ãnalytic excitation include HPBW, BW_{null}, antenna directivity and radiation efficiency, and the disadvantage of

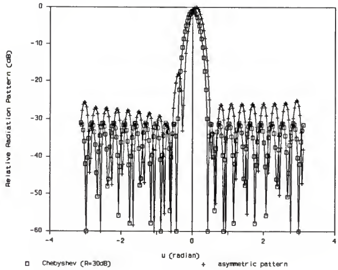

(a)

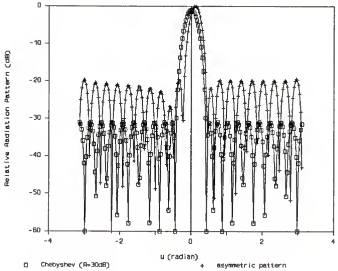

(b)

Figure 3.9 The Chebyshev (R=30dB) and the corresponding realized asymmetric radiation patterns.
(a) The Chebyshev and realized asymmetric array pattern $F_{tc}(u)$ R=25.
(b) The Chebyshev and realized asymmetric array pattern $F_{tc}(u)$ R=18.

Table 3.3 The characteristics of the broadside narrow beamwidth radiation patterns excited by the Dolph-Chebyshev and the two corresponding ãnalytic excitations.

type of pattern	HPBW (Rad)	BW_{null} (Rad)	MLWR (None)	η (None)	D (none)	SLL_{peak} (dB)	SLR_{peak} (dB)
$F_c(u)\{30\}$	.330	.880	-	.869	18.242	-30.00	-30.00
$F_{tc}(u)$ R=25	.310	.789	1.13	.912	19.165	-18.06	-25.96
$F_{tc}(u)$ R=18	.287	.691	1.38	.940	19.758	-19.61	-19.84
$F_c(u)\{26\}$	.314	.793	-	.913	19.163	-26.00	-26.00

the realized asymmetric patterns is the higher sidelobe scenario. Furthermore, the advantages gained from the ãnalytic excitation really depend on the MLWR parameter, the Main-Lobe Width Ratio, and the advantages are limited by the required sidelobe ratio in the realized asymmetric radiation pattern.

Very often, an asymmetric sidelobe scenario, such as (18dB/26dB) sidelobes of $F_{tc}(u)$ R=25 in Table 3.3, can be acceptable. Thus, a fair performance comparison is assumed to be made between the $F_{tc}(u)$ R=25 and the symmetric broadside Dolph-Chebyshev pattern with the sidelobe ratio R=26 dB, whose characteristics are listed in the last row of Table 3.3 as $F_c(u)\{26\}$. Comparing the performance of these two patterns indicats that the advantages gained from an ãnalytic excitation seem to be modest. However, the practical consideration of the applications of an asymmetric sidelobe radiation pattern is not merely based on these modest advantages.

From the simulation results of Example 1 and 2, the most unfavorable characteristic in the asymmetric radiation pattern corresponding to an ãnalytic excitation is the peak sidelobe generated by the mainbeam mis-match which results from the periodic convolution in the realization of an ãnalytic excitation. Theoretically, the larger the number of array elements N, the narrower the mainlobe width of the spectrum of the truncation window. Therefore, the number of array elements N could be used to improve this mainbeam mis-match phenomenon. It is interesting and worthwhile to check this theoretical concept by letting N be an independent variable. Let's again assume that the sidelobe ratio R=30dB Dolph-Chebyshev array system is the original real excitation, and the truncation window used to realize the corresponding ãnalytic excitation is Dolph-Chebyshev window with R=25dB, and the number of array elements N has changed from 11 to 25. The two sides of the peak sidelobe of the realized asymmetric radiation pattern as function of the number of array elements N are plotted in Figure 3.10.

In Figure 3.10, the upper curve represents the peak sidelobe in the sidelobe region of $u < 0$, which depends on the extent of the mainbeam mis-match mentioned earlier, and the lower curve represents the peak sidelobe in the sidelobe region of $u > 0$, which depends on the peak sidelobes of both original symmetric pattern and realizable Hilbert transformed pattern. It can be seen from Figure 3.10 that both sides of the peak sidelobe are almost independent of the number of the

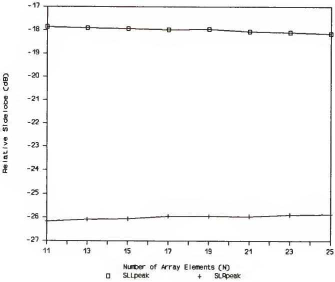

Figure 3.10 The peak sidelobe ratios of the asymmetric radiation patterns as function of the number of array elements.

array elements N. The reason for the independence of peak sidelobe with respect to N for the case of u>0 (lower curve) is simply that we keep the peak sidelobe constant in both original symmetric pattern and the spectrum of the truncation window and, consequently, in the realized Hilbert transformed pattern as well. However, for the case of u<0 (upper curve) the undesired peak sidelobe is independent of N because as we increase the number of the array elements, the mainlobe width of the spectrum of the truncation window becomes narrower. However, the mainbeam width of the pattern of the original real excitation is narrower as well, that is, the MLWR parameter almost remains constant with the increase in the number of the array elements. Therefore, the increase in the number of the array elements does not improve the mainbeam mis-match phenomenon in the realization of the ãnalytic excitation for an array antenna system.

3.4 Discussion and Summary

Based on above qualitative and quantitative analysis results, we could reach several statements related to radiation pattern of an array antenna system using ãnalytic excitation. They are stated as follows:

1. The far field radiation pattern produced by an ãnalytic excitation is inherently asymmetric, that is, the analytic signal theory can provide a generalized analytic method to design a practical desired asymmetric far field radiation pattern of an array antenna system.

2. In general, the asymmetric radiation pattern of an ãnalytic excitation has the advantages on every performance indices over the corresponding original broadside narrow beamwidth symmetric radiation pattern, except the peak sidelobe scenario. Therefore, a required low peak sidelobe of radiation pattern is implausible using a realizable ãnalytic excitation.

3. By adjusting the Main-Lobe Width Ratio (MLWR), and the peak sidelobe of the truncation window, we can obtain a design result. The larger the value of MLWR, the more advantages we obtain in the characteristics of HPBW, BW_{null}, directivity, radiation efficiency, and the lower the undesired peak sidelobe generated by the mainbeam mis-match which is

consequence of the periodic convolution in the realization of an ãnalytic excitation. However, the larger the value of MLWR, the higher the overall sidelobe level of the truncation window as well as the realized asymmetric radiation pattern. Therefore, the advantages are taken in the compromise between those pattern characteristics.

4. The increase in the number of array elements (N) does not affect the peak sidelobe scenario of the asymmetric radiation pattern of an ãnalytic excitation, because the parameter MLWR is normally independent from the number of array elements N.

5. The cause for producing the undesired peak sidelobe in the realization of an ãnalytic excitation explained earlier can be attributed to the realizable Hilbert transform that can not faithfully transform a radiation pattern. For the cases where the design of a desired radiation pattern can be started from a symmetric radiation pattern which has small amount of components in the u=0 direction, the utilization of the ãnalytic excitation will be found to be valuable.

The information extracted from the analysis results in this chapter provides both essential and valuable foundation for designing several practical array radiation patterns using the ãnalytic excitation, which will be developed in the following chapters.

CHAPTER IV

THE BROADSIDE NARROW BEAMWIDTH ASYMMETRIC SIDELOBE ARRAY RADIATION PATTERN DESIGN USING ANALYTIC EXCITATION

4.1 Introduction

To overcome the disadvantageous property of the Hilbert transformation in the realization of an ãnalytic excitation in the preceeding chapter, in this chapter, we exploit the utilization of the ãnalytic excitation which will generate useful broadside narrow beamwidth asymmetric sidelobe radiation patterns for an array antenna system.

The required shape of an antenna radiation pattern may very much depend on applications. There are many environmental situations where the asymmetric sidelobe radiation pattern is desired [28-34]. However, the design of an asymmetric sidelobe narrow beamwidth radiation pattern is not as straightforward as a symmetric radiation pattern. An iterative try and error numerical method is commonly adopted in dealing with such problems. This chapter will first present a new gneralized design concept, which combines the analytic signal concept and modulation theory, for designing the desired broadside narrow beamwidth asymmetric sidelobe radiation patterns of an array antenna system. Then, the design criteria and error analysis for the physical implementation of this generalized design concept will be carried out. Several practical design examples will show that the asymmetric sidelobe radiation patterns have various advantages over the symmetric radiation patterns, and the features of this design technique will be generalized. Finally, we will show that, by using the 2-D ãnalytic excitations and this design concept, an asymmetric sidelobe planar array radiation pattern can be obtained.

4.2. The Fundamental Theories for Designing a Broadside Narrow Beamwidth Asymmetric Sidelobe Array Radiation Pattern

Knowing that the realizable discrete-time Hilbert transformer can not handle the patterns which have a large amount of components around u=0 direction, we will derive a generalized modulated ãnalytic excitation which is generated by combining ãnalytic excitation and modulation theory, so as to shift the typical broadside narrow beamwidth radiation pattern off the u=0 and to reduce the distortion caused by the realizable Hilbert transfomation. As a result, we can generate a broadside narrow beamwidth radiation pattern which has a practical desired asymmetric sidelobe scenario.

Let's ideally assume that $J_r(n)$ is a real excitation for an N elements broadside linear array system, and its corresponding narrow beamwidth radiation pattern, denoted as $F_r(u)$, has a negligible response in the range $u_m<|u|<\pi$ (approximation to a beamlimited pattern). Then, in order to shift the pattern $F_r(u)$ off the u=0 direction, a modulated real excitation $J_{mr}(n)$ can be formed as

$$J_{mr}(n)=J_r(n)s(n) = J_r(n)\cos(u_c n) \tag{4.1}$$

where $s(n)=\cos(u_c n)$ represents a generalized sinusoidal excitation, where u_c is the modulation angle in radians. Due to the periodicity of the array pattern, the following condition is also assumed to be satisfied

$$[u_c + u_m] < \pi \tag{4.2}$$

Taking the discrete-time Fourier transform on both sides of Equation (4.1), and applying the modulation theory, the radiation pattern, denoted as $F_{mr}(u)$, of $J_{mr}(n)$ is

$$F_{mr}(u) = (1/2)[F_r(u-u_c)+F_r(u+u_c)] \tag{4.3}$$

Equation (4.3) shows that by applying modulation theory, we can shift a typical broadside narrow beamwidth radiation pattern away from u=0 direction. However, in order to eliminate one of the shifted patterns $[F_r(u-u_c)]$ or $[F_r(u+u_c)]$ presented in the visible range, we can apply the ãnalytic signal theory. Let's form a generalized modulated complex ãnalytic excitation $J_{ma}(n)$ as

$$J_{ma}(n) = J_{mr}(n) + jJ_{mi}(n) \tag{4.4}$$

where $J_{mi}(n)$ is the discrete-time Hilbert transform of $J_{mr}(n)$. Thus, $F_{mi}(u)$ denotes the pattern of $J_{mi}(n)$, and according to Equation (2.15),

$$F_{mi}(u) = \begin{cases} -jF_{mr}(u), & 0 < u < \pi \\ jF_{mr}(u), & -\pi \le u < 0 \end{cases}$$

Consider the facts that the pattern $F_r(u)$ corresponding to $J_r(n)$ is assumed to be beamlimited, and the value of u_c is set as Equation (4.2). Those assumptions assure that the pattern $F_{mi}(u)$ can be expressed as[1]

$$F_{mi}(u) = (1/2)[-jF_r(u-u_c) + jF_r(u+u_c)] \quad (4.5)$$

By taking Inverse Fourier transform of Equation (4.5), the excitation $J_{mi}(n)$ becomes

$$\begin{aligned} J_{mi}(n) &= (1/2)[-jJ_r(n)\ e^{ju_cn} + jJ_r(n)e^{-ju_cn} \\ &= J_r(n)\sin(u_cn) \quad (4.6) \end{aligned}$$

Then, the complex ãnalytic excitation in Equation (4.4) becomes

$$\begin{aligned} J_{ma}(n) &= J_{mr}(n) + jJ_{mi}(n) \\ &= J_r(n)[\cos(u_cn) + j\sin(u_cn)] \\ &= J_r(n)e^{ju_cn} \quad (4.7) \end{aligned}$$

By taking the discrete-time Fourier transformation, the narrow beamwidth radiation pattern, $F_{ma}(u)$, of the modulated ãnalytic excitation $J_{ma}(n)$ in Equation (4.7) is

---

[1] The error caused by the non-beamlimited (sidelobe component) of a typical array radiation pattern will be analyzed later.

$$F_{ma}(u) = F_r(u-u_c) \tag{4.8}$$

It is a single narrow beamwidth radiation pattern which remains within the visible range. Then, by using the phase shifting property of an array antenna system, the shifted pattern in Equation (4.8) can be shifted back, such that the boresight of the realized asymmetric sidelobe radiation pattern is pointed to the u=0 direction. That means, by controlling the parameter u_c, we can obtain a half-sided sidelobe radiation pattern (which is equivalent to saying that one of the two sides sidelobes can be eliminated) without sacrificing the system performance of an original broadside symmetric radiation pattern, provided that the sidelobe ratio of the original radiation pattern is reasonably low enough. Thus, the ãnalytic signal theory really provides a generalized theory for designing desired broadside narrow beamwidth asymmetric sidelobe radiation patterns of an array antenna system.

A generalized theory has been found to design narrow beamwidth asymmetric sidelobe radiation patterns, and will be explained in the following sections.

4.3 System Design Constraint

Using a modulated ãnalytic excitation, a portion of the half-side sidelobe of a broadside symmetric radiation pattern can be eliminated. The extent of sidelobe elimination depends on the value of the modulation angle u_c. However, from practical application points of view, the purpose of using such a modulated ãnalytic excitation is to reduce one of the two sides sidelobes in an array radiation pattern without sacrificing the system characteristics. Thus, the system design constraint is that the value of u_c is restricted to be exactly equal to half of the mainbeam width of the original broadside symmetric pattern ($u_c=BW_{null}/2$). Thus the basic concept of this design methodology is simply to shift the mainbeam of the radiation pattern to the pass-band of the spectrum of the realizable Hilbert transformer, and to position the first null of the pattern on the u=0, so as to reduce the distortion caused by the realizable Hilbert transformer about u=0, and to eliminate the sidelobe left on the reverse.

4.4 System Analysis and Performance Evaluation

With the constraint value of u_c, there are two factors that will determine the achievements of this design methodology. They are presented and analyzed as follows:

Consider a typical real even symmetric excitation $J_r(n)$ and its corresponding broadside symmetric narrow beamwidth radiation pattern $F_r(u)$ which is depicted in Figure 4.1(a). The modulated real excitation is then $J_{mr}(n)=J_r(n)\cos(u_c n)$ and its radiation pattern becomes $F_{mr}(u)=(1/2)[F_r(u-u_c)+F_r(u+u_c)]$. The pattern of $F_{mr}(u)$ with the modulation angle $u_c=(BW_{null}/2)$ can be further decomposed into mainbeam pattern and sidelobe pattern as depicted in Figure 4.1(b) and (c).

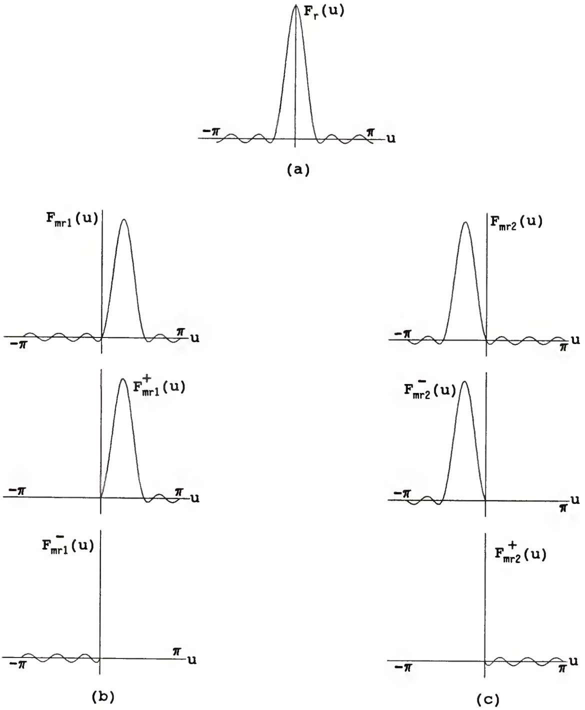

Figure 4.1 The decomposed mainbeam and sidelobe patterns of a real modulated excitation.
(a)The real symmetric pattern $F_r(u)$
(b)The $F_{mr1}(u)$ and its decomposed patterns.
(c)The $F_{mr2}(u)$ and its decomposed patterns.

Thus,

$$\begin{aligned} F_{mr}(u) &= (1/2)[F_r(u-u_c) + F_r(u+u_c)] \\ &= (1/2)[F_{mr1}(u) + F_{mr2}(u)] \\ &= (1/2)[F^{+}_{mr1}(u) + F^{-}_{mr1}(u) + F^{+}_{mr2}(u) + F^{-}_{mr2}(u)] \end{aligned} \tag{4.9}$$

where $F_{mr1}(u)=F_r(u-u_c)$, $F_{mr2}(u)=F_r(u+u_c)$, and

$$F^{+}_{mr1}(u)=\begin{cases} F_{mr1}(u), & 0<u<\pi \\ 0, & -\pi\le u<0 \end{cases} \qquad F^{-}_{mr1}(u)=\begin{cases} 0, & 0<u<\pi \\ F_{mr1}(u), & -\pi\le u<0 \end{cases}$$

$$F^{+}_{mr2}(u)=\begin{cases} F_{mr2}(u), & 0<u<\pi \\ 0, & -\pi\le u<0 \end{cases} \qquad F^{-}_{mr2}(u)=\begin{cases} 0, & 0<u<\pi \\ F_{mr2}(u), & -\pi\le u<0 \end{cases}$$

Then, the radiation pattern $F_{mi}(u)$ corresponding to the excitation which is the Hilbert transform of $F_{mr}(u)$ is

$$\begin{aligned} F_{mi}(u) &= -j\,\mathrm{sgn}(u)F_{mr}(u) \\ &= (-j/2)[F^{+}_{mr1}(u)+F^{+}_{mr2}(u)]+(j/2)[F^{-}_{mr1}(u)+F^{-}_{mr2}(u)] \end{aligned} \tag{4.10}$$

From Equation (4.9) and (4.10), the resulting asymmetric sidelobe radiation for the corresponding realizable modulated ãnalytic excitation, $F_{ma}(u)$, becomes

$$
\begin{aligned}
F_{ma}(u) &= F_{mr}(u) + jF_{mi}(u) \\
&= (1/2)[F^{+}_{mr1}(u) + F^{-}_{mr1}(u) + F^{+}_{mr2}(u) + F^{-}_{mr2}(u)] \\
&\quad + (1/2)[F^{+}_{mr1}(u)+F^{+}_{mr2}(u)] - (1/2)[F^{-}_{mr1}(u)+F^{-}_{mr2}(u)] \\
&= F^{+}_{mr1}(u) + F^{+}_{mr2}(u) \qquad (4.11)
\end{aligned}
$$

The first term on the right-hand side of Equation (4.11) represents the desired asymmetric sidelobe radiation pattern, and the second term is the undesired sidelobe which leaks into the desired asymmetric sidelobe radiation pattern. Thus, because of the sidelobe leakage effect, the first factor that influences the accomplishments of this design method is the sidelobe level of the original broadside symmetric pattern. The distortion caused by this sidelobe leakage effect indicates that the lower the sidelobe in the original symmetric radiation pattern $F_{mr}(u)$, the more advantages we gain in the resulting asymmetric sidelobe radiation pattern. The second factor is that the small amount of components in the shifted pattern $F_{mr}(u)$ around the u=0 will still be distorted by a realizable Hilbert transformer. However, due to the shifting of $F_{mr}(u)$, the amount of distortion is greatly reduced. Although the distortion appears to be unavoidable, it will be shown that the generation of an asymmetric sidelobe radiation pattern using a realizable modulated analytic excitation is both practical and valuable.

In evaluation of the performances of the asymmetric sidelobe radiation pattern, in addition to these characteristic indices defined in Section 3.3, Chapter III, there are two more characteristic indices which are required to assess the figure of merits of the asymmetric sidelobe radiation pattern compared to the original broadside symmetric radiation pattern of a linear array antenna system. These are defined as follows and the related parameters can be refered to Figure 4.2.

a. The peak sidelobe suppression gain (SSG_{peak}) is defined as the difference (dB) of the peak sidelobes between the original symmetric and the asymmetric sidelobe radiation patterns in the supressed side (u<0). Let u<0 represent the left-hand side, the SSG_{peak} can be expressed as

$$SSG_{peak}(dB) = SLL_{speak}(dB) - SLL_{apeak}(dB)$$

where SLL_{speak} and SLL_{apeak} denote the peak sidelobe of the symmetric and asymmetric patterns at the left-hand side (u<0).

b. The supressed radiation power ratio (SRPR) is defined as the ratio of the radiation powers of the asymmetric sidelobe radiation pattern to the original symmetric radiation pattern in the suppressed side (u<0). Mathematically, it can be expressed as

$$SRPR = \frac{\int_{-\pi}^{anull_1} |F_{ma}(u)|^2 \, du}{\int_{-\pi}^{snull_1} |F_r(u)|^2 \, du} \tag{4.12}$$

where the $F_{ma}(u)$ and $F_r(u)$ represent the asymmetric sidelobe and the symmetric radiation patterns, and $anull_1$ and $snull_1$ are the first null in the supressed side of $F_{ma}(u)$ and $F_r(u)$ with respect to the mainbeam.

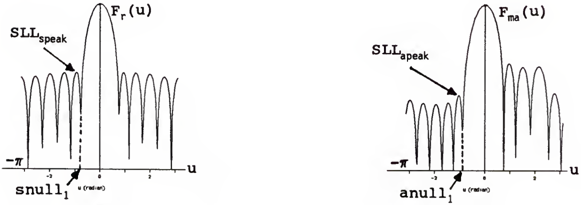

(a) (b)

Figure 4.2 The parameters used to define the SSG_{peak} and SRPR. (a)the SLL_{speak} and $snull_1$. (b)the SLL_{apeak} and $anull_1$

4.5 System Design Procedure

The design procedure of a broadside narrow beamwidth asymmetric sidelobe radiation pattern of an array antenna system using modulated ãnalytic excitation starts from a well-developed real excitation, and can be formally summaried as:

(a) Select a suitable real excitation $J_r(n)$ and evaluate its mainbeam width (BW_{null}).

(b) Form the real modulated excitation $J_{mr}(n)$ as given by Equation (4.1) with a modulating angle $u_c=(BW_{null}/2)$.

(c) Acquire the required modulated ãnalytic excitation $J_{ma}(n)$ as given by Equation (4.4) by carrying out the discrete-time Hilbert transform.

(d) Evaluate the system performance.

Since the ideal modulated ãnalytic excitation in Equation (4.7) is unobtainable, as long as the original symmetric radiation $F_{mr}(u)$ is not beamlimited, the acquisition of the modulated ãnalytic excitation $J_{ma}(n)$ in step (c) should be carried out as follows

$$J_{ma}(n) = J_r(n)\cos(u_c n)+j\{[J_r(n)\cos(u_c n)]*h(n)\}w(n) \quad (4.13)$$

where h(n) is the discrete-time Hilbert transform defined in Equation (2.18), and w(n) is a truncation window function. Thus, the realized asymmetric sidelobe radiation pattern, $F_{ma}(u)$, corresponding to the modulated ãnalytic excitation of $J_{ma}(n)$ in Equation (4.13) becomes

$$F_{ma}(u) = F_{mr}(u) + j[F_{mr}(u)H(u)]*W(u) \quad (4.14)$$

where $F_{mr}(u)$ is the pattern of $J_r(n)\cos(u_c n)$, and H(u) and W(u) are the spectrums of h(n) and w(n) respectively, and * indicats the discrete-time convolution. The purpose of the window function w(n) in realization of this asymmetric sidelobe radiation pattern as given by Equation (4.13) is the same as that in Chapter III. However, the effects of the truncation window on the asymmetric sidelobe radiation pattern are different from those discussed in Chapter III. The major difference is that there is no discontinuity in the shifted pattern $F_{mr}(u)$, and consequently, there is no roll-off region in the pattern $\{[F_{mr}(u)H(u)]*W(u)\}$. However, because of the convolution process, the spectrum of the window function will utimately leak into the pattern $[F_{mr}(u)H(u)]$, and result in a ripple on the waveform of $[F_{mr}(u)H(u)]$.

After recalling the effects of the truncation window in the realization of a modulated ãnalytic excitation, we can consider the question of what is the best selection of the truncation window under this circumstance. Here, the major concern is to eliminate one of two sides sidelobes of an array radiation pattern. Furthermore, the truncation window should have the negligible influence on the shape of $[F_{mr}(u)*H(u)]$, not only on the mainbeam but also on the sidelobe. In order to achieve this result, the more important characteristic of the spectrum of the desired truncation window (in addition to the narrow mainlobe width) is that the mainlobe should contain as much of the energy as possible and the sidelobe should decrease rapidly as u moves toward to π.[2] Thus, the solution of the best chosen truncation window in implementation of a realizable modulated ãnalytic excitation, in countrary to Chapter III,[3] converges to the Kaiser window [12,57,64] which is claimed to be an approximation to a class of functions called the prolate spheroidal wave functions [36] which possess the desired properties mentioned above. The Kaiser window is expressed as [57]

---

[2] This is because a window function that has this property produces the least amount of ripple on the convolved waveform.

[3] The major concern in Chapter III is to seek a window function which has minimun mainlobe width given a peak sidelobe ratio, in order to reduce the roll-off region at the discontinuity of a spectrum. That leads to the Dolph-Chebyshev window function as the best selection.

$$w_k(n) = \frac{I_0[\beta(1-[2n/(N-1)]^2)^{1/2}]}{I_0[\beta]}, \; -((N-1)/2) \le n \le ((N-1)/2) \tag{4.15}$$

where N is odd, and $I_0[\cdot]$ represents the modified Bessel function of first kind of order zero, and ß is a constant that determines the tradeoff between the peak sidelobe and the mainlobe width. The larger the ß, the lower the sidelobe, and the wider the mainlobe width of the spectrum. It should be noted that when ß=0, the Kaiser window becomes the uniform rectangular window.

There is an additional point that needs to be considered. If the value of u_c is given as the first null of the original selected symmetric pattern with some tolerance, then, the shifted pattern $F_{mr}(u)$ corresponding to $J_r(n)\cos(u_c n)$ will have component exactly at the u=0 that will produce a noticable distortion due to the realizable Hilbert transformer. Therefore, in order to allow for some error in the value of u_c in the physical calculation of the modulated ãnalytic excitation, the procedure used to compute the modulated ãnalytic excitation in Equation (4.13) can be judiciously modified as

$$J_{ma}(n)=J_r(n)\sin(u_c n) + j\{[J_r(n)\sin(u_c n)]*h(n)\}w(n) \tag{4.16}$$

That is, instead of $\cos(u_c n)$, the real excitation $J_r(n)$ is modulated by $\sin(u_c n)$. Then, with a typical real even symmetric excitation $J_r(n)$, $J_r(n)\sin(u_c n)$ is always an odd symmetric excitation for any specific value of u_c, and its corresponding pattern will exactly have no component at u=0. That is, this modification assures that the pattern which will be transformed by a realizable Hilbert transformer has zero component at u=0, and consequently, minimize the distortion caused by the realizable Hilbert transformer. It is trivial to show that the modification of the modulated ãnalytic excitation in Equation (4.16) does not change the shape or characterictics of the asymmetric sidelobe radiation pattern as indicated in Equation (4.14), except a phase constant that does not affect any shape or performances of a desired pattern.

There are three parameters that allow us to consider to generate the asymmetric sidelobe radiation pattern. They are the number of the array elements (N), the peak sidelobe of the original symmetric pattern, and the characteristics of the truncation window. Normally, the number of array elements does not affect the sidelobe level, provided that N is large enough. Thus, once the best choice of window function is determined, the levels of the sidelobes in the realized asymmetric sidelobe pattern will be controlled by the original selected symmetric patterns. A rule of thumb design strategy will be demonstrated in the following design Example 2.

4.6 Design Examples

Example 1 For demonstration of the generation of an asymmetric sidelobe radiation pattern utilizing the modulated ãnalytic excitation, we use the Hamming excitation $J_h(n)$ (refer to Example 1, Chapter III) as an original real symmetric excitation, the number of array elements is kept the same as that used in Chapter III, N=21, and the truncation window is Kaiser $w_k(n)$ with $\beta=0$. First, the mainbeam width of the array radiation pattern excited by $J_{ham}(n)$ is computed to be $BW_{null}=1.359$(rad). Then, the modulated real excitation is $J_{mr}(n)=[J_{ham}(n)\sin(0.679n)]$. Following the design procedures described in previous Section 4.5, the corresponding realizable modulated ãnalytic excitation $J_{ma}(n)$ as given by Equation (4.16) can be obtained by carrying out the Hilbert transform and truncation process. The original symmetric Hamming pattern and the shifted radiation pattern $F_{ma}(u+u_c)$ ($u_c=0.679$) corresponding to the realized modulated ãnalytic excitation $J_{ma}(n)$ are plotted together in Figure 4.3. By examining the shape of the pattern $F_{ma}(u+u_c)$ in Figure 4.3, we find that the sidelobe in the range of $u<0$ has been greatly suppressed. Furthermore, it is interesting to compare the asymmetric pattern in Figure 4.3 with the asymmetric pattern in Figure 3.8(b). Both patterns are excited by an ãnalytic excitation generated by using Hamming excitation as an original real excitation. We find that the undesired high peak sidelobe in the $u<0$ range in Figure 3.8(b) disappears in

Figure 4.3. The improvement is actually attributed to the modulation theory which has been applied to the ãnalytic excitation that produces the asymmetric sidelobe radiation pattern of Figure 4.3. In other words, the disadvantageous property of an asymmetric radiation pattern occured in Chapter III can be overcome by applying modulation theory.

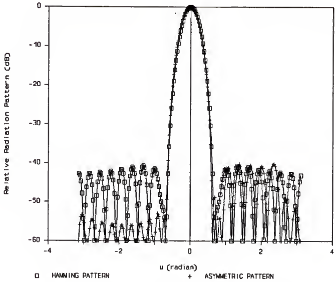

Figure 4.3 The Hamming $F_{ham}(u)$ and the corresponding realized asymmetric sidelobe $F_{ma}(u+u_c)$ radiation patterns.
(N=21, and tuncation window is Kaiser with ß=0)

Table 4.1 The characteristics of the radiation patterns excited by Hamming and the corresponding modulated ãnalytic excitations. (N=21)

Type of pattern	HPBW (Rad)	BW_{null} (Rad)	D (None)	η (None)	**SLL_{peak} (dB)**	SLR_{peak} (dB)	SSG (dB)	**SRPR (dB)**
$F_{ham}(u)$	.401	1.359	14.885	.709	-40.64	-40.64	-12.4	41.6
$F_{ma}(u+u_c)$	.404	1.312	14.697	.700	**-53.07**	-40.29	12.4	**-41.6**

Table 4.1 lists the characteristics of the radiation patterns for which $F_{ham}(u)$ represents the pattern excited by Hamming function and $F_{ma}(u+u_c)$ represents the pattern of the realized asymmetric sidelobe radiation pattern. By comparing the quantitative results of the two patterns listed in Table 4.1, we find that those system performances of the original symmetric pattern are almost maintained in the realized asymmetric sidelobe pattern, except the peak sidelobe at the left-hand side region (SLL_{peak}), where the asymmetric sidelobe radiation pattern has tremendous advantage over the original symmetric pattern by lower than 12.4dB (SSG_{peak}=12.4dB). Moreover, the suppressed radiation power (SRPR) in the supressed side ($u<0$) of the asymmetric sidelobe pattern is 41dB lower than that of the original symmetric pattern. This characteristic shows one of the reasons why the asymmetric sidelobe radiation pattern is attractive for the areas where interferences come from wide range of angle in the space. Moreover, this example demonstrates the fact that the foregoing ãnalytic signal theory really can provide an effective method to design a desirable asymmetric sidelobe radiation pattern. In the next design example, we will show a design strategy for generating a practical and useful asymmetric sidelobe radiation pattern.

Example 2 In this design example, by using the sampled Taylor aperture distribution, we will show how to design an asymmetric sidelobe radiation pattern using modulated analytic excitations that are practical and useful. Then, the performance comparisons are made between the symmetric radiation pattern excited by the sampled Taylor aperture distribution and the realized aymmetric sidelobe radiation pattern. The reasons for choosing the sampled Taylor aperture distribution in this design example are that it not only provides a flexible method to obtain various sidelobe levels of array radiation patterns but also is widely adopted in the practical realization of an array antenna system, because it has higher directivity as well as excitation (radiation) efficiency than the Dolph-Chebyshev array system.

It was recognized that the continuous counterpart (aperture distribution) of the Dolph-Chebyshev array system is physically unrealizable [20]. By changing the locations of the zeros of the radiation pattern, Taylor was able to modify the uniform aperture distribution to approximate the Dolph-Chebyshev aperture distribution. The Taylor pattern can be expressed as [20]

$$F(z,A,\bar{n}) = \frac{\left(\frac{\sin \pi z}{\pi z}\right) \prod_{n=1}^{\bar{n}-1} \left\{1-\frac{z^2}{\sigma^2[A^2 + (n-(1/2))^2]}\right\}}{\prod_{n=1}^{\bar{n}-1} \left(1-\frac{z^2}{n^2}\right)} \qquad (4.17)$$

where $z=(L/\lambda)\cos\theta$, with L the length of the aperture in units of wavelength, θ the angle measured from the endfire direction, and λ is the wavelength. The shape of the Taylor pattern is clearly understandable by examining Equation (4.16). The term $(\sin \pi z/\pi z)$ in the numerator is the typical uniformly excited aperture pattern, which has zeros at $\pm n$, $n=1,2,3,\cdots,\infty$. Then, the first $(\bar{n}-1)$ pairs of inner nulls of $(\sin \pi z/\pi z)$ are to be modified, so that the first $(\bar{n}-1)$ pairs of inner peak sidelobes of the pattern $(\sin \pi z/\pi z)$ are converted to the desired Dolph-Chebyshev equal peak sidelobe scenario. Thus, the product term in the denominator

$$\prod_{n=1}^{\bar{n}-1} \left(1- \frac{z^2}{n^2}\right)$$

is used to remove the first $(\bar{n}-1)$ pairs of inner zeros of function $(\sin \pi z/\pi z)$. These removed nulls are replaced by the zeros of the product term in the numerator

$$\prod_{n=1}^{\bar{n}-1} \left\{1- \frac{z^2}{\sigma^2[A^2+(n-(1/2))^2]}\right\} \tag{4.18}$$

which is derived from the Dolph-Chebyshev array pattern by letting the number of array elements to be indefinitely increased, where A is an adjustable real parameter such that $(\cosh \pi A)=b$, with b the desired voltage sidelobe ratio, and σ is defined by

$$\sigma = \frac{\bar{n}}{[A^2 + (\bar{n}-(1/2))^2]^{1/2}}$$

The aperture distribution corresponding to the Taylor pattern as given by Equation (4.17) can be obtained by using the Fourier transform relations between the aperture distribution and the far field pattern. After doing so, the aperture distribution, $J(x)$, is found to be

$$J(x) = (1/L)\{1 + 2 \sum_{m=1}^{\bar{n}-1} [F(m,A,\bar{n}) \cos(2\pi mx/L)]\}, \quad |x| \leq (L/2) \tag{4.19}$$

where $F(m,A,\bar{n})$ is defined in Equation (4.17), with z replaced by m. From Equation (4.17), the shape of the Taylor pattern is fully specified by two parameters, $\bar{n}$ and A. The required value of $\bar{n}$ for different levels of sidelobes can be obtained from Taylor [20, p.23, Table II]. In this design example, $\bar{n}$ is set to 4, which is chosen to cover the sidelobe levels from 0dB to 30dB, unless otherwise specified.

Applying the aperture sampling method [65-66], the continuous Taylor aperture distribution can be applied to an array antenna as well. Consider an array of (N+1) (N is even) elements with interelement distance d whose unit is wavelength, then the length of an aperture is assumed to be L=(N+1)d, so that the length of the aperture extends a distance (d/2) over the two ends of the array. Thus, the array excitation $J_r(n)$ corresponding to the Taylor aperture distribution are the sampled values of $J(x)$, that is $J_r(n)=J(x_n)$, where

$$x_n = nd, \qquad n = 0, \pm 1, \pm 2, \pm 3, \cdots, \pm(N/2) \qquad (4.20)$$

Using the sampled Taylor aperture distribution, and with the number of array elements N=21, a Taylor pattern for the case of 25dB peak sidelobe with $\bar{n}=4$ is plotted in Figure 4.4(a). With the same parameters of N and $\bar{n}$, the BW_{null} of the Taylor patterns with peak sidelobes from 20dB to 30dB are plotted in Figure 4.4(b).

Having acquired the Taylor excitation,[4] we are able to design various desired asymmetric sidelobe radiation patterns. Let's keep the number of array elements to be 21. The design goal here is assumed to meet the practical applications. That is, the levels of the peak sidelobes on both sides of the radiation pattern vary from 20dB to 35dB. However, it allows the two sides of the sidelobes to be asymmetric.[5] After an experimental judgement, we could start to establish the design

---

[4] Hereafter, the Taylor excitation will be used to represent the sampled Taylor aperture distribution for an array antenna system.

[5] The most practical case is that one of the sidelobes be about 20dB, and the other side to be variable. However, the lower the sidelobe, the poorer the excitation (radiation) efficiency. Therefore, a very low sidelobe level is also impractical.

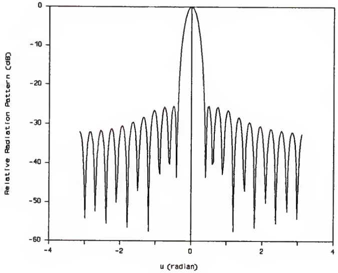

(a)

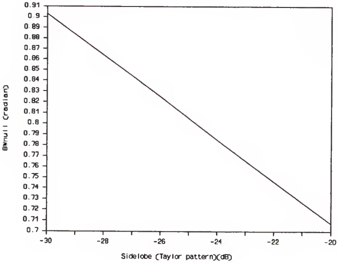

(b)

Figure 4.4 The 25 dB Taylor pattern and mainbeam widths.

(a) The Taylor pattern with N=21, $\bar{n}$=4, SL_{peak}=25dB.
(b) The BW_{null} of the Taylor pattern with N=21, $\bar{n}$=4, and SL_{peak} from 20dB to 30 dB.

information which contains the relations between the levels of the asymmetric sidelobes (SLL_{peak} or SLR_{peak}) and the symmetric Taylor patterns with various peak sidelobes. That is, by changing the sidelobes of the Taylor patterns from 21dBto 27dB, and applying the procedures for generating the corresponding modulated ãnalytic excitation and the asymmetric sidelobe patterns described in Section 4.5, for which the required values of u_c can be obtained from Figure 4.4(b), and Kaiser truncation window with ß=0,[6] the various asymmetric sidelobe levels (SLL_{peak} and SLR_{peak}) corresponding to the symmetric Taylor patterns can be obtained and are plotted in Figure 4.5, where SLL_{peak} and SLL_{peak} symbolize the left and right side of the peak sidelobes in unit of dB of the asymmetric sidelobe radiation pattern.

From the system design point of view, we should be able to acquire the array excitation which produces the desired asymmetric sidelobe radiation pattern. Let's use a practical requirement as an example to show how to obtain the array excitation of an asymmetric sidelobe radiation pattern. Assume that the requirements of the sidelobe levels of the radiation pattern of an array antenna system are (SLL_{peak}=35dB) and (SLR_{peak}>20dB). Then, from the results plotted in Figure 4.5,

---

[6] We can also vary ß to control the level of the asymmetric sidelobe. However, the larger the ß, the more distortion the asymmetric pattern. ß=0 shows the best result in the realization of a practical useful modulated ãnalytic excitation.

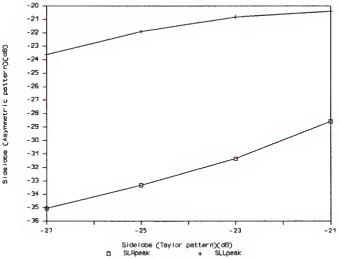

Figure 4.5 The relations of the asymmetric sidelobes SLL_{peak} and SLR_{peak} and the Taylor patterns with various peak sidelobes.

we find that using 27dB peak sidelobe of Taylor pattern as an original symmetric pattern and the Kaiser truncation window with $\beta=0$ can generate an asymmetric radiation pattern whose sidelobe levels satisfy the system requirements. Thus, the Taylor excitation $J_r(n)$ can be calculated by using Equation (4.19) and (4.20). The corresponding modulated analytic excitation $J_{ma}(n)$ is then computed from Equation (4.16) with $u_c=0.424$(radian) which is obtained from Figure 4.4(b) (half of the BW_{null} of 27dB Taylor pattern), and the truncation window is Kaiser with $\beta=0$. The resulting shifted (35/23) asymmetric sidelobe radiation pattern[7] and the 35 dB Taylor pattern (N=21, $\bar{n}=5$) are plotted together in Figure 4.6 for comparison (will be discussed later), and the analytic excitation for the (35/23) asymmetric sidelobe radiation pattern is tabulated in Table 4.2. For the shifted (35/23) asymmetric sidelobe radiation pattern as plotted in Figure 4.6, the phase in each array excitation is the sum of the tabulated value and nu_c, where $u_c=0.424$(radian). The quantitative characteristics of the realized shifted (35/23) asymmetric sidelobe radiation pattern and the 35 dB Taylor pattern are listed in Table 4.3.

---

[7] Let (SLL_{peak}/SLR_{peak}) be used to symbolize the left-hand side and right-hand side peak sidelobes with respect to the main beam of an arbitrary radiation pattern. Thus, (35/23) indicates the 35dB and 23dB peak sidelobes at the left-hand and right-hand sides of an asymmetric sidelobe radiation pattern respectivity.

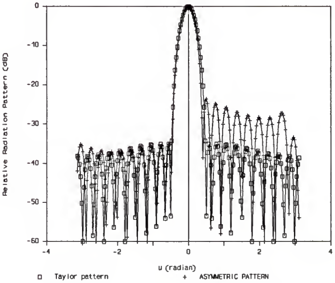

Figure 4.6 The realized shifted (35/23) asymmetric sidelobe and the Taylor symmetric sidelobe (35dB) radiation patterns.(N=21).

Table 4.2 The analytic excitation for (35/23) asymmetric sidelobe radiation pattern. [N=21, $J_{ma}(-n)=J^*_{ma}(n)$].

array number	$J_{ma}(n)$	
n	amplitude	phase
0	1.019	90.000
1	.988	-65.715
2	.964	-42.242
3	.891	-17.021
4	.809	5.891
5	.718	31.796
6	.594	54.641
7	.515	80.217
8	.381	-74.164
9	.349	-50.966
10	.282	4.958

Table 4.3 The characteristics of the shifted (35/23) asymmetric sidelobe and (35/35) Taylor symmetric sidelobe radiation patterns.

type of pattern	HPBW (Rad)	BW_{null} (Rad)	D (None)	η (None)	SLL_{peak} (dB)	SLR_{peak} (dB)
(35/23)	.334	.884	18.114	.863	-35.045	-23.629
Taylor(35)	.353	.997	16.971	.808	-35.046	-35.046

Let's assume that the requirement of a broadside array antenna system on the sidelobes can be stated as follows: one side of the sidelobes is required to achieve the level indicated as SLL_{peak}, while the other side of the peak sidelobes can be a specific level which is higher than SLL_{peak}. That is, the peak sidelobe in left-hand side with respect to the mainbeam is required to be lower than that of right-hand side. Further assume that the (SLL_{peak}/SLR_{peak}) asymmetric radiation pattern can satisfy the system requirement. Thus, in order to satisfy the system peak sidelobe requirements, the symmetric Taylor pattern should be designed with the symmetric peak sidelobe of SLL_{peak}. The fair comparison is then made between the symmetric Taylor pattern with peak sidelobe of SLL_{peak} and an asymmetric sidelobe pattern with sidelobe (SLL_{peak}/SLR_{peak}). Using the patterns plotted in Figure 4.6 and the results listed in Table 4.3, let's compare the (35/23) asymmetric sidelobe pattern to the Taylor pattern with peak sidelobe 35dB. It is obvious that the asymmetric sidelobe radiation pattern, as expected, has a substantial amount of advantages in all characteristic indices over the symmetric Taylor pattern. The incremental beamwidth resolutions, directivity, and excitation (radiation) efficiency of the asymmetric sidelobe radiation pattern can be attributed to having let the sidelobes on the right side rise from the level SLL_{peak} to the level SLR_{peak}.

The consequences of the design examples show that the proposed design method does not allow a strong control on the right-hand side sidelobe (SLR_{peak}) of an asymmetric sidelobe pattern due to the convolution process. However, the result is close enough to achieve the most practical utilization of the asymmetric sidelobe radiation pattern, and it is reasonable to have a conclusion that the design methodology using a modulated ãnalytic excitation provides an effective and straightforward method to produce a desirable broadside narrow beamwidth asymmetric sidelobe radiation pattern. As long as a practical asymmetric radiation pattern is concerned, the design procedures described above are generalized. For instance, those procedures can be applied to a Dolph-Chebyshev array system and the same results can be obtained. In the following sections, we extend this design concept in the linear array system to the 2-D planar array system.

4.7 The Generation of Narrow Beamwidth Asymmetric Sidelobe Planar Array Radiation Pattern

The 2-D ãnalytic signals whose spectrums are either half-plane or quadrant-plane and their associated Hilbert transformers have been defined and derived in Chapter II. Once, the key transformation tool--Hilbert transformer has been obtained, the general theory, system analysis and design procedures involved in the generation of an asymmetric sidelobe planar array pattern using the concept of the modulated ãnalytic excitation are theoretically the same as those applied in the linear array system, because the properties of a realizable 2-D Hilbert transformer and the modulation theory remain the same in the 2-D case. Nevertheless, we want to show that this design methodology can be extended to the plannar array system as well. However, we will omit the details of the fundamental theory and system analysis,[8] and directly get into the generation of the planar asymmetric sidelobe patterns.

---

[8] Since they are the same as the linear case, except some symbolic manipulation.

4.7.1 The generation of half-plane asymmetric sidelobe radiation pattern using Type-II ãnalytic excitation

Let's first consider the case that we want to generate a half-plane asymmetric sidelobe radiation pattern in the u plane. Thus, let's assume that we are given a 2-D real excitation $J_r(m,n)$ whose pattern is denoted as $F_r(u,v)$. Using the same concept in the linear array system, in order to minimize the distortion caused by the realizable 2-D Hilbert transformer (Type II) around the line of u=0, and to eliminate the half-plane sidelobe, we can generate a 2-D modulated real excitation as

$$J_{mr}(m,n) = J_r(m,n)\sin(u_c n) \qquad (4.21)$$

where u_c is the angle(in radians) of the half mainbeam width of the $F_r(u,v)$ at u plane. Thus, applying the modulation property of the Fourier transform, the pattern corresponding to the excitation in Equation (4.21), denoted as $F_{mr}(u,v)$, is

$$F_{mr}(u,v) = (j/2)[F_r(u+u_c,v) - F_r(u-u_c,v)] \qquad (4.22)$$

That is, the original pattern $F_r(u,v)$ has been shifted off the line of u=0 by the modulation process. Then, by using the Type-II Hilbert transformer and a suitable window function, we can obtain a 2-D modulated ãnalytic excitation $J_{ma}(m,n)$ as

$$J_{ma}(m,n) = J_{mr}(m,n) + j\{[J_{mr}(m,n)**h_{II}(m,n)]w(m,n)\} \qquad (4.23)$$

where ** indicates the 2-D discrete-time convolution, $h_{II}(m,n)$ is the impulse response of the type II Hilbert transformer, and $w(m,n)$ is the 2-D truncation window. Note that because $h_{II}(m,n)$ as given by Equation (2.55) is equivalent to $h(m)$, the convolution in Equation (4.23) can be carried out as a 1-D convolution and $w(m,n)$ becomes $w(m)$. Thus, the best choice of the truncation window $w(m)$ should be the same as that discussed in the linear array system, that is, it is the Kaiser window with $\beta=0$. Accordingly, the resulting radiation pattern, denoted as $F_{ma}(u,v)$, corresponding to the 2-D modulated ãnalytic excitation $J_{ma}(m,n)$ in Equation (4.23) should have a suppressed sidelobe in $u<0$ half-plane, and should gain various advantages compared to the conventional symmetric planar array pattern. Let's first use a nonseparable 2-D circular Kaiser window function as a symmetric planar array excitation to illustrate the generation of a desired half-plane asymmetric sidelobe array pattern using the methodology discussed above.[9] The equivalent 2-D nonseparable circular Kaiser excitation can be expressed as [61]

$$J_r(m,n) = w_k(m,n) = \begin{cases} \dfrac{I_o[\alpha(1-[(m^2+n^2)/25])^{1/2}]}{I_o^2[\alpha]}, & m^2+n^2 \leq 25 \\ 0, & \text{otherwise.} \end{cases} \tag{4.24}$$

---

[9] This example is for demonstration only, due to the very poor excitation (radiation) efficiency of the heavily tapered Kaiser window.

where $I_0[\cdot]$ is the modified Bessel function of the first kind of order zero, and α is the parameter used to adjust the sidelobe level and the mainbeam width. With $\alpha=4$ and $m=n=5$, the symmetric planar radiation pattern is plotted in Figure 4.7(a), where the sidelobe level is about 30dB. The contour of the 3dB beamwidth (HPBW) of the symmetric Kaiser planar pattern is ploted in Figure 4.7(b). The corresponding realized half-plane asymmetric sidelobe pattern $F_{ma}(u,v)$ and its 3dB beamwidth (HPBW) contour are plotted in Figure 4.7(c) and (d) respectively. As seen from Figure 4.7(c), the sidelobe of the planar pattern $F_{ma}(u,v)$ in the $u<0$ half-plane has been greatly suppressed, and its peak sidelobe levels become 38dB and 27dB in the $u<0$ and $u>0$ half-planes respectively. However, by comparing the contour plots in Figure 4.6(b) and (d), we find that the 3dB beamwidth (HPBW) of the realized asymmetric sidelobe planar pattern remains the same as (at least very close to) that of the original symmetric planar array pattern, except the shifted mainbeam maximum due to the modulation process.

Next, by applying the principle of separability of the planar array excitation in Equation (3.14), we can form a symmetric planar pattern as

$$F_r(u,v) = [F_r(u)F_r(v)] \tag{4.25}$$

where $F_r(u)$ and $F_r(v)$ are assumed to be the Taylor pattern with $\bar{n}=4$ and 27dB sidelobe level. Let the number of the array elements be (11x11). The symmetric Taylor planar pattern generated by using Equation (4.25) and its 3dB beamwidth contour plot are plotted in Figure 4.8(a) and (b), and the corresponding asymmetric sidelobe planar array pattern and its 3dB beamwidth (HPBW) contour plot are plotted in Figure 4.8(c) and (d).

By comparing Figure 4.8(a), (b) to Figure 4.8(c), (d) respectively, we can find the same results as shown in previous Kaiser circular planar array patterns. That is, the planar array pattern excited by the corresponding modulated ãnalytic excitation has a suppressed sidelobe in the u<0 half-plane and has about the same 3dB beamwidth as the original symmetric Taylor planar pattern. It is interesting to note that the asymmetric sidelobe levels which appear in Figure 4.8(c) are 34.5dB and 22.5dB in the u<0 and u>0 half-planes, which is close enough to the results of the linear array system (refer to Example 2 in Section 4.6). Thus, it is reasonable to conclude that the analysis results and the design procedures of an asymmetric sidelobe pattern in the linear array system can be applied to the half-plane asymmetric sidelobe planar array pattern, provided that the excitation for a planar array system is separable.

4.7.2 The generation of quadrant-plane asymmetric sidelobe radiation pattern using Type I ãnalytic excitation

There are two kinds of Type I 2-D ãnalytic excitations which correspond to the ãnalytic signals of Case 1a and 1b in

Chapter II respectively. The generation of the Type I ãnalytic excitation of Case 1a involved two stages of transformations (refer to Figure 2.6). However, as far as the excitation (radiation) efficiency of an array excitation is concerned, we found that the ãnalytic excitation of Case 1a is physically inapplicable in the realization of the quadrant-plane asymmetric sidelobe planar array radiation patterns since the excitation at the output of the first transformation in Figure 2.6 is formed by directly substracting two real excitations (not quadratually) that will greatly reduce the efficiency of the realized array excitation. However, by using the Case 1b ãnalytic excitation which is equivalent to applying the pattern multiplicative theory of the array antenna system, a quadrant-plane asymmetric sidelobe planar array radiation pattern can be easily realized, and consequently, the generation of a quadrant-plane asymmetric sidelobe planar pattern is nothing more than the generation of two asymmetric sidelobe linear array patterns. For purpose of the conceptual simplicity, we will not further simulate the quadrant-plane asymmetric sidelobe planar array pattern, as long as the pattern multiplicative concept is applied.

4.8. Discussion and Summary

There are two major contributions in this chapter. First, the potential advantages of the asymmetric sidelobe array patterns compared to the conventional symmetric array patterns have been quantitatively shown. Second, an effective and analytic method has been introduced to the design of the desired broadside narrow beamwidth asymmetric sidelobe radiation patterns. It is the philosophy of associating the modulation theory and the analytic signal concept that makes the design of an asymmetric sidelobe broadside array radiation pattern so straightforward. Finally, it is found that the design concept and procedures for an asymmetric sidelobe linear array radiation pattern can be extended to the design of a half-plane asymmetric sidelobe planar array radiation pattern.

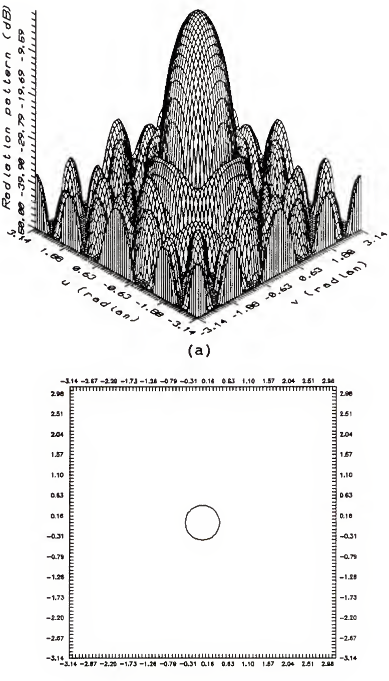

Figure 4.7 The nonseparable Kaiser circular and the corresponding half-plane asymmetric sidelobe planar array patterns.
(a) The symmetric Kaiser planar array pattern.
(b) The 3dB beamwidth contour plot of (a).
(c) The half-plane asymmetric sidelobe array pattern.
(d) The 3dB beamwidth contour plot of (c).

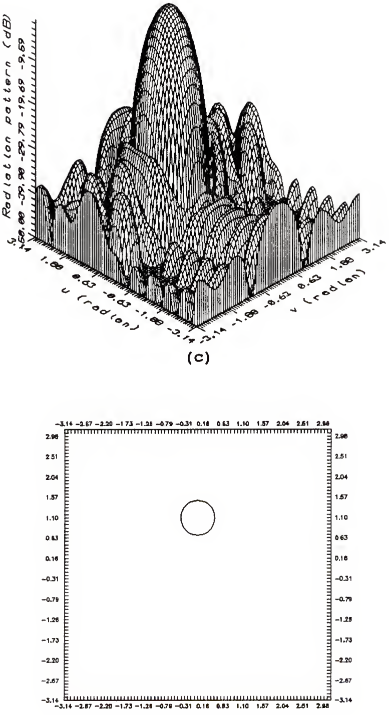

(c)

(d)

Figure 4.7 --- continued

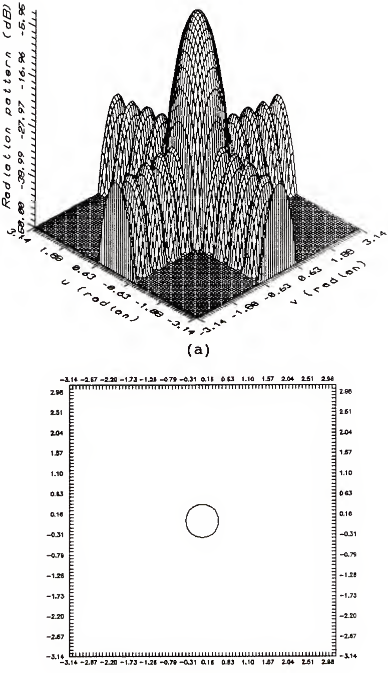

(a)

(b)

Figure 4.8 The 11x11 separable Taylor and the corresponding half-plane asymmetric sidelobe planar array patterns.
(a)The symmetric Taylor planar array pattern.
(b)The 3dB beamwidth contour plot of (a).
(c)The half-plane asymmetric sidelobe array pattern.
(d)The 3dB beamwidth contour plot of (c).

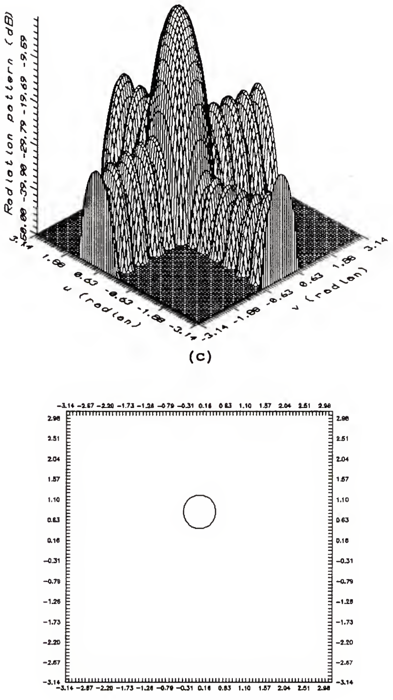

(c)

(d)

Figure 4.8 --- continued

CHAPTER V

THE SHAPED BEAM ARRAY ANTENNA RADIATION PATTERN DESIGN USING ANALYTIC EXCITATION

5.1 Introduction

By extending the design concept and technology in the preceeding chapter, we proceed to design the shaped beam radiation patterns of an array antenna system using an ãnalytic excitation.

In addition to the narrow beamwidth radiation pattern, the design of the wide angle shaped beam radiation pattern is another important subject in the area of antenna system. For instance, a cosecant-squared ($\csc^2\theta$) power radiation pattern is widely applied in the ground-mapping and air-search radar systems. The most popular methods used in realization of a shaped beam pattern were the Fourier series expansion and the Woodward's voltage pattern sampling method [7,21,35] which result in a minimum mean-square-error (MMSE) approximation to the desired shaped beam pattern. Several design methods for improving the shape of either a voltage or a power shaped beam pattern using iterative numerical methods have been found in the literature [37-42]. Since the polynomial representation of an asymmetric shaped beam pattern is normally complex, the design of a shaped beam pattern using numerical iterative method is not as effective and straightforward as the symmetric pattern which can always be represented as a real polynomial. For a large array system, the procedures become very ineffective, cumbersome and sometimes impossible. Moreover, the usual wide shaped beamwidth further exacerbates the fundamental difficulties in designing the shaped beam pattern using iterative numerical method, and skill and luck are often required in the numerical manipulation.

In this chapter, a totally new method is introduced for designing a typical shaped beam pattern using an ãnalytic excitation. It will be shown that this design method has greatly alleviated the computational effort, and has provided an idea to effectively apply the well-developed equiripple (or minimax) design criterion in the realization of an asymmetric shaped beam pattern. Furthermore, the inherent distortion which results from a realizable Hilbert transformer can be minimized, and a desirable asymmetric sidelobe shaped patttern can be easily generated. Thus, this design methodology is increasingly attractive from the points of view of practical utilization of the shaped beam pattern of an array antenna system.

5.2 The Basic Concepts for Shaped Beam Radiation Pattern Design using Analytic Excitation

A desired shaped beam radiation pattern is always ill-defined, and the design of a shaped beam pattern becomes an approximation problem. The concepts of designing a shaped beam radiation pattern using an analytic excitation are first realizing a symmetricalized desired shaped beam pattern, secondly applying the analytic signal theory to eliminate the half side of the symmetricalized shaped beam pattern, and thirdly, following the phase shifting property of the array antenna system to shift the realized shaped beam pattern back to the required angular position.

Assume a typical desired shaped beam pattern of an N=2M+1 elements array system, denoted as $F_d(u)$, with shaped beamwidth u_s depicted as in Figure 5.1(a), where without loss of any generality, $F_d(u)$ is assumed to be real, and its starting angle of the shaped region is assumed to be exactly positioned at $u=0$. Then, the symmetricalized shaped beam pattern, denoted as $F_{ds}(u)$, can be expressed as

$$F_{ds}(u) = \begin{cases} F_d(u-u_c), & 0 < u < \pi \\ 0, & u=0 \\ F_d(-u-u_c), & -\pi \leq u < 0 \end{cases} \tag{5.1}$$

where the value of u_c is required to allow a roll-off region[1] which occurs in the realization of $F_{ds}(u)$ and to eliminate the distortion caused by the realizable Hilbert transformer (will be discussed in next section). The symmetricalized shaped beam pattern as given by Equation (5.1) can be depicted as in Figure 5.1(b),

---

[1] The roll-off region here is defined as the angular width between the first null and the desired magnitude of the realized pattern (or spectrum).

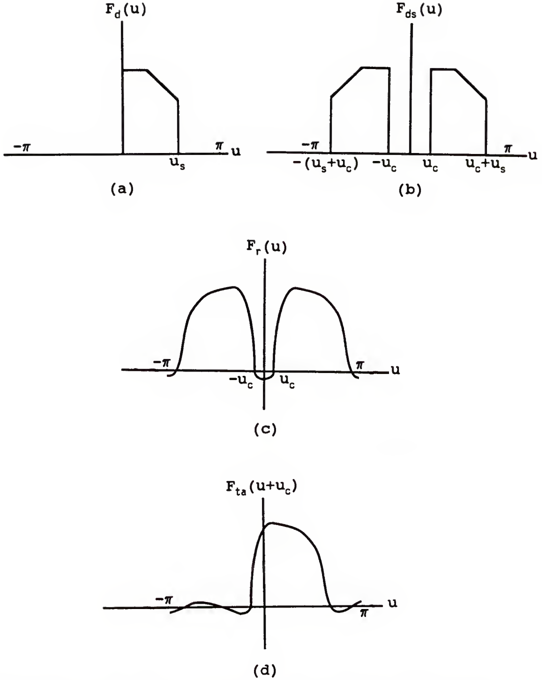

Figure 5.1 Sketches of the desired shaped beam, the symmetricalized shaped beam pattern and the realized shaped beam pattern.

(a) The ideal desired shaped beam pattern $F_d(u)$.

(b) The symmetricalized shaped beam pattern $F_{ds}(u)$.

(c) The realized symmetricalized shaped beam pattern $F_r(u)$.

(d) The realized shaped beam pattern $F_{ta}(u+u_c)$.

After the symmetricalization process and according to the property of the discrete-time Fourier transform, the excitation for the symmetricalized shaped beam pattern, denoted as $J_{ds}(n)$, should be real and symmetric. Thus, the array shaped beam pattern $F_{ds}(u)$ in Equation (5.1) can be expressed as

$$F_{ds}(u) = \sum_{n=0}^{\infty} a(n)\cos(un) \tag{5.2}$$

where $a(0)=J_{ds}(0)$ and $a(n)=2J_{ds}(n)$ for $n\neq 0$. Note that a desired shaped beam pattern may only be realized with an infinite number of array elements. From the mathematical representation of the symmetricalized shaped beam pattern as given by Equation (5.2), it is easy to see that the symmetricalization process not only converts the complex polynomial representation of an asymmetric shaped beam pattern into a real polynomial representation, but also allows us to consider only half of the array excitations and pattern, and thus greatly simplifies the design complexity and reduces the computational effort. Furthermore, because of the form of (5.2), the well-developed equiripple (minmax) design criterion [1,13,56-57] can then be applied to the design of the symmetricalized shaped beam pattern $F_{ds}(u)$.

It is the analytic signal theory that makes the above symmetricalization process possible. Let's assume that a design method has been applied to realize the ideal symmetricalized shaped beam pattern $F_{ds}(u)$, and let the realized symmetricalized shaped beam pattern and its corresponding excitation be represented as $F_r(u)$ and $J_r(n)$ respectively. Note that $J_r(n)$ becomes an N elements array excitation. Let the realized symmetricalized shaped beam pattern $F_r(u)$ be depicted as Figure 5.1(c). Then, by applying the analytic signal theory, we can obtain a realizable ãnalytic excitation such that to eliminate one of the shaped beams of $F_r(u)$ presented within the visible range. That is, the ãnalytic excitation, denoted as $J_{ta}(n)$, can be formed as

$$J_{ta}(n) = J_r(n) + jJ_{ti}(n) \qquad (5.3)$$

where $J_{ti}(n)$ denotes a truncated N elements array excitation generated from $J_r(n)$ by using the realizable discrete-time Hilbert transformer. The radiation pattern $F_{ta}(u)$ corresponding to the ãnalytic excitation of $J_{ta}(n)$ in Equation (5.3) is

$$F_{ta}(u) = F_r(u) + jF_{ti}(u) \qquad (5.4)$$

where $F_{ti}(u)$ is the pattern corresponding to $J_{ti}(n)$. Accordingly, $F_{ta}(u)$ represents the realized pattern which has single shaped beam remaining within the visible range of an array antenna system. Because of the symmetricalization process, the realized shaped beam pattern $F_{ta}(u)$ is shifted with angle u_c. Then, using the shifting property of an array antenna system with a linear phase gradient which is the value of u_c, $F_{ta}(u)$ can be shifted back to the original required angular position. Thus, the ultimate realized shaped beam pattern, denoted as $F_{ta}(u+u_c)$, is depicted as in Figure 5.1(d). Since the symmetricalization process is a linear operation, the shape of the pattern in the to-be shaped region remains the same as the one which is synthesized without shifting process. However, based on the property of an ãnalytic excitation, at least, parts of half-side sidelobe of the realized shaped beam pattern can be eliminated (at least suppressed). As discussed in Chapter IV, the phenomenon of the eliminated sidelobe is always a desirable property in the practical application of an antenna system. This is an important advantage obtained from this design methodology.

5.3 System Design Constraint

In order to minimize the distortion caused by a realizable Hilbert transformer in the physical implementation of the shaped beam pattern using ãnalytic excitation, the quantity of u_c in Equation (5.1) is required to shift the realized symmetricalized shaped beam pattern $F_r(u)$ to the pass-band of the realizable Hilbert transformer. Let's delineate the roll-off regions (at the u=0 end) of both realized symmetricalized shaped beam pattern $F_r(u)$ and spectrum H(u) of the Hilbert transformer as in Figure 5.2, where Δu_h denotes the roll-off region of H(u), Δu_r represents the roll-off region of $F_r(u)$ and Δu_{null} represents the angular distance between the first null of the $F_r(u)$ and the starting angle of the shaped region of the desired symmetricalized beam pattern $F_{ds}(u)$. It is obvious that the value of u_c should at least satisfy the following condition:

$$(\Delta u_{null}+\Delta u_h) \leq u_c \text{ and } (u_c+u_s+\Delta u_{null}+\Delta u_h) < \pi \qquad (5.5)$$

and $F_r(u)$ should have a small amount of component around the u=0 direction to assure that the distortion caused by a realizable Hilbert transform can be minimized.

However, in the practical application, it is advantageous to eliminate (at least suppress) one of two sides sidelobes of the shaped beam pattern. Thus, the value of u_c is the possible value of Δu_{null}.[2]

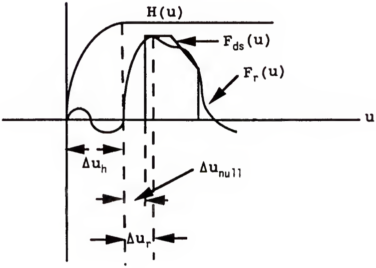

Figure 5.2 The definitions of the roll-off regions of the realized symmetricalized shaped beam pattern and the spectrum of the realizable Hilbert transformer.

---

[2] It allows a negligible incremental of distortion in the shaped beam pattern caused by the realizable Hilbert transformer.

The extent of the system constraint in Equation (5.5) is actually very much dependent on the number of array elements. The larger the number of array elements, the smaller the limitation on the angular width of the shaped beamwidth which can be realized by using this proposed design method.

5.4 System Design Example using Windowing Method

Due to the conceptual simplicity, it is easy to visualize the design process in the realization of a shaped beam pattern using an ãnalytic excitation. It is obvious that an equiripple criteria of numerical design method is possible and preferred in realizing such a symmetricalized shaped beam pattern as given by Equation (5.2). However, by using the windowing method, we are able to analytically generate a shaped beam pattern, and to demonstrate the simplicity and feasibility of this new design methodology. That is the windowing method is more appropriate for the purpose of illustration of this design method introduced.

The most popular shaped beam pattern is the $\text{cosec}^2\theta$ power pattern. Since it gives a constant echo-signal power which is independent from θ for a target moving at the same altitude, it was widely used in an air-search and the ground-mapping radar system. A typical requirement of a shaped beam pattern in the radar application is that from 1° to 5° is the vertical main beam (that is the beamwidth in the elevation direction is 4°) and with cosecant-squared shaped beam from 5° to 30°. Using the linear array system as discussed in Section 3.2.2

Chapter II, let the phase reference be shifted to the array center point and the interelement distance to be half of the wavelength ($d=\lambda/2$), the normalized desired cosecant voltage shaped pattern is[3]

$$F_d(\theta) = \begin{cases} 1, & 85^\circ \le \theta \le 89^\circ \\ \dfrac{\sin(5^\circ)}{\sin(90^\circ-\theta)}, & 60^\circ < \theta \le 85^\circ \\ 0, & \text{elsewhere} \end{cases} \tag{5.6}$$

where $\sin(5^\circ)$ is used to normalize the shaped beam pattern. Note that $u=\pi\cos(\theta)$ for half wavelength interelement distance. After changing the variable of θ to u, the normalized shaped voltage beam pattern becomes

$$F_d(u) = \begin{cases} 1, & u_1 \le u \le u_2 \\ \dfrac{u_o}{u}, & u_2 < u \le u_3 \\ 0, & \text{elsewhere} \end{cases} \tag{5.7}$$

where $u_1=\pi\cos(89^\circ)$, $u_o=u_2=\pi\cos(85^\circ)$, and $u_3=\pi\cos(60^\circ)$. The desired shaped voltage beam pattern as described by Equation (5.7) is plotted in Figure 5.3.

---

[3] Note that the angle θ in the Figure 3.2 of the linear array system is measured from the endfire direction.

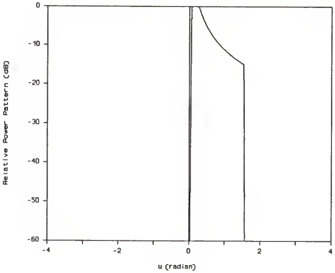

Figure 5.3 The desired cosecant-squared shaped beam power pattern.

Having defined the desired shaped beam pattern, we can symmetricalize the desired shaped beam pattern by determining the value of u_c in Equation (5.1). According to Equation (5.5), the value of u_c is actually determined by the number of array elements N as well as the characteristics of the windowing functions which are also functions of the number of array elements. The number of array elements determines the degree of the approximation of the realized pattern to the desired shaped pattern. There are two window functions involved in using the windowing method to realize this design technology. The first one is used to realize the ideal symmetricalized shaped beam pattern, and the other one is used to implement the finite elements of the ãnalytic excitation.

Since the mainlobe widths of the window functions are to be less than the pass band of the desired shaped beam pattern and the spectrum of the ideal Hilbert transformer, based on the convolution process, a fairly accurate qualitative estimation of the angular width of Δu_{null} and the roll-off region Δu_h is possible. That is, the angular width Δu_{null} which is the angular width between the first null point in the realized symmetricalized shaped beam pattern and the discontinuity in the ideal symmetricalized shaped beam pattern is to be half of the mainlobe width of the first window function,[4] and the roll-off region Δu_h at u=0 end of the realized Hilbert transformer is to be the half of the mainlobe of the second window function. The first window function will determine the angular width Δu_{null} and the level of the sidelobe in the realized symmetricalized shaped pattern. In order to have a narrower roll-off region (it is a desirable requirement in designing a shaped beam pattern) the first window should be Dolph-Chebyshev window. However, in order to possibly suppress one of two sides sidelobes, the best choice for the second window becomes the Kaiser window with $\beta=0$. The reasons to choose such window functions are actually the same as those stated in the preceeding chapters.

After determining the type of the windows, let's assume that the number of array elements is 17 [40], and a sidelobe ratio R=15dB Dolph-Chebyshev window is used to realize the symmetricalized shaped beam pattern.[5] Then, the values of Δu_h and Δu_{null} can be estimated from the mainlobe widths of the chosen window functions, that is $\Delta u_h=(2\pi/17)$ which is equal to half of the mainlobe width of a uniform window function and $\Delta u_{null}=(1.9\pi/17)$ which is equal to half of the mainlobe width of the Dolph-Chebyshev window with R=15dB. Accordingly, the value of $u_c=0.7$(radian) can satisfy the constraint in Equation (5.5), and the symmetricalized cosecant shaped voltage beam pattern can be represented as

---

[4] The value of u_c is assumed to be larger or equal to the half of the mainlobe width of the first window function.

$$F_{ds}(u) = \begin{cases} 1, & u_c \le |u| \le (u_c+u_2-u_1) \\ \dfrac{u_o}{(u-u_c+u_1)}, & (u_c+u_2-u_1)<|u|\le (u_c+u_3-u_1) \\ 0, & \text{elsewhere} \end{cases} \qquad (5.8)$$

According to Equation (5.2), the corresponding excitation for $F_{ds}(u)$ in Equation (5.8) can be obtained by using the inverse Fourier transform. After doing the Inverse transformation and truncation process, the excitation for the realized symmetricalized shaped beam voltage pattern can be expressed as

$$J_r(n) = a(n)w_1(n) \qquad -M \le n \le M \qquad (5.9)$$

---

[5] The mainlobe width of the Dolph-Chebyshev window can be obtained from Figure A.1 in Appendix, where the mainlobe width is equal to the mainbeam width ratio times $(4\pi/N)$.

where M=8, $w_1(n)$ is the Dolph-Chebyshev window with sidelobe ratio R=15dB, and a(n) is the excitation for the ideal symmetricalized shaped beam pattern $F_{ds}(u)$ as given by Equation (5.8), which is calculated as

$$a(n) = \frac{1}{\pi} \int_0^{\pi} F_{ds}(u)\cos(un)\,du \qquad (5.10)$$

It can be seen that because of the symmetric property of $F_{ds}(u)$, the calculation of the excitation is simplified.

The resulting symmetricalized shaped beam pattern corresponding to the excitation $J_r(n)$ is plotted in Figure 5.4(a). Then applying the Hilbert transform and truncation process, the ãnalytic excitation $J_a(n)$ corresponding to the real excitation $J_r(n)$ in Equation (5.9) can be obtained as

$$J_a(n) = J_r(n) + j[J_r(n)*h(n)]w_2(n) \qquad (5.11)$$

where * indicated the discrete-time convolution, h(n) is the impulse response of the discrete-time Hilbert transformer, and $w_2(n)$ is the uniform window function. The realized cosecant shaped beam pattern corresponding to the ãnalytic excitation $J_a(n)$ in Equation (5.11) after shifting back to the original required position is plotted in Figure 5.4(b). The realized pattern in Figure 5.4(b) shows that the levels of the sidelobe in the non-shaped region and the ripple in the shaped region are high. By changing the sidelobe ratio of the Dolph-

Chebyshev window function in the realization of the symmetricalized shaped pattern in Equation (5.8), we can control the levels of the sidelobe and the pass band ripple. Thus, by applying the same procedures and using the Dolph-Chebyshev window with R=20dB in realization of the symmetricalized shaped beam pattern, the corresponding realized cosecant shaped beam pattern is plotted in Figure 5.4(c), where the value of u_c is set to 0.5(radian). When we use a Dolph-Chebyshev window with R=30dB to implement the symmetricalized shaped voltage pattern, and adjust the first null point of the symmetricalized pattern to be at u=0, where the value of u_c can easily be estimated to be u_c=0.54(radian) ($u_c=\Delta u_{null}$=half of the mainlobe width of the Dolph-Chebyshev window with R=30dB), the resulting shaped cosecant-squared power pattern is plotted in Figure 5.4(d). Comparing those patterns in Figure 5.4(b), 5.4(c) and 5.4(d), it is easy to see that the lower the sidelobe of the Dolph-Chebyshev truncation window used to realize the symmetricalized shaped beam pattern, the lower the sidelobe level and pass band ripple, but, the broader the shaped region in the realized cosecant-squared power pattern. The pattern plotted in Figure 5.5 illustrates the improvement of the approximation by increasing the size of the array elements from 17 to 51, and the window function in realization of the symmetricalized shaped beam pattern is the Dolph-Chebyshev with R=30dB.

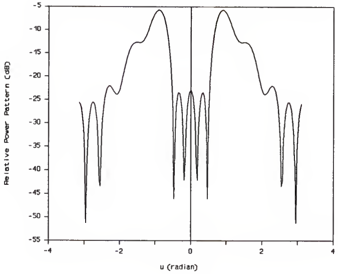

(a)

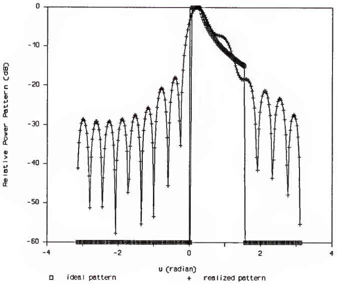

(b)

Figure 5.4 The desired and realized cosecant-squared shaped power patterns.
(a) The realized symmetricalized shaped beam pattern.
(b)(c)(d) are the realized cosecant-squared power patterns corresponding to R=15dB, 20dB and 35dB of Dolph-Chebyshev truncation windows.

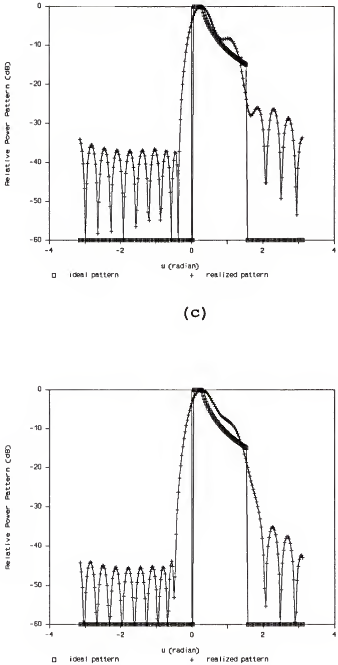

(c)

(d)

Figure 5.4 --- continued

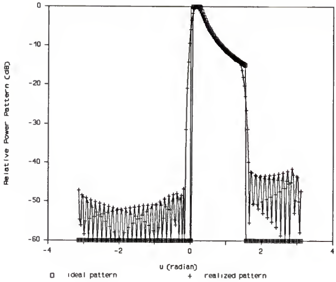

Figure 5.5 The realized cosecant-squared shaped power pattern with increasing number of array elements. (N=51).

The excitations for the shaped beam cosecant-squared power pattern in Figure 5.4(b), 5.4(c) and 5.4(d) are tabulated in Table 5.1, where the desirable complex conjugate symmetric property of an array excitation is maintained. Actually the phase in each array element should be the summation of the tabulated value and its corresponding linear phase gradient which is n times u_c, where u_c is the value used to symmetricalize the shaped pattern in each realization case. Thus by adding the linear phase nu_c to each corresponding number of element, we are able to shift the realized shaped patterns back to the original required angular position shown in Figure 5.4(b), 5.4(c) and 5.4(d). The characteristics of these three realized cosecant-squared shaped beam power patterns are also listed in Table 5.2, where the parameter of J_{max}/J_{min} is the ratio of the maximum to the minimum amplitude in the element excitations, which is related to the excitation (radiation) efficiency of the array antenna system.

Table 5.1 The excitations of the realized cosecant-squared power patterns. N=17, $J(-n)=J^*(n)$

array number	Figure 5.4(b)		Figure 5.4(c)		Figure 5.4(d)	
	Amplitude	phase	amplitude	phase	amplitude	phase
0	.222	.000	.222	.000	.222	.000
1	.202	68.486	.201	57.078	.200	59.399
2	.153	-46.509	.151	-69.535	.146	-64.910
3	.098	9.520	.094	-26.097	.087	-19.561
4	.067	44.569	.063	-2.579	.055	7.286
5	.068	83.714	.057	27.748	.045	37.797
6	.054	-45.359	.044	64.942	.032	79.734
7	.042	-25.856	.039	-76.331	.021	-59.851
8	.055	18.775	.031	-8.132	.012	-3.971

Table 5.2 The characteristics of the realized cosecant-squared power patterns.

type of pattern	J_{max}/J_{min} (None)	SLL_{peak} (dB)	SLR_{peak} (dB)
Figure 5.4(b)	5.29	-18.12	-21.48
Figure 5.4(c)	7.16	-36.57	-26.38
Figure 5.4(d)	18.50	-43.87	-35.16

The results in Table 5.2 show that, as expected, the lower the sidelobe, the poorer the excitation efficiency of the realized ãnalytic excitation. Furthermore, as shown in Figure 5.4(c) and 5.4(d), the sidelobe levels below the horizontal (SLL_{peak}) of the resulting shaped beam patterns using ãnalytic excitations can be heavily suppressed. In the practical environmental situation where the clutters which come from ground or sea-surface are more severe than those from the space, the level of the lower side sidelobe (below the horizon) is desired to be lower than that of upper side, which implies that the asymmetric sidelobe levels shown in Figure 5.4(c) and 5.4(d) may satisfy the sidelobe requirement of an antenna system. Then, by using the asymmetric sidelobe shaped beam pattern, we will be able to gain the advantages such as excitation efficiency, narrower roll-off region compared to the symmetric sidelobe shaped beam pattern. Actually, this is one of the common and attractive properties of an ãnalytic excitation.

5.5 Discussion and Summary

A new design technology for synthesizing a shaped beam array radiation pattern has been introduced in this chapter. From the example, we can reach a reasonable conclusion that the new design method provides a great reduction in the computational effort compared to the Fourier expansion and the iterative numerical method, and provides a simple skill to control the sidelobe level compared to the Woodward's voltage pattern sampling method. The most important idea and contribution conveyed by this method is that the well-developed equiripple design criterion can be equally applied to the design of any desired shaped array antenna radiation pattern provided that Equation (5.5) is satisfied.

Furthermore, it is worthwhile to be emphasized that a desirable asymmetric sidelobe shaped beam pattern [27] can be easily generated by using this design methodology.

Chapter VI

ANALYSIS AND DESIGN OF RADIATION PATTERNS FOR A MONOPULSE ARRAY ANTENNA SYSTEM USING ANALYTIC SIGNAL THEORY

6.1 Introduction

A monopulse tracking radar system usually requires two kinds of patterns, a sum pattern and a difference pattern. The sum pattern is responsible to detect and measure the range of the target, and the difference pattern is used to acquire the angular information of a moving target. Traditionally, the sum and difference patterns of an amplitude monopulse array antenna radar system are formed as the summation and the difference of two squint patterns [5], as shown in Figure 6.1, where u_s in radians is usually called the squant angle, and $\Sigma(u)$ and $\Delta(u)$ denote the sum and difference patterns respectively. However, as the modern technology continues to advance, it becomes increasing attractive to produce the sum and difference patterns using dual excitations in an array antenna system [67-68]. Actually, this separation concept has already been widely adopted in dealing with the problems related to the difference patterns of a monopulse tracking radar system [5,69-75].

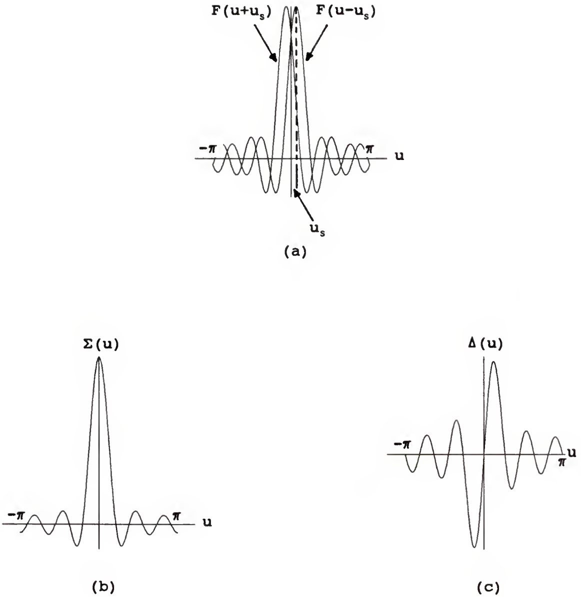

Figure 6.1 Sketches of the typical radiation patterns of an amplitude monopulse array antenna radar system.
(a) The overlapping of two squint patterns.
(b) The sum pattern $\Sigma(u)$.
(c) The difference pattern $\Delta(u)$.

Theoretically, any odd symmetric excitation could be used to generate a desired difference pattern.[1] It has been shown in Chapter III that the Hilbert transform of an even symmetric function is always an odd symmetric function. As the matter of fact, we will show that the real and the imaginary part of a theoretical ãnalytic signal represent an ideal excitation pair for the monopulse array antenna radar system. It is therefore interesting and worthwhile to exploit the concept using the ãnalytic signal to generate the sum and difference patterns for the monopulse array antenna radar system.

6.2 The Generations of Radiation Patterns for a Monopulse Array Antenna Radar System using Analytic Signal Concept

Before studying the utilization of the ãnalytic signal concept to generate the radiation patterns for a monopulse array antenna radar system, let's figure out some characteristic indices used to measure the performance of the sum and difference patterns. The characteristic indices used to describe the performance of the sum pattern for a monopulse radar system are exactly the same as those of the narrow beamwidth radaition pattern described in Chapter III, that is, the beamwidth resolutions, directivity, excitation efficiency, and sidelobe level. For a difference pattern, they are directivity, difference slope at the boresight and sidelobe level. The definition of the directivity of the difference pattern, denoted as D_d, is the same as that defined in Equation (3.15), with $F(\theta_o,\phi_o)$ and $F(\theta,\phi)$ replaced by $\Delta(\theta_m,\phi_m)$ and $\Delta(\theta,\phi)$, where $\Delta(\theta_m,\phi_m)$ is the mainbeam maximum of the difference pattern. The difference slope at the boresight (u=0 or $\theta=\pi/2$) of a difference pattern, denoted as $\Delta'(0)$, is defined as [5]

---

[1] Generally, the difference pattern is an odd symmetric pattern, such that the angular information of a moving target can be obtained.

$$\Delta'(0) = \left.\frac{d\Delta(u)}{du}\right|_{u=0} \qquad (6.1)$$

where $\Delta(u)$ is the difference pattern, and $u=kd\cos\theta$, θ is measured from the endfire direction. $\Delta'(0)$ is a very important performance index of a difference pattern, since it is related to the tracking accuracy of the monopulse radar system[64].

Since the sum pattern can be any broadside narrow beamwidth radiation pattern using this ãnalytic excitation concept, it is not discussed here. In the following, we will show that by applying the concept of analytic signal (ãnalytic excitation), we can generate a difference pattern which possesses many desirable properties.

It has been shown earlier that a theoretical analytic excitation $J(n)=J_r(n)+jJ_i(n)$ will produce a positive-sided radiation pattern, and its dual $J_d(n)=J_r(n)-jJ_i(n)$ has a negative-sided pattern, where both $J_r(n)$ and $J_i(n)$ are real, and $J_i(n)$ is the Hilbert transform of $J_r(n)$. Let $F_P(u)$ and $F_N(u)$ represent the positive-sided pattern corresponding to $J(n)$ and the negative-sided pattern corresponding to $J_d(n)$, respectively. Accordingly, a desired sum pattern $\Sigma(u)$ can be the summation of $F_P(u)$ and $F_N(u)$; that is,

$$\begin{aligned}\Sigma(u) &= F_P(u) + F_N(u) \\ &= \sum_n [(J_r(n)+jJ_i(n)) + (J_r(n)-jJ_i(n))]e^{-jun} \\ &= 2 \sum_n J_r(n)e^{-jun} = 2\, F_r(u) \qquad (6.2)\end{aligned}$$

where $F_r(u)$ is the typical broadside narrow beamwidth radiation pattern corresponding to $J_r(n)$. The difference pattern can be formed as the difference of $F_P(u)$ and $F_N(u)$; that is,

$$\begin{aligned}\Delta(u) &= F_P(u) - F_N(u) \\ &= 2j \sum_n J_i(n)e^{-jun} \\ &= 2jF_i(u) \qquad (6.3)\end{aligned}$$

where $F_i(u)$ is the radiation pattern corresponding to $J_i(n)$. Furthermore,

$$\begin{aligned}\Delta(u) &= 2j[-j\,\mathrm{sgn}(u)F_r(u)] \\ &= 2F_r(u)\,\mathrm{sgn}(u) \\ &= \Sigma(u)\,\mathrm{sgn}(u) \qquad (6.4)\end{aligned}$$

where $F_i(u)=[-jF_r(u)\,\mathrm{sgn}(u)]$ is applied. The results in Equation (6.2) and (6.3) indicate that if an ãnalytic excitation is obtainable, then the sum pattern is just the pattern excited by its real part, and the difference pattern is the one excited by its imaginary part. From Equation (6.4), the difference pattern is just that of sum pattern except inverse in the region of u<0, and both of them have exactly the same power pattern. The result shown in Equation (6.4) represents one of the most desirable relations between the sum and difference patterns for a monopulse radar system. Furthermore, according to Equation (6.1), the difference slope of the difference pattern is

$$\Delta'(0) = \frac{d\Delta(u)}{du}\bigg|_{u=o} = [\frac{d[\Sigma(u)\mathrm{sgn}(u)]}{du}\bigg|_{u=0}$$

Due to the discontinuity of the pattern [Σ(u)sgn(u] at u=0, the derivative of [Σ(u)sgn(u)] can mathematically be expressed as

$$\Delta'(0) = [R(u) + \delta(u)]\bigg|_{u=0} = \delta(0) = \infty \qquad (6.5)$$

where R(u) represents the derivative function of the pattern [Σ(u)sgn(u)] over all u, except u=0. Thus, the difference slope of the difference pattern excited by the imaginary part of a theoretical ãnalytic excitation is infinite.

As mentioned eariler, the real part of an ãnalytic excitation used to generate the sum pattern for a monopulse array antenna radar system can be a well-designed excitation which produces a broadside narrow beamwidth radiation pattern that may have various desired characteristics. Then, based on the relation between the sum and difference pattern as indicated in Equation (6.4), it is easy to see that the characteristic in the sum pattern will always be preserved in the difference pattern which is excited by the imaginary part of the corresponding ãnalytic excitation.

Based on the above deduction, let's summarize the properties of the radiation patterns of the monopulse array antenna radar system using a theoretical ãnalytic excitation, that is, the real part of the ãnalytic excitation is the excitation for sum pattern and the imaginary part for the difference pattern. First, both of the sum and difference patterns have the same power patterns, that is both sum and difference patterns cover the same illuminated volume in the space. Secondly, the difference pattern has an infinite difference slope at the boresight. Third, the characteristics of both sum and difference patterns are simultaneously controllable to meet the system requirments, such as directivity, beamwidth resolution, and sidelobe level. Actually, those properties form the most desirable patterns for a monopulse array antenna radar system. Thus, we have reached the following important assertion:

Assertion 6.1 The most desirable radiation patterns for a monopulse array antenna system can be generated through a ideal ãnalytic excitation.

The sum pattern and the corresponding most desirable difference pattern of a monopulse array antenna radar system are plotted together in Figure 6.2, where the excitation for the sum pattern is uniform.

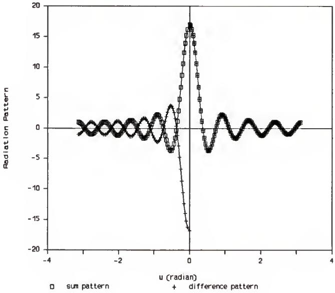

Figure 6.2 The desirable radiation patterns of an amplitude monopulse array antenna radar system. (sum and difference patterns).

6.3 Analysis of Radiation Patterns of a Monopulse Array Antenna Radar System using Realizable Hilbert Transformer

As stated in Assertion 6.1, the most desirable odd excitation for the difference pattern of a monopulse array antenna radar system can be obtained from the even symmetric excitation for the sum pattern by using an ideal Hilbert transformer. It is this elegent consequence that stimulates us to investigate the properties of the difference pattern generated from a sum pattern using a realizable Hilbert transformer. The generation of an odd symmetric excitation from an even symmetric excitation by a realizable Hilbert transformer has been discussed in Chapter III, where it was considered to generate an ãnalytic excitation for a broadside narrow beamwidth radiation pattern. However, the purpose and results here will be totally different.

Let's denote the even symmetric excitation for a desired sum pattern of an N=2M+1 elements monopulse array antenna radar system as $J_s(n)$. Then, according to Equation (6.3), the normalized ideal excitation for the difference pattern is $\{jJ_i(n)\}$ where $J_i(n)$ is generated from $J_s(n)$ through an ideal Hilbert transformer. However, by using a window function, the realizable odd symmetric excitation for the difference pattern, denoted as $J_d(n)$, can be obtained and expressed as

$$J_d(n) = j\{[J_s(n)*h(n)]w(n)\} \tag{6.6}$$

where h(n) is impulse response of the discrete-time Hilbert transform, and w(n) is a typical truncation window. As usual, let's denote the sum pattern corresponding to $J_s(n)$ as $\Sigma(u)$ and the difference pattern corresponding to $J_d(n)$ as $\Delta(u)$. Then, by applying the convolution and multiplicative law, the realized difference pattern $\Delta(u)$ can be expressed as

$$\Delta(u) = [\Sigma(u)\mathrm{sgn}(u)]*W(u) \tag{6.7}$$

where [-jsgn(u)] is the spectrum of the discrete-time Hilbert transformer, and W(u) is the spectrum of the selected truncation window. Thus, the difference slope $\Delta'(0)$ of the realizable difference pattern can be evaluated by

$$\Delta'(0) = \left.\frac{d\Delta(u)}{du}\right|_{u=0} = \left.\frac{d\{[\Sigma(u)\,\mathrm{sgn}(u)]*W(u)\}}{du}\right|_{u=0} \tag{6.8}$$

However, according to the Fourier relations between the radiation pattern and its excitation, the evaluation of the difference slope in Equation (6.8) is equivalent to the following

$$\Delta'(0) = \left.\frac{d\Delta(u)}{du}\right|_{u=0} = \left.\frac{d\{\Sigma(j\{[J_s(n)*h(n)]w(n)\})e^{-jun}\}}{du}\right|_{u=0}$$

$$= \sum_{n}(n\{[J_s(n)*h(n)]w(n)\}) \tag{6.9}$$

The result in Equation (6.9) provides a neat formula to calculate the difference slope of a difference pattern derived from a realizable Hilbert transformer. It is said that the difference slope is the weight sum of the element's number and the weight is determined by the truncation window and the excitation which is the Hilbert transform of the even symmetric excitation for the sum pattern. It is interesting to note that the best truncation window for maximizing the difference slope is the uniform rectangular window.

Based on the results in Equation (6.7) and (6.9), for a given sum pattern $\Sigma(u)$, the characteristics of the difference pattern can be controlled by the number of array elements N and the selected trancation window. As just mentioned, the best window to maximize the difference slope is uniform, however, the best chosen window to minimize the beamwidth of the difference pattern with a controllable sidelobe level is exactly the same as that discussed in Section 3.3.2, that is the truncation window should have narrowest mainlobe width with a specified sidelobe level, which leads to the Dolph-Chebyshev window. By using the windowing method, we will show the flexibility and the properties of the difference pattern which are obtained from a practical sum pattern by using the realizable discrete-time Hilbert transformer. Then, from those analysis results, a specific difference pattern for the monopulse array antenna radar system can be created.

6.4 System Analysis and Design Example

In this analysis example, let's assume the specific sum pattern to be the Taylor pattern with peak sidelobe 30dB and $\bar{n}=4$ (refer to Example 2, Section 4.6, Chapter IV), due to its popularity. First, the directivity and the difference slope of the difference pattern are analyzed as function of the number of the array elements N. That is, the number of the array element N is treated as an independent variable. The truncation windows used to generate the realizable odd excitation as given by Equation (6.6) are assumed to be the uniform and the Dolph-Chebyshev with R=20dB for comparison. The analysis results with N=11, 13, 15, 17, 19, 21, 23, 25 are listed in Table 6.1, where D_d and SL_{peak} indicate the directivity and the peak sidelobe of the difference pattern.

Table 6.1 The characteristics of the difference pattern as functions of the number of array elements N.

number of elements	truncation window					
	uniform			Chebyshev (R=20dB)		
N	$\Delta'(0)$ (None)	D_d (None)	SL_{peak} (dB)	$\Delta'(0)$ (None)	D_d (None)	SL_{peak} (dB)
11	17.53	6.70	-12.08	12.01	6.53	-14.84
13	24.49	7.90	-12.28	17.21	7.63	-14.92
15	32.61	9.11	-12.40	23.37	8.68	-14.67
17	41.90	10.31	-12.45	30.51	9.69	-14.59
19	52.34	11.52	-12.45	38.62	10.65	-14.61
21	63.94	12.73	-12.48	47.71	11.58	-14.56
23	76.70	13.93	-12.55	57.79	12.46	-14.56
25	90.62	15.14	-12.53	68.85	13.33	-14.43

The analysis results of directivity and difference slope in Table 6.1 are plotted in Figure 6.3(a) and (b) respectively, where a linear interpolation scheme is adopted. Figure 6.3(a) shows that the directivity of a difference pattern generated by using the Hilbert transform method is linearly increasing with the number of array elements N, and in Figure 6.3(b) the difference slope increases more prominently than linear relation with increasing N. The result in the difference slope just reflects the property of the nonlinear distortion decreasing with the increasing number of the

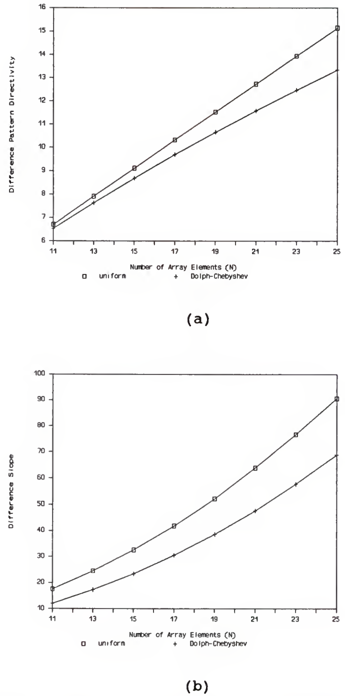

(a)

(b)

Figure 6.3 The directivity and difference slope of a difference pattern as functions of the number of array enements N. (a) Directivity. (b) Difference slope.

truncation points of the Hilbert transformer.[2] Therefore, the larger the number of array elements, the more advantage we can obtain in the difference slope of the difference pattern by using the Hilbert transform method. Moreover, the selected truncation windows control the slopes in both directivity and difference slope, and the uniform truncation window has advantages in both pattern characteristics, because the ratio of the mainlobe width of the uniform window to the mainbeam width of the assumed Taylor sum pattern is smaller than that of the Dolpf-Chebyshev with R=20dB to the Taylor sum pattern, and also the uniform window is the best choice in terms of difference slope. However, the peak sidelobes of the difference patterns shown in Table 6.1 do not vary with the number of array elements N. They are leaked and therefore determined by the peak sidelobes of the selected truncation windows.

Next, we can further analyze the manner in which the truncation windows control the performances of the difference pattern. Let the specific sum pattern remain the same as before, and the number of array element N is set to 21. Then, the uniform, Dolph-Chebyshev with R=20dB, 25dB, 30dB, and 35dB are used as the truncation windows for generating the odd excitation in Equation (6.6). The characteristics of the difference patterns corresponding to those truncation windows are tabulated in Table 6.2, and, again, Figure 6.4(a) and (b) plot the analysis results of the difference slopes and the peak sidelobes of the realized difference patterns using a linear interpolation method, where the characteristics values corresponding to -13dB sidelobe on the abscissas of Figure 6.4(a) and (b) are the results of the uniform truncation window.

---

[2] Recall that the impulse response of the Hilbert transform is $h(n)=(1-\cos(n\pi))/n\pi$ which is a decreasing function of $(1/n)$.

Table 6.2 The characteristics of the difference patterns as functions of the truncation windows.(N=21)

truncation windows	D_d	$\Delta'(u)$	SL_{peak}
uniform	12.73	63.94	-12.48
Chebyshev(R=20dB)	11.58	47.71	-14.56
Chebyshev(R=25dB)	11.96	37.27	-18.98
Chebyshev(R=30dB)	11.59	30.45	-23.45
Chebyshev(R=35dB)	11.04	25.66	-27.98

It has been shown in Table 6.2 and Figure 6.4 that using the different peak sidelobes of the window functions, we can control the peak sidelobe of the difference pattern generated by the Hilbert transform method, provided that the sidelobe of the original sum pattern is low enough (it is always the case). However, the advantage of the lower sidelobe is obtained by sacrificing the diffence slope. Furthermore, the effect of the truncation windows on the directivity of the difference patterns seem minute. Therefore the directivity ofthe difference pattern largely depends on the number of the array elements N.

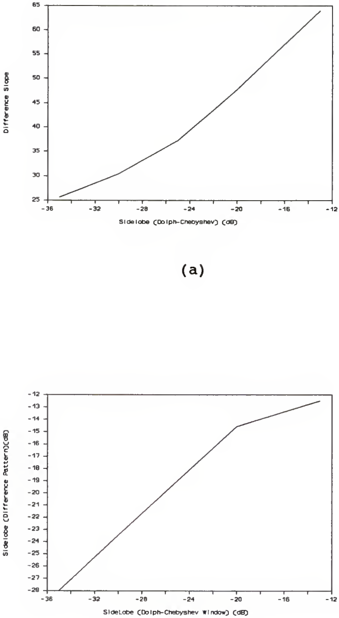

(a)

(b)

Figure 6.4 The difference slopes and the peak sidelobes of a difference pattern as functions of the truncation windows.(N=21)
(a)The difference slopes. (b)The peak sidelobes.

From the analysis result, it is obvious that the generation of the difference pattern from a sum pattern by using the Hilbert transform exactly provides a flexible and meaningful method to control the performance indices of the difference pattern. Normally, the number of the array elements is determined by the system requirements such as beamwidth resolutions, and array size. A sum pattern can then be specified. Thus, given the number of array elements N and a specific sum pattern and by applying the analysis proceduresdemonstrated above, it is easy to establish a set of data shown in Figure 6.4, which is relevant to the difference slopes and sidelobe levels of the difference patterns by using the Hilbert transform method. Thus a difference pattern which satisfies the system requirement that involves a compromise between the difference slope and the sidelobe level can be obtained.[3] As an immediately practical example, let the array number N and the sum pattern be the same as those just used in the analysis example above, and a 23 dB sidelobe of the difference pattern assumed to be another system requirement (ignore the difference slope). Then, checking from Figure 6.4(b), a Dolph-Chebyshev window with R=30dB can be used to generate the odd excitation as given by

---

[3] It is possible to simultaneously satisfy the system requirements on both difference slope and sidelobe level of the difference pattern by increasing the number of the array elements.

Equation (6.6) for the required difference pattern. After carrying out these computation routines, the realized sum and difference patterns are plotted together in Figure 6.5, and the corresponding excitations for the realized sum and difference patterns are tabulated in Table 6.3. The performance of the realized difference pattern is shown in the fourth row of Table 6.2.

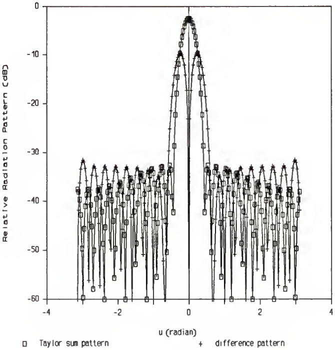

Figure 6.5 The realized sum and difference patterns using the Hilbert transform method.

Table 6.3 The excitations for the realized sum and difference patterns of a monopulse array antenna radar system. (where $J_s(-n)=J_s(n)$, and $J_d(-n)=-J_d(n)$).

array number	sum pattern $J_s(n)$	difference pattern $J_d(n)$
0	1.00000	.00000
1	.98578	.13523
2	.94416	.25555
3	.87801	.33899
4	.79138	.39067
5	.68929	.39124
6	.57821	.36785
7	.46691	.30392
8	.36666	.24389
9	.29010	.16604
10	.24846	.22614

It should be clear that the design methodology presented in this chapter for the linear array monopulse radar system can be easily extended to the planar array system. The difference pattern in either u plane or v plane can be obtained by using the Type-II 2-D ãnalytic signal and the associated Hilbert transform (Type II) which are defined and derived in Chapter II.

6.5 Discussion and Summary

The conceptual association of the analytic signal with the radiation patterns of a monopulse array antenna radar system has stimulated a new approach to design radiation patterns for monopulse array antenna radar systems. The concept of ideal ãnalytic signal represents the most desirable excitations (its real and imaginary parts) for the sum and difference patterns for the monopulse array antenna radar system. Using the realizable Hilbert transformation, the performances have been analyzed, and the design procedures have been formalized for the difference pattern of the monopulse array antenna radar systems. Furthermore, we claim that this concept can be equally applied to the design of both linear and planar monopulse array antenna systems.

Another attractive property of this design method is that once an excitation for the sum pattern is specified, the excitation for the difference pattern can be analytically obtained.

CHAPTER VII

CONCLUSION

There are three major results and a new discovery in this dissertation. First, the analytic signal concept has been extended to two-dimensional signal domain.[1] Secondly, the application of analytic signal concept to the design of both broadside narrow beamwidth array antenna systems and monopulse array antenna radar systems has been introduced and extensively investigated. Third, by associating the analytic signal concept with the modulation theory, a new generalized design methodology has been developed to generate practical desirable asymmetric sidelobe array antenna radiation patterns. The new discovery is that a design concept has been shown that enables the equiripple (minmax) design criterion to be applied to the synthesis of asymmetric shaped beam patterns.

In Chapter II, the concept of the analytic signal in analog signal domain has been extended to one-dimensional and two-dimensional discrete-time signal domains.[1] Based on the definitions, two types of two-dimensional ãnalytic signals and associated discrete-time Hilbert transfroms have been developed. They are differentiated as Type I and Type II. Furthermore, there are three interesting results related to the generation of two-dimensional ãnalytic signals either by using two stages of transformations or by using one and two dimensional discrete-time Hilbert transforms, and the results are formulated by three Lemmas in Chapter II.

---

[1] The extended analytic signal is denoted by ãnalytic signal (where the tilde is used). The ãnalytic signal is defined by Definition 2.1. The ãnalytic signal is not analytic since its derivatives do not exist and, consequently, it does not satisfy the Cauchy-Riemann conditions given by (2.1).

It needs to be emphasized that the 2-D ãnalytic signals are defined from the application points of view and the conclusion in Lemma 2.1 is obtained from the case of the separability of the kernel of the 2-D discrete-time Hilbert transform. As for further study, it would be interesting to deduce a generalized 2-D analytic signal and to derive the properties of the 2-D Hilbert transform whose impulse response may not be separable by using the method of z-transfrom, although this could be a challenging and difficult problem.

The ãnalytic excitations (corresponding to the ãnalytic signals) for broadside narrow beamwidth array antenna systems are discussed and stated by three Assertions presented in Chapter III. These results are based on the hypothesis that an ideal Hilbert transform is available. By using windowing functions, practical design procedures are developed. Radiation patterns resulting from the use of a realizable Hilbert transformer are examined and the performance is evaluated, where the measures of performance include half-power beamwidth, first-null beamwidth, antenna directivity, excitation (radiation) efficiency and sidelobe level. The results show that the array radiation patterns excited by the realizable ãnalytic excitations are inherently asymmetric and have the advantages in all measures of performance compared to the typical broadside symmetric array radiation patterns, except the sidelobe level. The cause of the high sidelobe level in the realized asymmetric radiation patterns is attributed to the realizable Hilbert transformer which can not faithfully transform the radiation patterns if the original patterns possess large spectral components around the u=0 direction.

A new generalized design methodology for desirable asymmetric sidelobe radiation patterns has been developed for narrow beamwidth linear and planar array pattens (Chapter IV) as well as shaped beam patterns (Chapter V). The kernel of this design method is the philosophy of associating the analytic signal concept with the modulation theory. The excitation generated by this design method is called modulated ãnalytic excitation. However, there is a minor diference in the design procedure used to generate an asymmetric sidelobe broadside narrow beamwidth and the shaped beam patterns.

In Chapter IV, the purpose of the modulation process for designing asymmetric sidelobe narrow beamwidth array radiation patterns is to shift the mainbeam of the broadside array pattern off u=0 direction, so as to minimize the distortion caused by a realizable Hilbert transformer. By adjusting the modulation angle, such that the first null of a symmetric broadside pattern is exactly positioned in the u=0, we can obtain various broadside narrow beamwidth asymmetric sidelode radiation patterns.

In Chapter V, the procedures for designing an asymmetric shaped pattern are to symmetricalize the desired shaped beam pattern and to shift the shaped beam region off u=0 direction, so as to minimize the distortion caused by the realizable Hilbert transformer and to suppress one of the sidelobes. It is the symmetricalization process that enables us to apply the preferred equiripple (minmax) design criterion to the realization of an asymmetric shaped beam pattern, although the realized asymmetric shaped beam pattern may not obtain equiripple result because of the process of Hilbert transformation.

Finally, in Chapter VI, by association of the analytic signal concept with the required patterns of an amplitude monopulse array antenna radar system, a new design method has been created for the difference pattern of the monopulse radar system. That is, the difference pattern can be generated from the sum pattern by using the Hilbert transform. Based on the system requirements on difference slope at boresight direction and the sidelobe level, the design procedures have been formalized.

In summary, new design methods have been developed using the analytic signal theory for the design of array antenna radiation patterns. The features of these design methods are conceptual simplicity, and computational effectiveness while yielding satisfactory results. Furthermore, these design methods allow the use of existing theory of symmetric broadside array antenna design that is well developed. This makes these design methods even more straightforward and attractive.

APPEXDIX

THE DOLPH-CHEBYSHEV LINEAR ARRAY SYSTEM

The Dolph-Chebyshev linear array system was originally developed for optimal synthesization of an in-phase excitation for an equal interelement distance linear broadside array system. It is optimal in the sense that, once the sidelobe ratio is specified, the mainbeam width is minimun, or if the mainbeam width is specified, the sidelobe ratio is minimum. This is due to the properties of the Chebyshev polynomial stated as follows. A Chebyshev polynomial is expressed as

$$\begin{aligned} T_n(x) &= \cos(n \cos^{-1}x) && \text{for } |x| \leq 1 \\ &= \cosh(n \cosh^{-1}x) && \text{for } |x| > 1 \end{aligned} \qquad \text{(A.1)}$$

Let $\phi=\cos^{-1}x$, it can be recursively expressed as

$$T_{n+1}(x) = 2xT_n(x) - T_{n-1}(x)$$

where $T_0(x)=1$ and $T_1(x)=x$. Normally, $T_N(x)$ is a N^{th} order polynomial of x (or $\cos\phi$), let it be expressed as

$$T_N(x) = \sum_{n=0}^{N} c(n)\ x^n \qquad \text{(A.2)}$$

where c(n) is the coefficient of the x^n term. The Chebyshev polynomial of $T_N(x)$ is characterized by

1. The polynomial oscillates between ± 1, for $|x| < 1$
2. It has N roots in the interval $-1<x<1$, those roots are located at $x_k=\cos \phi_k$, $\phi_k=\{[(2k-1)\pi]/2n\}$, k is from 1 to n.
3. It has N-1 extreme values(±1) in the interval $-1<x<1$, those extreme values are located at $x_m=\cos\phi_m$, $\phi_m=(m\pi)/n$, m is from 1 to n-1.
4. $T_N(x)$ monotonically increases or decreases as x^N for $|x|>1$. (depending on whether N is even or odd)

The pattern of an 2N+1 array elements (for 2N array elements follow the same procedures [19]) real even symmetric excitation J(n), denoted as F(u), is proportional to

$$F(u) = \sum_{n=0}^{N} J(n)\cos(un) \tag{A.3}$$

Note that, it has been implicitly assumed that the weight of the excitation in the phase reference element(n=0) is [2J(0)] in representing the pattern of an odd number of array elements as given by Equation (A.3). Let the pattern in Equation (A.3) be alternatively expressed as

$$F(u) = \sum_{n=0}^{N} J(n)\cos[2n(u/2)] \tag{A.4}$$

Note that the following two equations always hold

$$\cos(un)=\binom{n}{k}(\cos(u))^{n-k}(\sin(u))^{k}, \text{ for k even and } K \leq n \qquad (A.5)$$

and

$$\sin^2 u = 1 - \cos^2 u \qquad (A.6)$$

Substituting Equation (A.5) and (A.6) into Equation (A.4), the array pattern can be expressed as

$$F(u) = \sum_{n=0}^{N} d(2n)(\cos^{2n}(u/2)) \qquad (A.7)$$

where d(2n) is function of array excitation J(n) and represents the coefficient of the $\cos^{2n}(u/2)$ term. After those mathematical manipulation, the pattern representation in Equation (A.7) has exactly the same form as the Chebyshev polynomial in Equation (A.2) with the order of the polynomial increased from N to 2N, except the independent variables x and cos(u/2). Two problems remain: we need to transform the appropriate region of x into cos(u/2), and to equate the coefficients between the corresponding two polynomials. For transformation the sidelobe region of the pattern of an array system is identified with the oscillated region of the Chebyshev polynomial, and the mainbeam region is associated with the monotonically increasing region. The Dolph's transformation [19] is given by $\cos(u/2)=(x/x_0)$, and x_0 is chosen such that

$$T_{2N}(x_0) = R \qquad (A.8)$$

where R is the desired ratio of mainbeam maximum to the peak sidelobe. The Dolph's transformation between the variables of x and u can be seen as follows: as u varies from $-\pi$ to π, x varies from 0 to 1 in the sidelobe region, up to x_0 at the mainbeam maximum at u=0, and then back through 1 and other sidelobes to 0 at $u=\pi$. Once R is determined, x_0 can be calculated from Equation (A.1) as

$$x_0 = \cosh(\cosh^{-1}R/n) \tag{A.9}$$

Then, subsituting $x=x_0\cos(u/2)$ into Equation (A.2) with N replaced by 2N, gives the pattern of the Dolph-Chebyshev linear array system

$$F(u) = T_{2N}(x_0 \cos(u/2)) \tag{A.10}$$

By equating Equation (A.7) and (A.10), the coefficient d(2n) as well as the array excitation J(n) can be calculated, and the corresponding pattern will have the equal peak sidelobe with the ratio R. Also, it has been shown that the mainbeam width of the pattern is minimized. For a large number of array elements, the coefficients equating procedure is tedious. However, the procedure can be easily carried out by use of computer [76]. The comparison of the mainbeam width between the Dolph-Chebyshev and the uniform linear array antenna systems is plotted in Figure A.1, where the number of array elements is 21. From Figure A.1, given a specific sidelobe ratio R (in unit of dB) on the abscissa, the mainbeam width of the corresponding Dolph-Chebyshev array system is equal to the mainbeam width ratio on the ordinate times ($4\pi/N$), where N is the number of array elements and ($4\pi/N$) is the mainbeam width of the uniform array system. For instance, with the same number of array elements and a (-16.3dB) sidelobe ratio, the corresponding Dolph-Chebyshev array system has the same mainbeam width as the uniform array system (corresponding to the unity of the mainbeam width ratio in Figure A.1).

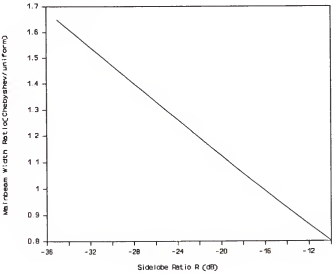

Figure A.1 The mainbeam width of the Dolph-Chebyshev linear array system with various peak sidelobe ratios R compared to that of the uniform linear array system.

REFERENCES

1. R. E. Collin and F. J. Zucker, **Antenna Theory Part I**, McGraw-Hill Book Co., New York, 1969.

2. R. E. Collin, **Antenna and Radiowave Propagation**, McGraw Hill Book Co., New York, 1985.

3. B. Rulf and G. A. Robertshaw, **Understanding Antenna for Radar, Communications, and Avionics**, Van-Nostrand Reinhold Co., New York, 1987, Ch. 1, 2, & 8.

4. M. I. Skolnik, **Introduction to Radar System**, McGraw-Hill Book Co., New York, 1980.

5. M. T. Ma, **Theory and Application of Antenna Arrays**, Wiley-Interscience, New York, 1974.

6. B. D. Steinberg, **Principles of Aperture and Array System Design**, John Wiley & Son, New York, 1976.

7. S. A. Schelkunoff, "A Mathematical Theory of Linear Arrays," **Bell System Tech. J.**, 22, 1943, pp. 80-107.

8. R. S. Elliot, "Beamwidth and Directivity of Large Scanning Arrays," **Microwave Journal, Part II**, 7, Jan. 1964, pp. 74-82

9. R. E. Collin, "Pattern Synthesis with Nonseparable Aperture Fields," **IEEE Trans. on AP**, AP-12, July 1964, pp. 502-503.

10. F. I. Tseng and D. K. Cheng, "Optimal Scannable Planar Arrays with an Invariant Sidelobe Level," **Proc. IEEE**, 56, Nov. 1968, pp. 1771-1778.

11. S. W. Autrey, "Approximate Synthesis of Nonseparable Design Responses for Rectangular Arrays," **IEEE Trans. on AP**, AP-35, Aug. 1987, pp. 907-912.

12. F. J. Harris, "On the Use of Windows for Harmonic Analysis with the Discrete Fourier Transform," **Proc. IEEE**, 66, Jan. 1978, pp. 51-83.

13. J. E. Evans, "Synthesis of Equiripple Sector Antenna Patterns," **IEEE Trans. on AP**, AP-24, May 1976, pp. 347-353.

14. E. N. Gilbert and S. P. Morgan, "Optimum Design of Directivity Antenna Arrays Subject to Random Variations," **Bell System Tech. J.**, 34, May 1955, pp. 637-663.

15. Y. T. Lo, S. W. Lee and Q. H. Lee, "Optimization of Directivity and Signal-to-Noise Ratio of an Arbitrary Antenna Array," **Proc. IEEE**, 54, Aug. 1966, pp.1033-1045.

16. D. K. Cheng and F. I. Tseng, "Elliptical Arrays," **Proc. IEE**, 114, May 1967, pp. 589-594.

17. C. Drane, Jr. and J. McILVENNA, "Gain Maximization and Controlled Null Placement Simultaneously Achieved in Aerial Array Patterns," **The Radio and Electronic Engineer**, 39, Jan. 1970, pp. 49-57.

18. D. K. Cheng, "Optimization Techniques for Antenna Arrays," **Proc. IEEE**, 59, Dec. 1971, pp. 1664-1674.

19. C. L. Dolph, "A Current Distribution for Broadside Arrays Which Optimalizes the Relationship Between Beam Width and Side Lobe Level," **Proc. IRE**, 34, June 1946, pp. 335-348.

20. T. T. Taylor, "Design of Line Source Antenna for Narrow Beamwidth and Low Sidelobes," **IRE Trans. on AP**, AP-4, Jan. 1955, pp. 16-28.

21. P. M. Woodward, "A Method of Calculating the Field over a Plane Aperture Required to Produce a Given Polar Diagram," **Proc. IRE**, 93, 1947, pp. 1554-1558.

22. L. W. Couch II, **Synthesis and Analysis of Real Single-Side-Band Signals for Communication System**, Ph.D. dissertation, University of Florida, 1968.

23. J. Dugundji, "Envelopes and Pre-Envelopes of Real Waveform," **Trans IRE**, IT-4, March 1958, pp. 53-57.

24. E. Bedrosian, "The Analytic Signal Representation of Modulated Waveforms," **Proc. IRE**, 50, Oct. 1962, pp. 2071-2076.

25. A. W. Rihaczek, **Principles of High-Resolution Radar**, McGraw-Hill Book Co., New York, 1969, ch. 2.

26. A. Papoulis, **Signal Analysis**, McGraw-Hill Book Co., New York, 1977.

27. A. R. Lopez, "Sharp Cutoff Radiation Patterns," **IEEE Trans. on AP**, AP-27, Nov. 1979, pp. 820-824.

28. R. S. Elliott, "Design of Line Source Antenna for Narrow Beamwidth and Asymmetric Low Sidelobes," **IEEE Trans. on AP**, AP-23, Jan. 1975, pp. 100-107.

29. R. S. Elliot, "Design of Circular Aperture for Narrow Beamwidth and Asymmetric Low Sidelobes," **IEEE Trans. on AP**, AP-23, July 1975, pp. 523-527.

30. R. S. Elliot, "Design of Line-Source Antennas for Sum Patterns with Sidelobes of Individually Arbitrary Heights," **IEEE Trans. on AP**, AP-24, Jan. 1976, pp. 76-83.

31. R. S. Elliot, "Synthesis of Rectangular Planar Arrays for Sum Patterns with Ring Side Lobes of Arbitrary Topography," **Radio Sci.**, 12, Sep.-Oct. 1977, pp. 653-657.

32. R. S. Elliott and G. J. Stern, "A New Technique for Shaped Beam Synthesis of Equispaced Arrays," **IEEE Trans. on AP**, AP-32, Oct. 1984, pp. 1129-1133.

33. H. J. Orchard, R. S. Elliott and G. J. Stern, "Optimising the Synthesis of Shaped Beam Antenna Patterns," **IEE Proc.**, 132, Pt. H, Feb. 1985, pp. 63-68.

34. Y. K. Kim and R. S. Elliott, "Phase-Only Control Of Side-Lobes in a Sum Pattern Produced by a Circular Grid Array," **IEEE International Symposium Antenna & Propagation Digest**, 1, June 1987, pp. 117-120.

35. D. R. Rhodes, "The Optimal Line Source for the Best Mean-Square Approximation to a Given Radiation Pattern," **IEEE Trans. on AP**, AP-22, July 1963, pp. 440-446.

36. D. Slepian and H. Pollak, "Prolate-spheroidal wave functions, Fourier analysis and uncertainty-I," **Bell Tel. Syst. J.**, 40, Jan. 1961, pp. 43-64.

37. H. Steyskal, "On Antenna Power Pattern Synthesis," **IEEE Trans. on AP**, AP-18, 1970, pp. 123-124.

38. C. A. Klein, "Design of Shaped-Beam Antennas Through Minmax Gain Optimization," **IEEE Trans. on AP**, AP-32, (9), Sep. 1984, pp. 963-968.

39. T. A. Milligan, **Modern Antenna Design**, McGraw-Hill Book Co., New York, 1985, Ch. 10.

40. K. Milne, "Synthesis Of Power Radiation Patterns for Linear Array Antennas," **IEE Proc.**, 134, Pt. H, June 1987, pp. 285-296.

41. R. F. E. Guy, "General Radiation-Pattern Synthesis Technique for Array Antennas of Arbitrary Configuration and Element Type," **IEE Proc.**, 135, pt. H, Aug. 1988, pp. 241-248.

42. G. Franceschetti, G. Mazzarella and G. Panariello, "Array Synthesis with Excitation Constraints", **IEE Proc.**, 135, Pt. H, Dec. 1988, pp. 400-407.

43. K. W. Cattermole, **Mathematical Foundations for Communication Engineering**, John Wiley & Sons, New York, 1985, pp. 98-107.

44. Harry Urkowttz, "Hilbert Transforms of Band-Pass Functions," **Proc. IRE**, 50, Oct. 1962, p. 2143.

45. H. Stark, " An Extension of the Hilbert Transform Product Theorem," **Proc. IEEE**, 59, Sept. 1971, pp. 1359-1360.

46. J. L. Brown, Jr., "Analytic Signals and Product Theorems for Hilbert Transforms," **IEEE Trans. on Circuits and Systems**, CAS-21, Nov. 1974, pp.790-792.

47. J. L. Brown, Jr., "A Hilbert Transform Product Theorem," **Proc. IEEE**, 74, March 1986, pp. 520-521.

48. R. E. Bogner,"Frequency Sampling Filter-Hilbert Transformers and Resonators", **Bell Tech. J.**, 48, March 1969, pp. 501-510.

49. G. D. Cain, "Hilbert Transform Description of Linear Filtering," **Electron. Lett.**, 8, July 1972, pp. 380-382.

50. M. S. Sabri and W. Steenaart, "Discrete Hilbert Transform Filtering," **IEEE Trans. on ASSP**, ASSP-25, Oct. 1977, pp. 452-454.

51. R. C. Cabot, "A Note on the Application of the Hilbert Transform to Time Delay Estimation," **IEEE Trans. on ASSP**, ASSP-29, June 1981, pp. 607-609.

52. K. L. Peacock, "Kaiser-Bessel Weighting of the Hilbert Transform High-Cut Filter," **IEEE Trans. on ASSP**, ASSP-33, Feb. 1985, pp. 329-331.

53. A. Papoulis, **Probability, Random Variables, and Stochastic Processes**, McGraw-Hill Book Co., New York, 1984.

54. P. Z. Peebles, Jr., **Digital Communication System**, Prentice-Hall, Inc., Englewood Cliffs, N.J., 1987, Ch. 2.

55. B. Gold, A. V. Oppenheim, C. M. Rader, "Theory and Implementation of the Discrete Hilbert Transform," **Proc. Symp. Computer Processing in Communication**, Vol. 19, Polytechnic Press, New York, 1970, pp. 235-249.

56. A. V. Oppenheim and R. W. Schafer, **Discrete-Time Signal Processing**, Prentice-Hall, Inc., Englewood Cliffs, N.J., 1989.

57. L. R. Rabiner and B. Gold, **Theory and Application of Digital Signal Processing**, Prentice-Hall, Inc., Englewood Cliffs, N.J., 1975, pp. 70-73.

58. C. Ray Wylie, **Advanced Engineering Mathematics**, McGraw-Hill Book Co., New York, 1975, pp. 750-754.

59. J. W. Dettman, **Applied Complex Variables**, Dover Publications, Inc., New York, 1965.

60. L. W. Couch II, **Digital and Analog Communication System**, Macmillan Publishing Co., New York, 1987, pp. 74-87.

61. Dan E. Dudgeon and R. M. Mersereau, **Multidimensional Digital Signal Processing**, Prentice-Hall, Inc., Englewood Cliffs, N.J., 1984.

62. W. H. Press, B. P. Flannery, S. A. Teukolsky and W. T. Vetterling, **Numerical Recipes**, Cambridge University Press, Cambridge, 1986.

63. James Keesling, **Lecture Notes on Numerical Analysis**, University of Florida, 1987.

64. J. F. Kaiser, "Nonrecursive Digital Filter Design Using The I_0-Sinh Window Function," **Proc. 1974 IEEE International Symp. on Circuit and System Digest**, April 1974, pp. 20-23.

65. R. S. Elliott, "On Discretizing Continuous Aperture Distributions," **IEEE Trans. on AP**, AP-25, Sep. 1977, pp. 617-621.

66. A. T. Villeneuve, "Taylor Patterns for Discrete Arrays," **IEEE Trans. on AP**, AP-32, Oct. 1984, pp. 1089-1093.

67. T. Takeshima, "Slot Array Antennas for Simultaneous Radiation," **IEEE Trans. on AP**, AP-13, 1965, pp. 472-473.

68. D. C. D. Chang, W. N. Klimczak, G. C. Susche, "An Experimental Digital Beamforming Array," **1988 IEEE International Symposium Antenna & Propagation Digest**, June, 1988, pp. 1300-1303.

69. G. M. kirkpatrick, "Final Engineering Report on Angular Accuracy Improvement", **General Electrical Company Report**, Aug. 1952. Reprinted in **Radars**, Vol. 1, Monopulse Radar, edited by D. K. Barton, Artech House, Inc., Dedham, Massachusetts, 1977.

70. E. J. Powers, "Utilization of the Lambda Functions in the Analysis and Synthesis of Monopulse Antenna Difference Patterns," **IEEE Trans. on AP**, AP-15, Nov. 1967, pp. 771-777.

71. O. R. Price and R. F. Hyneman, "Distribution Functions for Monopulse Antenna Difference Pattern," **IRE Trans. on AP**, AP-8, Nov. 1960, pp. 567-576.

72. P. W. Hannan, "Maximum Gain in Monopulse Difference Mode," **IRE Tran. on AP**, AP-9, May, 1961, pp. 314-315.

73. A. R. Lopez, "Monopulse Networks for Series Feeding an Array Antenna,". Reprinted in **Radars**, Vol. 1, Monopulse Radar, edited by D. K. Barton, Artech House, Inc., Dedham, Massachusetts, 1977, pp. 307-311.

74. D. K. Barton, **Radar**, Vol. 1, Monopulse Radar, Artech House, Inc., Dedham, Massachusetts, 1977.

75. N. Balakrishnan and S. Ramakrishna, "Optimun Difference Mode Excitations for Monopulse Arrays," **IEEE Trans. on AP**, AP-30, May 1982, pp. 325-330.

76. David M. Pozar, **Antenna Design Using Personal Computers**, Artech House, Inc., Dedham, Massachusetts, 1985.

BIOGRAPHICAL SKETCH

Ching-Song Chuang was born on April 20, 1951, in Tao-Yuan, Taiwan, R.O.C. He received the Diploma (equivalent to B. S. degree) with a major in electronic engineering from National Taipei Institute of Technology, Taipei, Taiwan, in June 1972. After two years military service, he was employed by the Timex Co., Ltd. in Taiwan as an electronic engineer. Since August 1976, he has been working in CSIST, Taiwan, as a research assistant. In May of 1980, he was awarded a Chinese government scholarship for graduate study in the United States and was admitted to the Electrical Engineering Department of North Carolina State University at Raleigh, and received his Master of Science degree in Dec. 1981. After graduation, he returned to the CSIST and worked as an assistant scientist, participating in the research and development of a radar system. In August 1986, he was re-awarded a government scholarship and enrolled in the Department of Electrical Engineering at the University of Florida for advanced research. He is scheduled to complete his Ph.D. program in August 1989.

I certify that I have read this study and that in my opinion it conforms to acceptable standards of scholarly presentation and is fully adequate, in scope and quality, as a dissertation for the degree of Doctor of Philosophy.

Leon W. Couch

Leon W. Couch, Chairman
Professor of Electrical Engineering

I certify that I have read this study and that in my opinion it conforms to acceptable standards of scholarly presentation and is fully adequate, in scope and quality, as a dissertation for the degree of Doctor of Philosophy.

Peyton Z. Peebles, Jr.

Peyton Z. Peebles
Professor of Electrical Engineering

I certify that I have read this study and that in my opinion it conforms to acceptable standards of scholarly presentation and is fully adequate, in scope and quality, as a dissertation for the degree of Doctor of Philosophy.

Julius T. Tou
Graduate Research Professor of
Electrical Engineering

I certify that I have read this study and that in my opinion it conforms to acceptable standards of scholarly presentation and is fully adequate, in scope and quality, as a dissertation for the degree of Doctor of Philosophy.

Jose C. Principe
Associate Professor of Electrical
Engineering

I certify that I have read this study and that in my opinion it conforms to acceptable standards of scholarly presentation and is fully adequate, in scope and quality, as a dissertation for the degree of Doctor of Philosophy.

James Keesling

James Keesling
Professor of Mathematics

This dissertation was submitted to the Graduate Faculty of the College of Engineering and to the Graduate School and was accepted as partial fulfillment of the requirements for the degree of Doctor of Philosophy.

August 1989

Hubert A. Bevis

Dean, College of Engineering

Dean, Graduate School